(4)

Experimental Investigation of a Planar Shock Wave over a Double Wedge

Final Technical Report

by

Prof. G. Ben-Dor

Period: Oct. 1, 1987 - Dec. 31, 1988

Contract: DAJA 45-87-0042
-C-

RYD 5838-PH-01

Introduction

The research project consisted of three different phases:

1) an analytical investigation

During this phase the various reflection processes which can occur when a plane shock wave reflects over a double wedge were predicted. In addition, the transition boundaries between the various reflection processes were established. Finally the domains of the different reflection processes and their boundaries were drawn in the (θ_w^1, θ_w^2) - plane for given values of M_i.

2) an experimental investigation

During this phase experiments were conducted ~~in order~~ to verify the above mentioned analysis. ~~In addition,~~ some other aspects regarding the reflection of a plane wedge over a double wedge were investigated experimentally. In particular, the wave configuration which is approached asymptotically should be mentioned. The results of this particular experimental study enables us to verify our shock polar analysis.

3) a numerical investigation

In addition to the above mentioned analytical and experimental investigations, a numerical code based on the TVD scheme was developed. The wave configurations as predicted by the numerical code were compared with those obtained experimentally and found to be in excellent agreement. This gave us some confidence in the numerical code and its predictions regarding the flow field generated during the reflection in general, and the pressure distribution along the wedge surface, in particular.

Publications

Some of the results of the investigation have been published in the following papers:

Ben-Dor, G., Dewey, J.M. & Takayama, K., "The Reflection of a Plane Shock Wave Over a Double Wedge", Journal of Fluid Mechanics, Vol. 176, pp. 483-520, 1987.

Ben-Dor, G., Dewey, J.M., McMillin, D.J. & Takayama, K., "Experimental Investigation of the Asymptotically Approached Mach Reflection Over the Second Surface in a Double Wedge Reflection", Experiments in Fluids, Vol. 6, pp. 429-434, 1988.

In addition to these publications, parts of the research project were presented in the following scientific conferences:

1. Ben-Dor, G., Takayama, K. and Dewey, J.M., "The Reflection of a Regular or a Mach Reflection over a Concave Double Wedge", The 5th Mach Reflection Symposium, Menlo Park, California, U.S.A., 1985.

2. Ben-Dor, G., Dewey, J.M. and Takayama, K., "The Reflection of a Mach Reflection over a Secondary Ramp", The 15th International Symposium on Shock Waves and Shock Tubes, San Francisco, California, U.S.A., 1985.

3. Dewey, J.M., Ben-Dor, G. and Takayama, K., "The Reflection of a Planar Shock from a Convex Double Wedge", The 15th International Symposium on Shock Waves and Shock Tubes, San Francisco, California, U.S.A., Published in the Proceedings, 1985.

4. Ben-Dor, G. and Dewey, J.M., "The Theory and Experimental Investigation of Regular and Mach Reflection over a Double Wedge. Part I: The Theory and Shock Polar Analysis", The 9th International Symposium on Military Applications of Blast Simulation, Oxford, England, Published in the Proceedings, 1985.

5. Ben-Dor, G. and Dewey, J.M., "The Theory and Experimental Investigation of Regular and Mach Reflection over a Double Wedge. Part II: Experimental Investigation", The 9th International Symposium on Military Applications of Blast Simulation, Oxford, England, Published in the Proceedings, 1985.

6. Dewey, J.M., Ben-Dor, G. and Takayama, K., "The Reflection of a Planar Shock Wave over a Double Wedge", The 6th Mach Reflection Symposium, Beer Sheva, Israel, Published in the Book of Abstracts, 1986.

7. Ben-Dor, G., "On the Asymptotically Approached Mach Reflection over the Second Surface in the Reflection of a Planar Shock Wave over a Double Wedge", The 7th Mach Reflection Sumposium, Albuquerque, N.M., U.S.A., 1987.

This report is divided into 3 parts:

Part 1. This part deals with the analytical prediction and the experimental verification of the domains and boundaries of the various types of the reflection processes of a plane shock wave over a double wedge.

Part 2. This part includes experiments regarding the wave configuration of the reflection which is approached asymptotically.

Part 3. This part contains some examples of the results which were obtained by the numerical code.

Part 1

Domains and Boundaries of the Various Types of the Reflection Processes of a Plane Shock Wave Over a Double Wedge

Analytical and Experimental Investigation

INTRODUCTION

Ben-Dor, Dewey and Takayama (1987) have studied, both analytically and experimentally, the reflection of a planar shock over a double wedge. In their analytical study they provided a detailed shock polar analysis of the reflection process, based on the assumption that the reflection over the second surface of the double wedge approaches asymptotically the reflection which would have been obtained over a single wedge with the same wedge angle.

A schematical illustration of a double wedge is shown in figure 1. θ_w^1 and θ_w^2 are the slopes of the first and second surfaces of the double wedge, respectively. The difference between these two slopes is $\Delta\theta_w = \theta_w^2 - \theta_w^1$. If $\Delta\theta_w > 0$ the double wedge is concave, (figure 1a), and if $\Delta\theta_w < 0$ the double wedge is convex (figure 1b).

The domains of different types of reflection process over a double wedge in the (θ_w^1, θ_w^2)-plane are shown in figure 2. The line $\Delta\theta_w = 0$ divides the (θ_w^1, θ_w^2)-plane into the domains of concave and convex double wedges. The line $\theta_w^1 = \theta_w^{det}$ determines the type of reflection over the first surface of the double wedge. If $\theta_w^1 < \theta_w^{det}$ then the incident shock wave reflects over the first surface as a Mach reflection (MR), and if $\theta_w^1 > \theta_w^{det}$ then the initial reflection is regular (RR). The line $\theta_w^2 = \theta_w^{det}$ determines the type of reflection which is finally obtained over the second surface. If $\theta_w^2 < \theta_w^{det}$ then the final reflection over the second surface is a MR, and if $\theta_w^2 > \theta_w^{det}$ then the final reflection over

the second surface is a RR. In the case of a concave double wedge ($\Delta\theta_w > 0$) and a Mach reflection over the first surface ($\theta_w^1 < \theta_w^{det}$) the Mach stem of the MR reflects eventually over the second surface. The type of its reflection depends upon whether $\Delta\theta_w$ is smaller or greater than θ_w^{det}. If $\Delta\theta_w < \theta_w^{det}$ then the Mach stem will reflect over the second surface as a MR, and if $\Delta\theta_w > \theta_w^{det}$ then it will reflect as a RR.

The above described transition boundaries give rise to seven domains of different types of reflection processes over a double wedge. They are numbered 1 to 7 in figure 2 and are summarized in more detail in table 1.

The three reflection processes which are investigated in this study are those appropriate to domains 3, 4 and 6, for only in these three domains the final reflection over the second surface of the double wedge is a MR. In the following a detailed description of the reflection process in each of these three domains is given.

Domain 3

- Since $\Delta\theta_w < 0$, the double wedge is convex.
- Since $\theta_w^1 < \theta_w^{det}$, the incident shock wave reflects over the first surface as a MR.
- Since $\theta_w^2 < \theta_w^{det}$, the final reflection of the incident shock wave over the second surface is also a MR.

A schematical illustration of this reflection process is shown in figure 3.

Domain 4

- Since $\Delta\theta_w < 0$, the double wedge is convex.
- Since $\theta_w^1 > \theta_w^{det}$, the incident shock wave reflects over the first surface as a RR.
- Since $\theta_w^2 < \theta_w^{det}$, the final reflection of the incident shock wave over the second surface is a MR.

A schematical illustration of this reflection process is shown in figure 4.

Domain 6

Unlike the previous two cases, here $\Delta\theta_w > 0$, and therefore the double wedge is concave. Since $\theta_w^1 < \theta_w^{det}$, the incident shock wave reflects over the first surface as a MR. When the Mach stem of this MR collides with the leading edge of the second surface, for which $\Delta\theta_w < \theta_w^{det}$, it reflects over it as a MR. The two Mach reflections interact to create the final MR of the incident shock wave over the second surface, whose slope satisfies $\theta_w^2 < \theta_w^{det}$. A schematical illustration of this reflection process is shown in figure 5. Note that the interaction of the two triple points, T_1 and T_2, at point Q, results in two new triple points: T_3, associated with the MR of the incident shock

wave over the second surface and an additional triple point, T_4, which 'splits' the reflected shock wave.

The previously mentioned assumption that the MR over the second surface approaches asymptotically the MR which would have been obtained by the same incident shock wave over a single wedge with an angle $\theta_w = \theta_w^2$ implies that the triple point trajectory angle χ of each of the Mach reflections shown in figures 3, 4 and 5, over the second surface should approach asymptotically the value which would have been obtained with the same incident shock wave over a single wedge with an angle $\theta_w = \theta_w^2$. The verification of this assumption, which is basic to Ben-Dor et al's (1987) analysis, is the subject of the present experimental study.

Present Study

In order to check the foregoing mentioned assumption, an experimental study was carried out in which the reflection process over a double wedge was recorded using high speed photography. Details of the high speed photography technique can be found in the papers by Dewey and Walker (1975) and Walker, Scotten and Dewey (1982). The system consists of a giant ruby laser which can be pulsed in 50 μsec intervals. The phenomenon was recorded with a rotating-mirror camera. Two experiments with very-nearly identical incident shock wave Mach numbers were conducted over each double wedge, with the first laser pulse of the second experiment delayed by 25 μsec with respect to the first pulse of the first experiment so that it was

possible to obtain multiple schlieran photographs of the reflection process over a double wedge in 25 μsec intervals.

Once the two experiments were recorded, the trajectories of the triple points and the points where the feet of the Mach stems touch the reflecting surfaces were digitized. The digitized data were then evaluated to obtain specific details regarding the direction of propagation of the various triple points, their velocities and the velocities of the feet of the Mach stems along the reflecting surfaces.

In order to obtain the values of the triple point trajectory angle, χ, the velocity of the triple point, V_T, and the velocity of the foot of the Mach stem, V_G, to which the MR over the second surface was assumed to approach asymptotically, the reflection of an incident shock wave with an identical Mach number over a single wedge with an angle $\theta_w = \theta_w^2$ was recorded. The values of χ, V_T and V_G, which are constant over a single wedge, were measured directly from the photographs. The triple point trajectory angle, χ, was measured with a protractor to an accuracy of ±0.5°. The velocities of the triple point and the foot of the Mach stem were obtained by dividing their respective distances from the leading edge of the wedge by the time passed from the moment the incident shock wave collided with the leading edge of the wedge to the moment the photograph was taken. This time was calculated from

$$\Delta t = \frac{L_i}{V_i}$$

where L_i is the horizontal distance of the incident shock wave from the

leading edge of the wedge and V_i is the velocity of the incident shock wave. The velocity of the incident shock wave was measured by two pressure transducers which were separated by 20 cm and were located just ahead of the test section of the shock tube.

RESULTS AND DISCUSSION

In the following, the experimental results of the foregoing described study are given for domains 3, 4 and 6 of figure 2. Note that only the asymptotic wave configuration is given over the second surface. The wave configurations which are obtained immediately after the reflection over the first surface interacts with the sudden change in the slope of the surface, are discussed in detail in Ben-Dor et al. (1987).

Domain 3

Experiments with two double wedges which are appropriate to domain 3 of figure 2 were performed. The geometry of the first double wedge was $\theta_w^1 = 40°$ and $\theta_w^2 = 25°$ ($\Delta\theta_w = -15°$). The incident shock wave Mach number was $M_i = 1.3$.

The triple point trajectory angle χ and its velocity in terms of Mach number, $M_T = V_T/a_0$, are shown in figure 6. The triple point trajectory angle over the first surface which has a slope of 40° is $\chi_1 = 1.2°$.

After the Mach stem of the MR over the first surface passes the leading edge of the second surface, the direction of propagation of the triple point, i.e. $\theta_w^1 + \chi_1$, decreases continuously and approaches the value appropriate to a MR with $M_i = 1.3$ over a single wedge with $\theta_w = 25°$, i.e., $\chi^s = 6.4°$. The velocity of the triple point, M_T, which was 1.74 over the first surface is also seen to be decreasing continuously and approaching asymptotically the value appropriate to a

single wedge, i.e., $M_T^s = 1.523$. The velocity of the foot of the Mach stem $M_G = V_G/a_0$, for this case is shown in figure 7. It is also seen to decrease continuously from its value of 1.7 over the first surface towards the value appropriate to a single wedge with $\theta_w = 25°$, i.e., $M_G^s = 1.387$.

At a distance of 18 cm from the leading edge of the double wedge the triple point trajectory angle χ and its velocity M_T have almost reached the values appropriate to a single wedge. However, M_G is still quite far from the asymptotic value it is assumed to reach at this distance (χ and M_T are about 1.5% and 1% larger than the asymptotic values, whereas M_G is still about 4.5% too large).

An additional experiment with a double wedge also appropriate to domain 3 of figure 2 is shown in figure 8. The geometry of the double wedge is $\theta_w^1 = 35°$, $\theta_w^2 = 15°$ ($\Delta\theta_w = -20°$) and the incident shock wave Mach number is again $M_i = 1.3$.

The experimental results again indicate that after the MR over the first surface passes the leading edge of the second surface the values of χ, M_T and M_G decrease towards the values appropriate to a single wedge with an angle $\theta_w = \theta_w^2$.

Unlike the previous case, here M_G is seen to reach its predicted asymptotic value at about x = 12 cm (x is measured from the leading edge of the double wedge) while M_T and χ are still about 1.5% and 4.9% larger than their assumed asymptotic values. Note that the ±0.5° error bar in the measured value of χ could have resulted in a different curve which

would still agree with all the measurements but would resemble a faster approach to the assumed asymptotic value. Such a curve is added to figure 8 in a dotted line. It results in a value which is only about 2.8% higher than the assumed limit.

Domain 4

The experimental results over a double wedge with $\theta_w^1 = 60°$ and $\theta_w^2 = 30°$ ($\Delta\theta_w = -30°$) and an incident shock wave with $M_i = 1.3$ are shown in figure 9. The reflection process over this double wedge starts with a RR over the first surface. When the reflection point of this RR reaches the leading edge of the second surface (point B), MR begins and a triple point forms.

The experimental results in figure 9 again indicate that χ, M_T and M_G approach asymptotically their assumed limiting values. At about x = 12 cm (x is again measured from the leading edge of the double wedge), χ, M_G and M_T are about 1.3%, 0.4% and 0.25% larger than their respective asymptotic values. These small differences imply that the MR configuration has almost reached a configuration which would have been obtained by an incident shock wave with $M_i = 1.3$ over a single wedge with $\theta_w = 30°$.

Domain 6

Due to the complexity of the reflection process in this domain compared to those presented earlier for domains 3 and 4 the experimental results for this case are shown in a different way than those presented earlier.

Figure 10 shows the experimentally recorded trajectories of the four triple points T_1, T_2, T_3 and T_4 of figure 5. The first triple point, T_1, is obtained when the incident shock wave with $M_i = 1.3$ reflects over the first surface which has an angle $\theta_w^1 = 15°$. The triple point trajectory angle of T_1 is $\chi_1 = 14.8°$. When the Mach stem of this MR collides with the leading edge, point B, of the second surface, which has an angle $\theta_w^2 = 35°$, it reflects over it as a secondary MR with triple point T_2. The experimental results indicate that unlike the trajectory of T_1 which is straight, the trajectory of T_2 is curved. This is probably due to the fact that the Mach stem (which serves as the incident shock wave in the secondary MR, see figure 5) is not a straight shock wave like the incident shock wave. Instead, it has a concave curvature. If, however, the trajectory of the T_2 is approximated by a straight line then it forms an angle, χ_2, of about 7° with the second surface. When the two triple points, T_1 and T_2, meet at point Q they interact to result in two new triple points, T_3 and T_4. T_3, the triple point of the MR of the incident shock wave over the second surface, is seen to approach a direction which is parallel to the trajectory which would have been obtained if an incident shock wave with $M_i = 1.3$ was reflected over a wedge with $\theta_w = 35°$, i.e., $\chi = 4°$. This direction is shown in figure 10 by a dash-dotted line. The trajectory of the triple point T_4, on the curved reflected shock wave, is also curved.

The evaluation of the velocity of T_3 resulted in $M_{T_3} = 1.659$. The velocity of an appropriate triple point over a single wedge would be

M_T = 1.673. The difference, which is less than 1%, clearly suggests that the triple point T_3 has almost reached the asymptotic value it is assumed to reach. The velocities of T_1 and T_2, i.e., M_{T_1} and M_{T_2}, are 1.479 and 1.650, respectively. It should also be noted that the trajectory of T_4, which as mentioned earlier is curved, is seen to approach a straight line. The direction of this line with respect to the x-axis is 62.9°.

Finally, it is of interest to note that if one assumes that the Mach stem of the MR of the incident shock wave is straight and perpendicular to the wedge surface, then the location of point Q where the trajectories of the first two triple points, T_1 and T_2, intersect, can be calculated analytically using the following geometrical expression:

$$\overline{AQ} = L \frac{\sin (\Delta\theta_w + \chi_2)}{\sin (\Delta\theta_w + \chi_2 - \chi_1)} \tag{1}$$

where $\overline{AQ}$ is the distance from the leading edge of the double wedge, point A, to point Q and L is the length of the first surface, i.e., $L = \overline{AB}$.

Thus the location of Q in the (x,y)-plane is:

$$x_Q = \overline{AQ} \cos (\theta_w^1 + \chi_1) \tag{2a}$$

$$y_Q = \overline{AQ} \sin (\theta_w^1 + \chi_1) \tag{2b}$$

The analytical solution of the reflection at hand results in: $\chi_1 = 13.286°$ and $\chi_2 = 7.028$ (recall that the experimental results were 14.8° and 7°, respectively). Inserting these values into equation (1), together with L = 72 mm yields $\overline{AQ} = 140.2$ mm. Thus, from equation (2), one obtains $x_Q = 123.4$ mm and $y_Q = 66.4$ mm. The corresponding measured results as evaluated from the digitized data are 125 mm and 68 mm, respectively. The comparison between these results suggests that equations (1) and (2) could be used to predict quite accurately the location of point Q where T_1 and T_2 meet.

It should also be mentioned that experiments with $M_i = 1.3$ were repeated using the double wedge configuration at hand, i.e., $\theta_w^1 = 15°$, $\Delta\theta_w = 20°$ and $\theta_w^2 = 35°$, but with different values of L (L is the distance from the leading edge of the first surface, point A, to the leading edge of the second surface, point B). The experimentally obtained location of point Q agreed with that predicted by equation (1) and (2) to within 2.5% for all values of L in the range $15 < L < 72$ mm.

Conclusions

The assumption that the MR of the incident shock wave over the second surface of a double wedge approaches the MR which would have been obtained by the same incident shock wave reflecting over a single wedge with an angle θ_w equal to the slope of the second surface of a double wedge, i.e., θ_w^2, was investigated experimentally.

The experimental results clearly indicate that the assumption is correct. The triple point velocity (including its direction of propagation) and the velocity of the foot of the Mach stem of the MR

are indeed found to approach the values appropriate to a reflection over a single wedge. This behavior can undoubtedly be attributed to the fact that shock wave stability is the governing mechanism of the phenomenon at hand.

It is also interesting to note that the experimental results presented in figures 6-10 indicate that the relaxation length, (i.e., the distance travelled by the incident shock wave over the second surface until the asymptotic reflection is nearly obtained) is of the order of a few lengths of the first surface of the double wedge. If the relaxation length is defined as the distance at which the reflection has come to within 5% of the asymptotic values, then the relaxation lengths of the four cases presented in this study are about 1.25, 2, 3.5 and 1.5 times the length of the first surface of the appropriate wedge.

As mentioned earlier, an experimental study aimed at investigating the influence of the length of the first surface on the relaxation process revealed that such an influence, if it exists, is minimal.

The present scudy was limited to cases where the reflection of the incident shock wave over the first and second wedges were supposed to be either regular or single-Mach reflection. For stronger incident shock waves both complex and double-Mach reflections might be possible over the two surfaces. This would undoubtedly complicate the reflection processes and might also increase the relaxation lengths. However, it is hypothesized here, that the final reflection over the second surface of a double wedge will be that which would have been obtained over a single wedge with the same incident shock wave, no matter if it is a single, a complex or a double-Mach reflection.

It should also be mentioned that the fact that the shock configurations which are approached asymptotically in the case of a reflection over a double wedge. are similar to those which would have been obtained by the same incident shock wave over an appropriate single wedge, does not necessarily imply that the flow fields are also similar. This can most easily be justified if one recalls the paper by Ben-Dor and Glass (1978) where it was shown that different computer codes were capable of resulting in almost identical wave configurations which differed very much in their flow fields.

In summary, the present experimental study supports the shock polar analysis which was presented by Ben-Dor et al. (1987) for studying the reflection process over a double wedge.

List of References

Ben-Dor, G. and Glass, I.I., "Nonstationary Oblique Shock Wave Reflections: Actual Isopycnics and Numerical Experiments", AIAA J., Vol. 16, pp. 1146-1153, 1978.

Ben-Dor, G., Dewey, J.M. and Takayama, K., The Reflection of a Planar Shock Wave over a Double Wedge, J. Fluid Mechanics, Vol. 176, pp. 483-520, 1987.

Dewey, J.M. and Walker, D.K., A Multiply Pulsed Double-Pass Laser Schlieren System for Recording the Movement of Shocks and Particle Tracers Within a Shock Tube, J. Appl. Phys., Vol. 46, pp. 3454-3458, 1975.

Walker, D.K., Scotten, L.N. and Dewey, J.M., Construction and Evaluation of an Simple and Inexpensive Rotating Prism Camera for Recording Movement of Shocks and Particle Tracers within a Shock Tube, Proc. 15th Int. Cong. High Speed Photography and Photonics, SPIE, Vol. 348, pp. 125-130, 1982.

	θ_{w_1}	θ_{w_2}	$\Delta\theta_w$	First surface	Second surface	Region
Convex	> det	> det	-	Regular	Regular	2
	< det	< det	-	Mach	Mach	3
	> det	< det	-	Regular	Mach	4
Concave	> det	> det	-	Regular	Regular	1
	< det	> det	> det	Mach	Regular→Regular	5
	< det	< det	< det	Mach	Mach→Mach	6
	< det	> det	< det	Mach	Mach→Regular	7

Table 1

A summary of the seven different reflection processes which can occur over convex and concave double wedges depending on the magnitude of the wedge angles θ_w^1, θ_w^2 and $\Delta\theta_w$ compared to the detachment wedge angle θ_w^{det} (referred to simply as 'det' above). The numbers in the final column refer to the regions in the θ_w^1, θ_w^2 plane of figure 2.

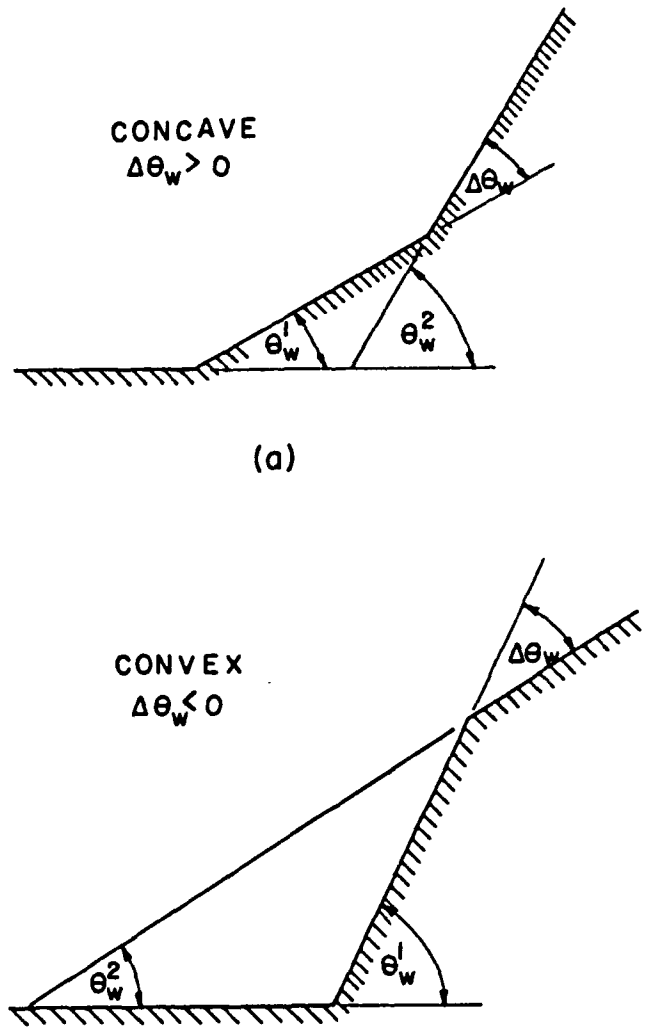

Figure 1: A schematical illustration of a double wedge: a) concave; b) convex.

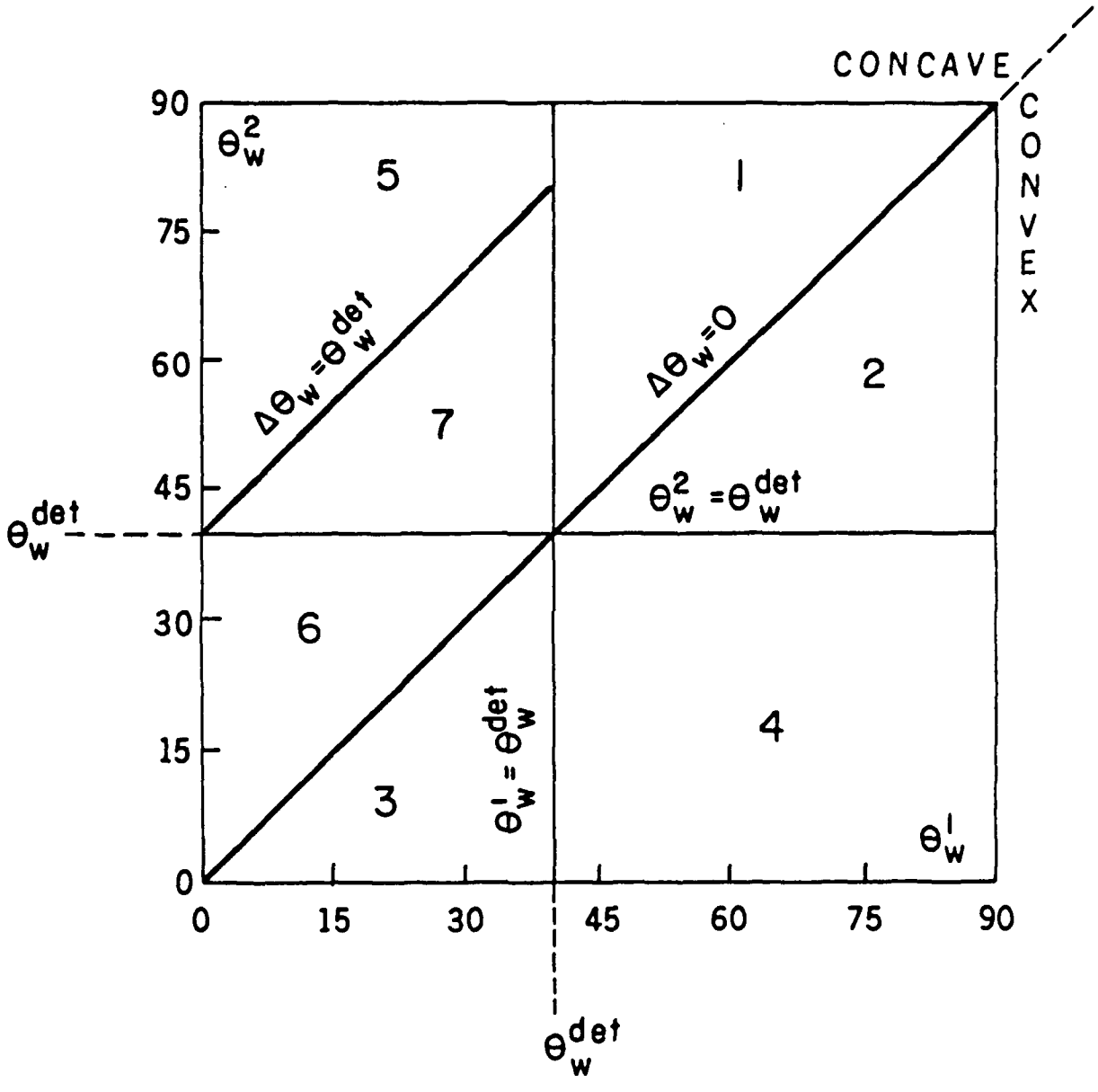

Figure 2: Domains of different types of reflection processes over a double wedge.

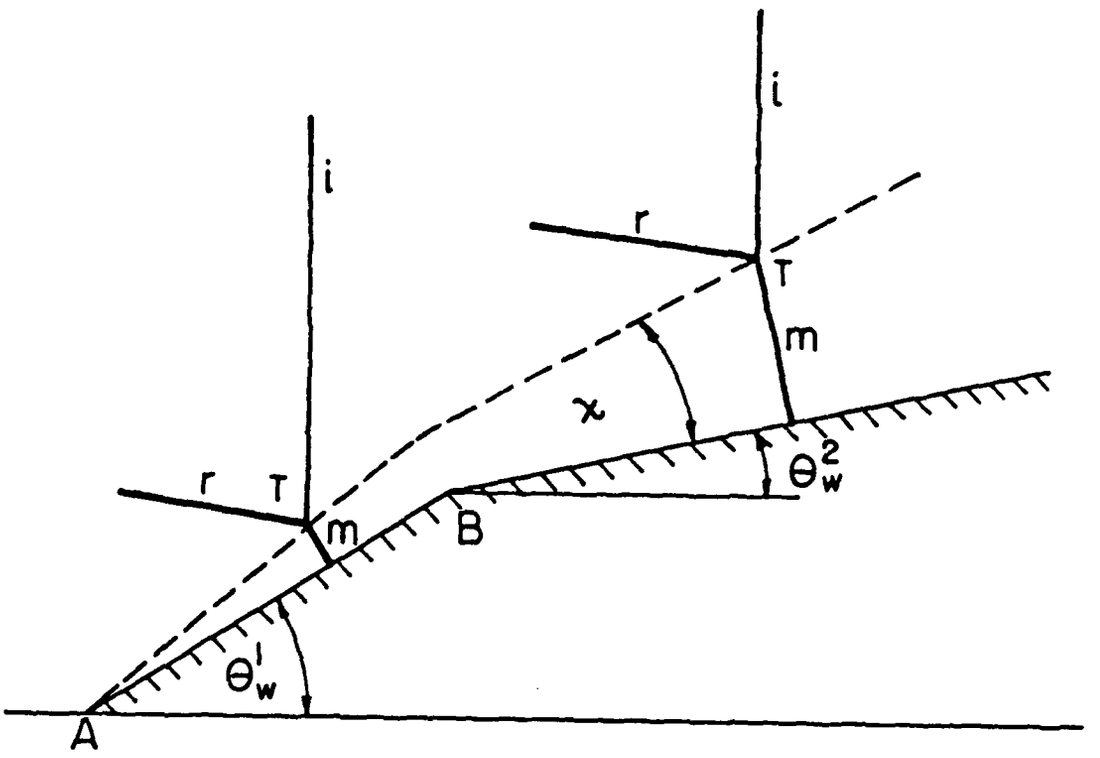

Figure 3: A schematical illustration of the reflection process in domain 3 of figure 2.

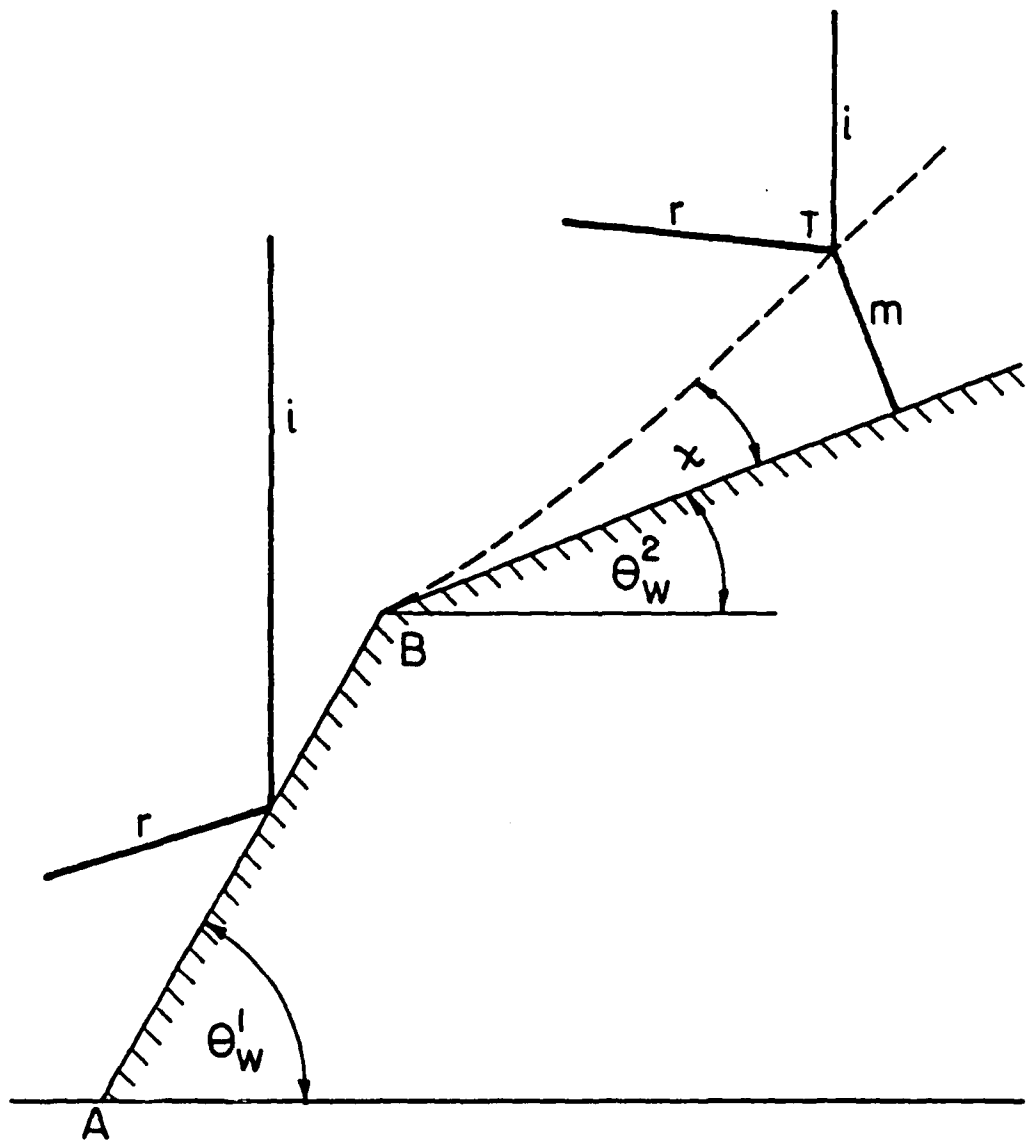

Figure 4: A schematical illustration of the reflection process in domain 4 of figure 2.

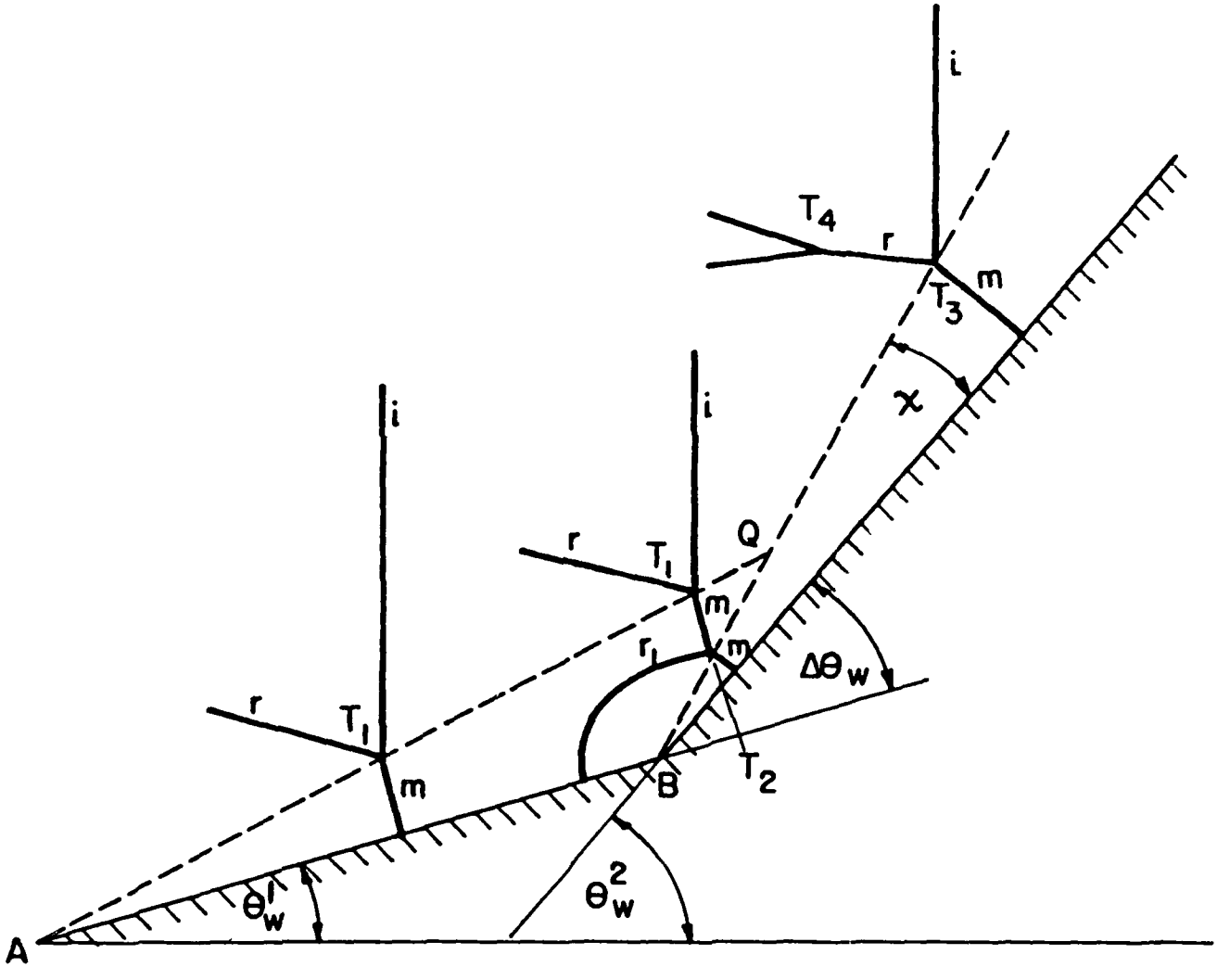

Figure 5: A schematical illustration of the reflection process in domain 6 of figure 2.

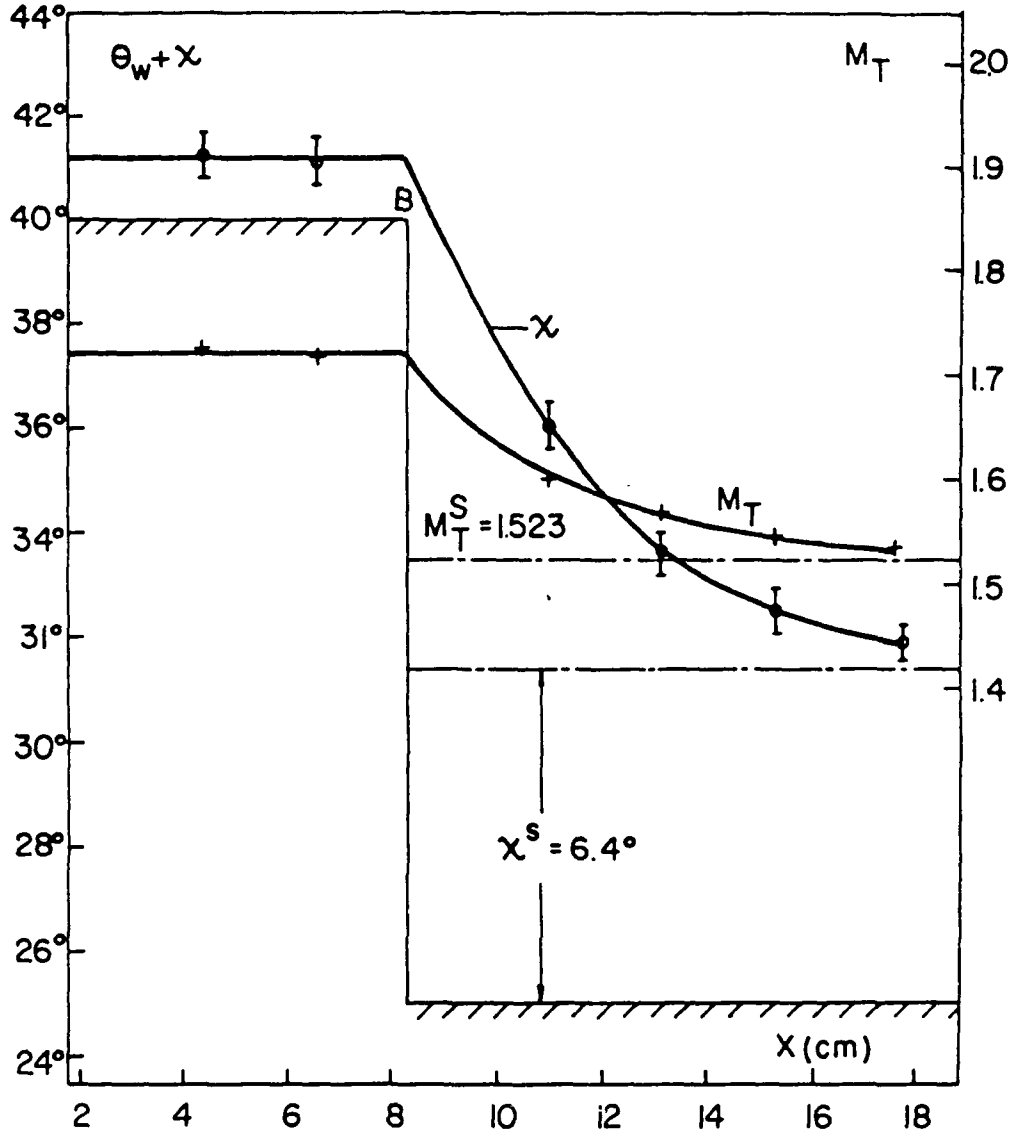

Figure 6: The instantaneous triple point trajectory angle, χ, and triple point Mach number , M_T, of the Mach reflection of an incident shock wave with $M_i = 1.3$ over the second surface of a double wedge with $\theta_w^1 = 40°$ and $\theta_w^2 = 25°$ (domain 3 of figure 2).

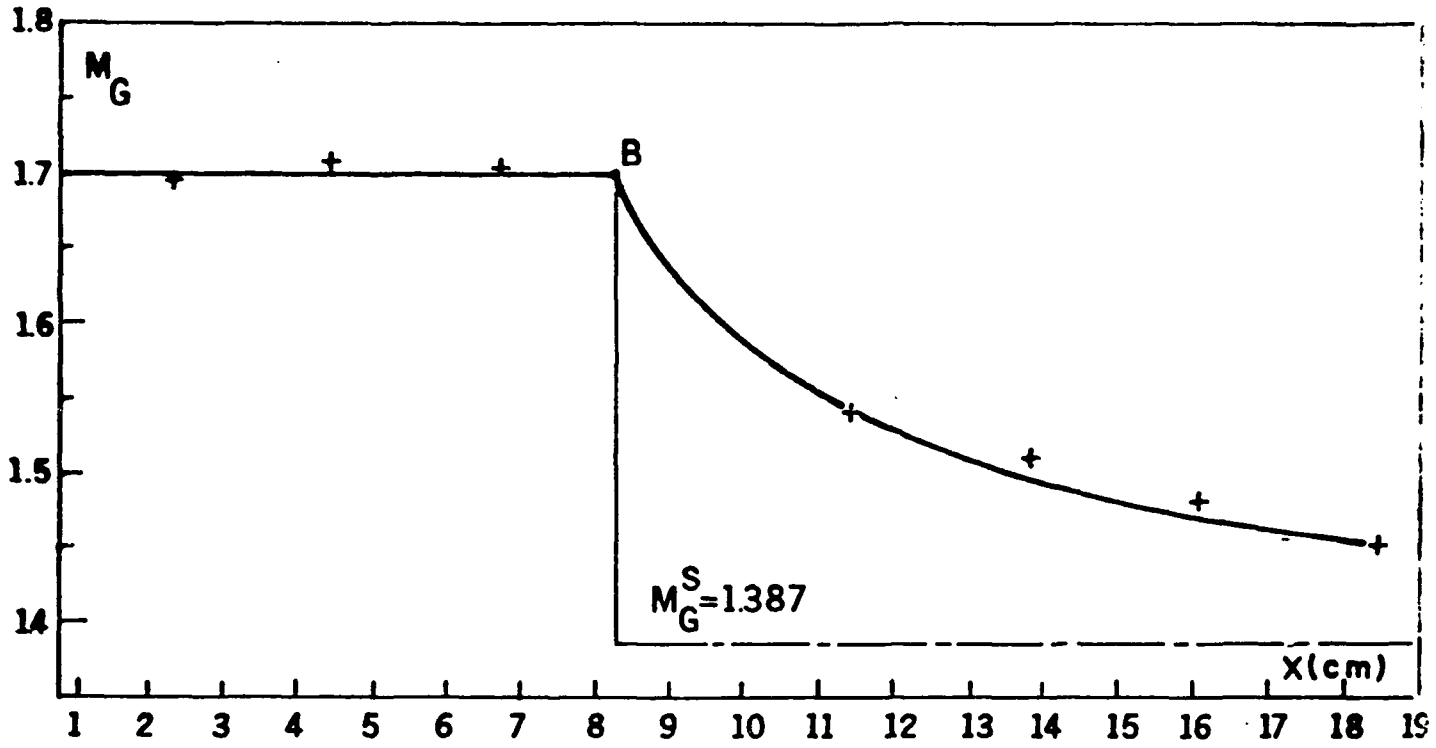

Figure 7: The instantaneous Mach number, M_G, of the foot of the Mach stem of the Mach reflection of an incident shock wave with $M_i = 1.3$ over the second surface of a double wedge with $\theta_w^1 = 40°$ and $\theta_w^2 = 25°$ (domain 3 of figure 2).

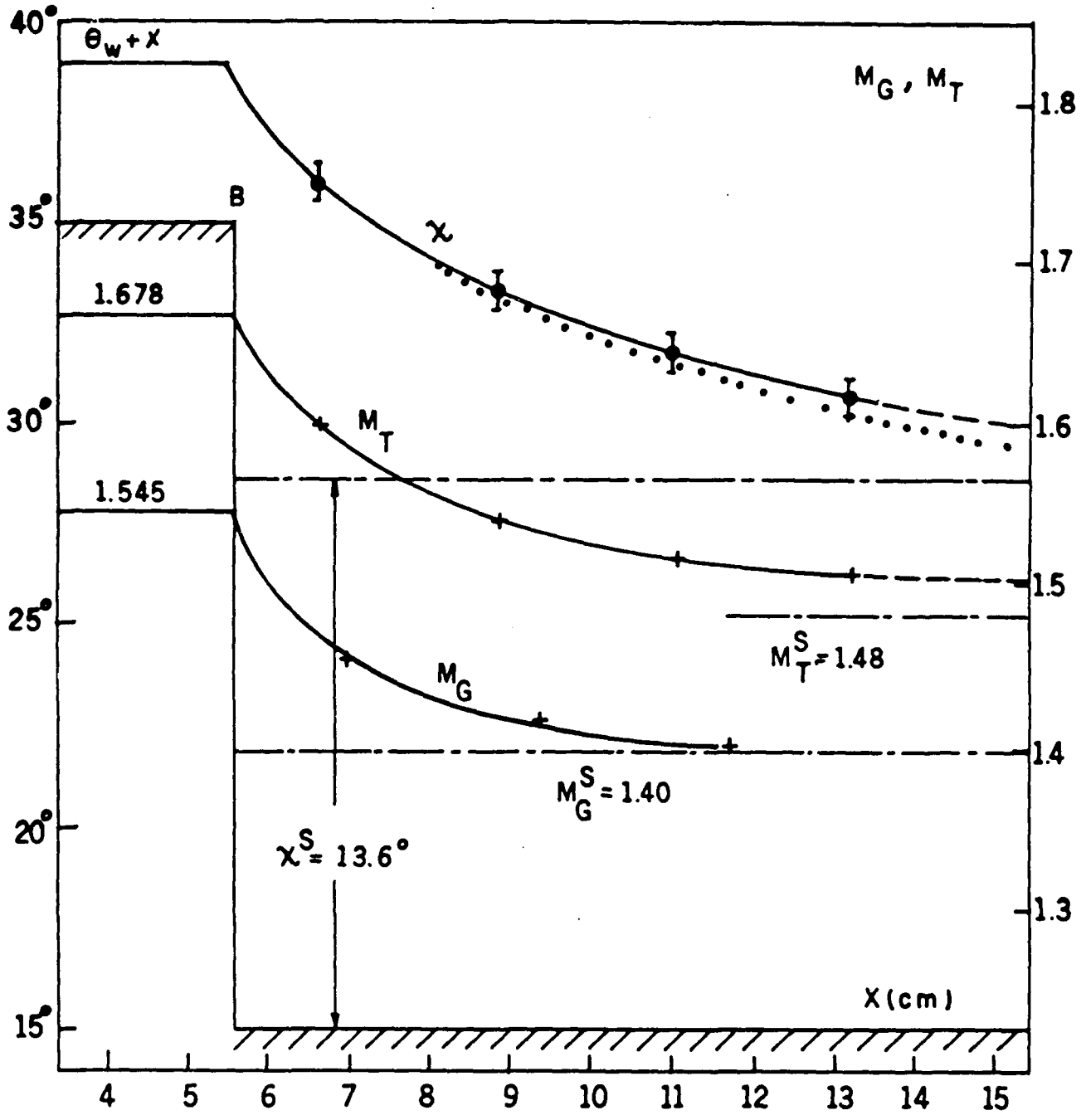

Figure 8: The instantaneous triple point trajectory angle and Mach numbers of the triple point and the foot of the Mach stem, of the Mach reflection of an incident shock wave with $M_i = 1.3$ over the second surface of a double wedge with $\theta_w^1 = 35°$ and $\theta_w^2 = 15°$ (domain 3 of figure 2).

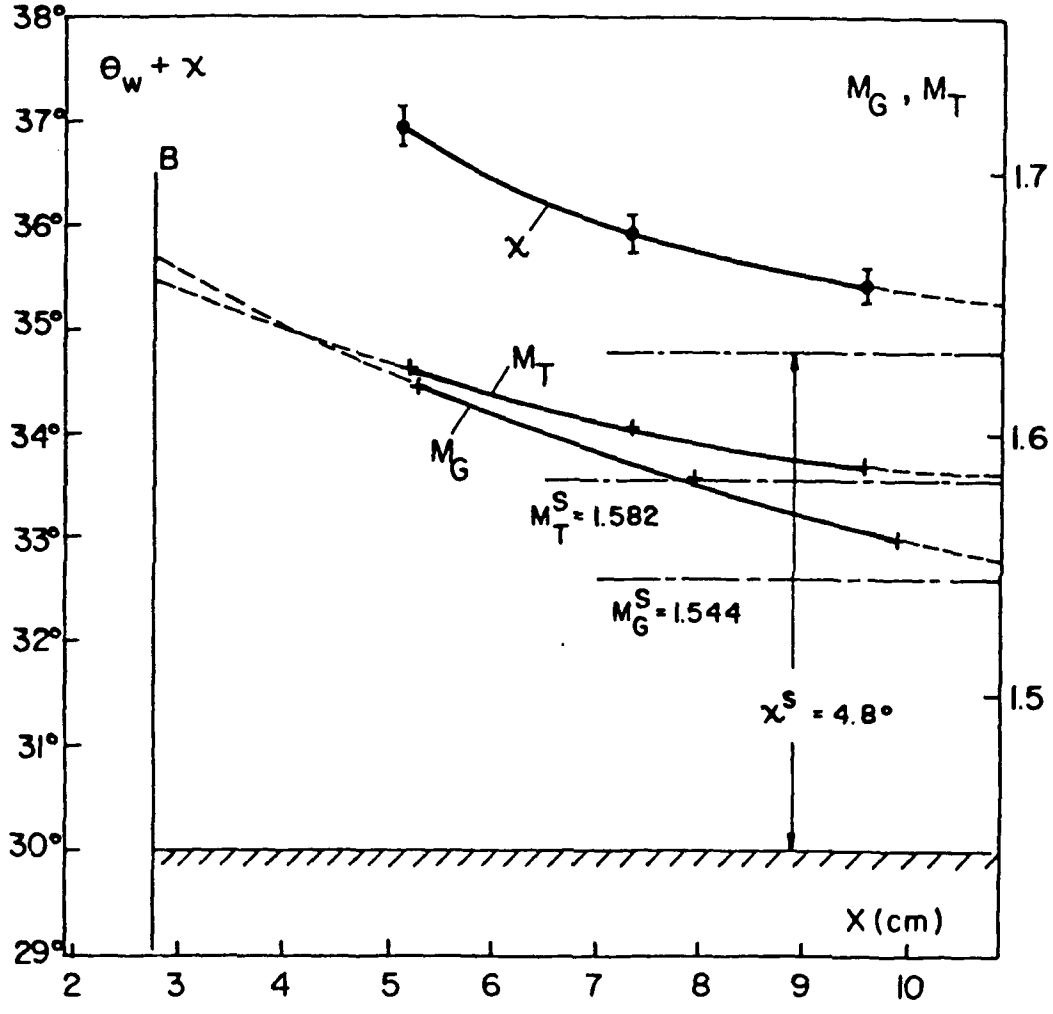

Figure 9: The instantaneous triple point trajectory angle, and Mach numbers of the triple point and the foot of the Mach stem, of the Mach reflection of an incident shock wave with $M_i = 1.3$ over the second surface of a double wedge with $\theta_w^1 = 60°$ and $\theta_w^2 = 30°$ (domain 4 of figure 2).

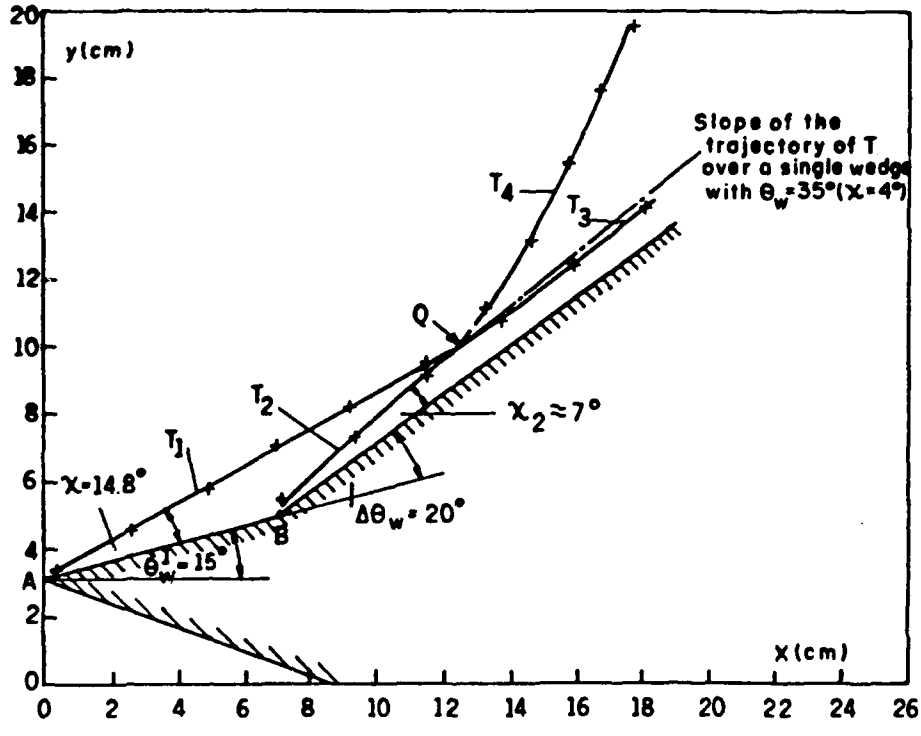

Figure 10: The experimentally recorded trajectories of the four triple points T_1, T_2, T_3 and T_4 shown in figure 5, of the Mach reflection of an incident shock wave with M_i = 1.3 over the second surface of a double wedge with θ_w^1 = 15° and θ_w^2 = 35° (domain 6 of figure 2).

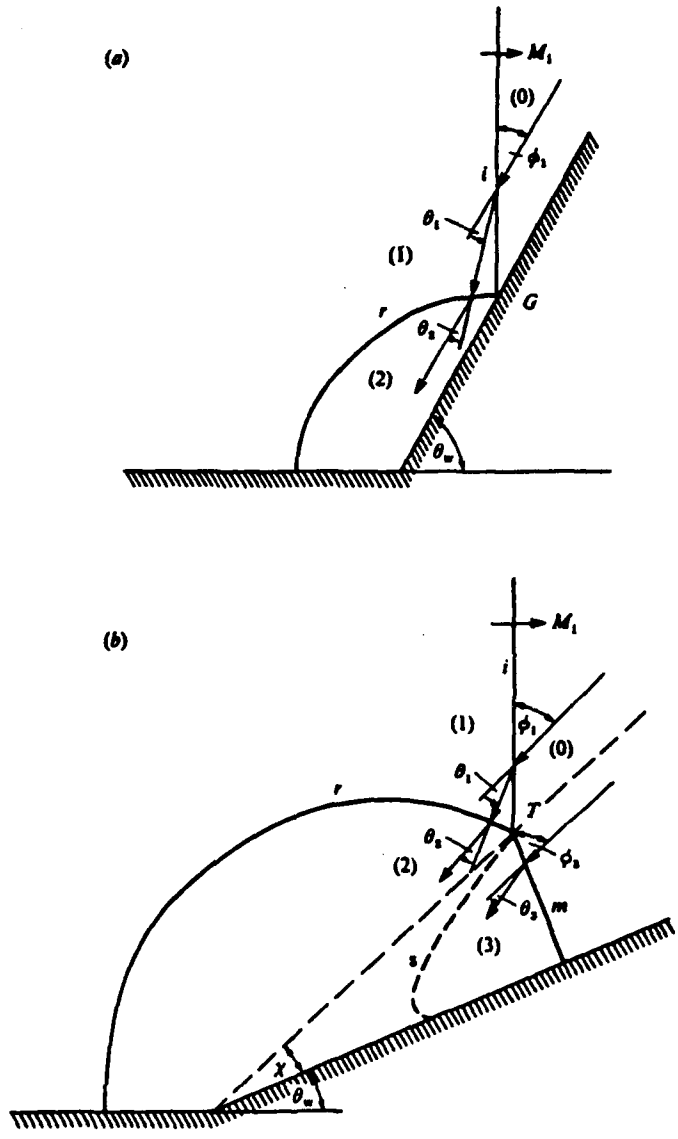

FIGURE 1. Schematic illustration of (*a*) regular reflection, and (*b*) Mach reflection, *i*, incident shock wave; *r*, reflected shock wave; *m*, Mach stem; *s*, slipstream; *G*, reflection point; *T*, triple point; θ_w, reflecting wedge angle; χ, triple point trajectory angle; ϕ, angle of incidence; θ, angle of deflection; (0)–(3), thermodynamic states.

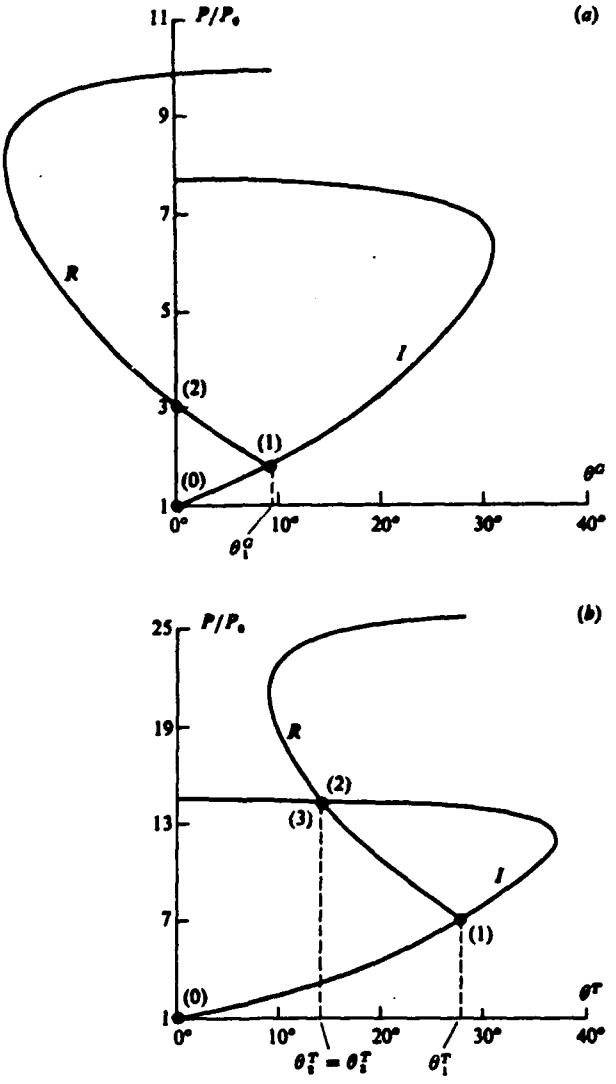

FIGURE 2. (P, θ) shock-polar solutions of (*a*) regular reflection ($M_1 = 1.3, \theta_w = 60°$) and (*b*) Mach reflection ($M_1 = 2.5, \theta_w = 40°, \chi = 5.29°$). The flow states are labelled (0) ahead of the incident shock wave, (1) behind the incident shock wave, (2) behind the reflected shock wave and (3) behind the Mach stem. *R* is the reflected shock polar, and *I* the polar for both the incident and Mach-stem shocks which encounter the same incident flow in a pseudo-steady frame of reference.

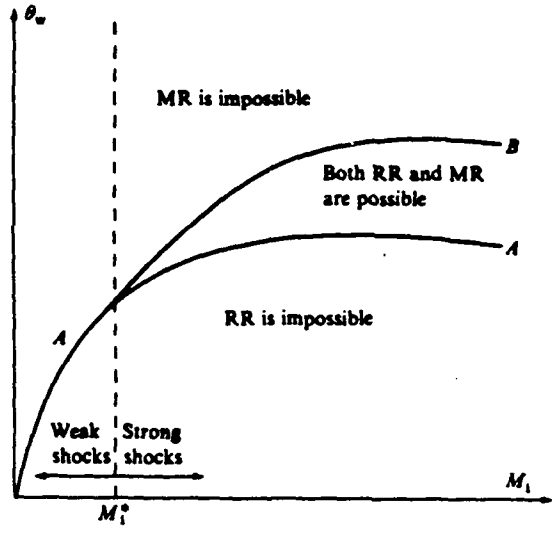

FIGURE 3. Regions of possible types of reflection in the (M_1, θ_w)-plane. M_1 is the incident-shock-wave Mach number, θ_w the reflecting wedge angle, and M_1^* the limiting Mach number separating weak and strong shocks. For $\gamma = \frac{7}{5}$, $M_1^* = 1.4565$.

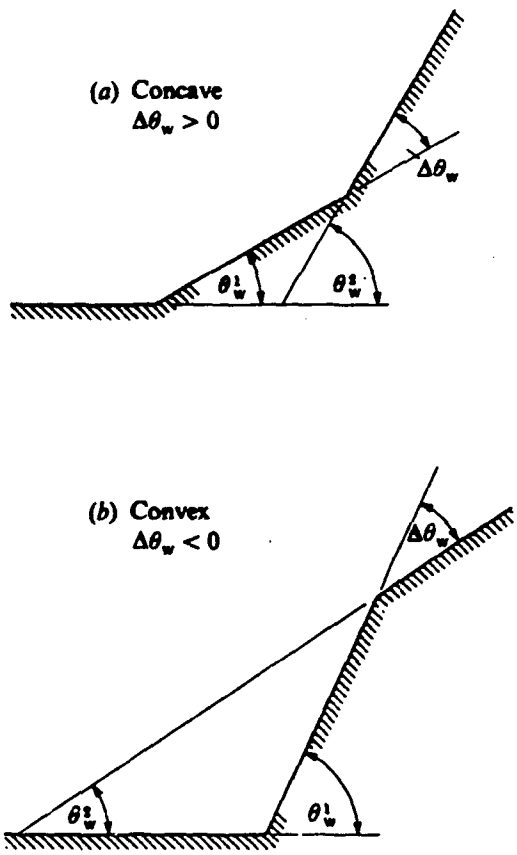

FIGURE 4. Two double wedge configurations, (*a*) concave and (*b*) convex. θ_w^1 is the first wedge angle, $\Delta\theta_w$ the second wedge angle with respect to the first wedge, and θ_w^2 the second wedge angle.

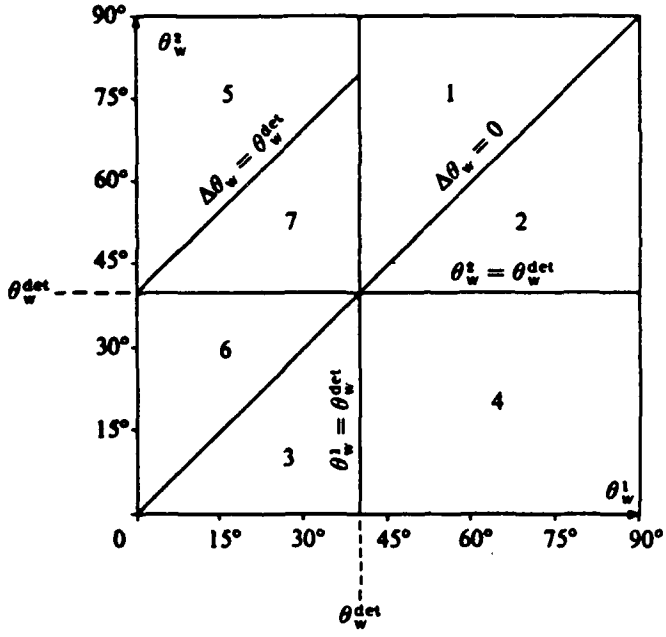

FIGURE 5. The seven regions in the (θ_w^1, θ_w^2)-plane which identify the different reflection processes of a shock wave over a double wedge. θ_w^1 is the first wedge angle, $\Delta\theta_w$ the second wedge angle with respect to the first wedge, θ_w^2 the second wedge angle, and θ_w^{det} the detachment wedge angle corresponding to the incident shock wave Mach number, M_1. The reflection processes in each region are given in table 1.

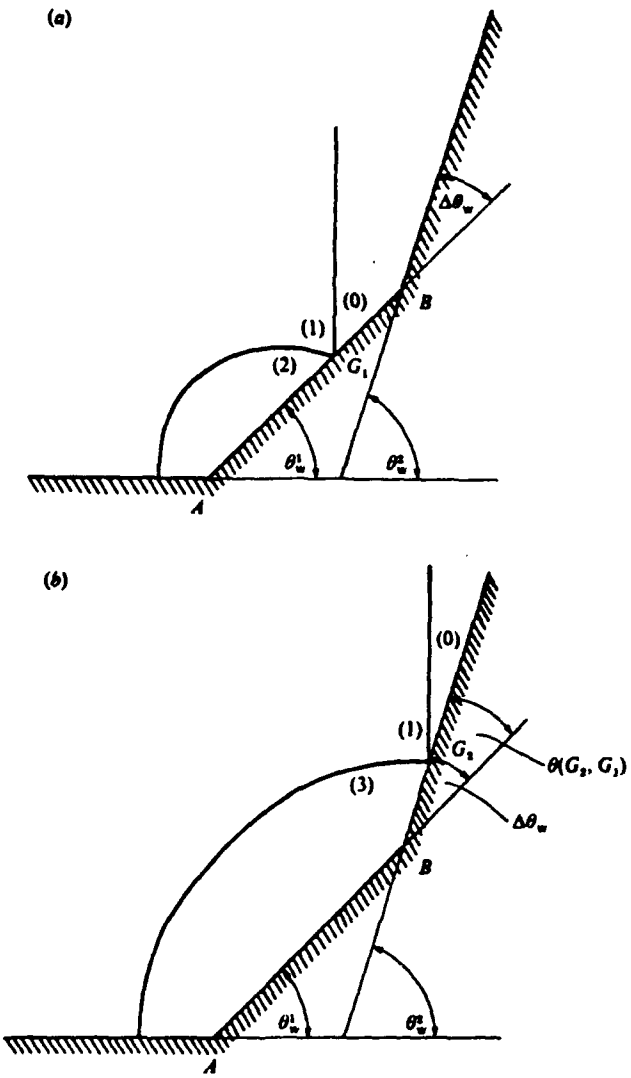

FIGURE 6. Schematic illustration of the shock wave reflections over (*a*) the first and (*b*) the second wedge for region 1 of figure 5.

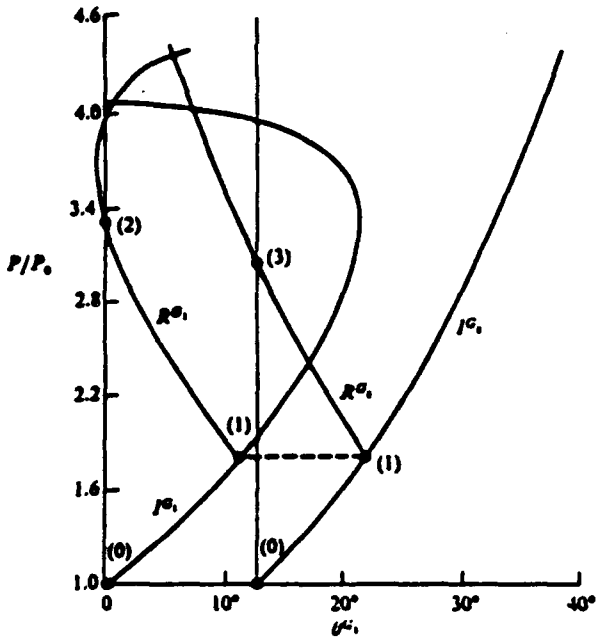

FIGURE 7. The shock-polar solution of the shock-wave reflection process for region 1. The polars are drawn accurately for an incident shock with Mach number $M_i = 1.3$, and a double concave wedge with inclinations $\theta_w^1 = 47°$ and $\theta_w^2 = 60°$. I^{G_1}, R^{G_1} and I^{G_2}, R^{G_2} are the incident and reflected shock polars for the pseudo-steady regular reflections over the first and second wedges, respectively.

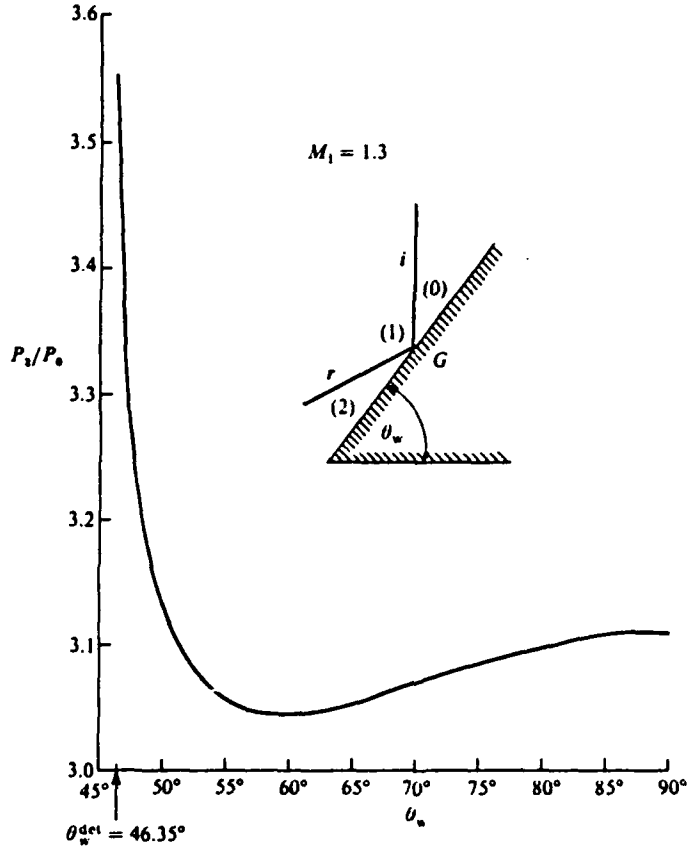

FIGURE 8. The ratio, P_2/P_0, of the pressures behind and ahead of the reflection point of a regular reflection as a function of the reflecting wedge angle, θ_w, for an incident-shock-wave Mach number $M_1 = 1.3$, calculated using two-shock theory.

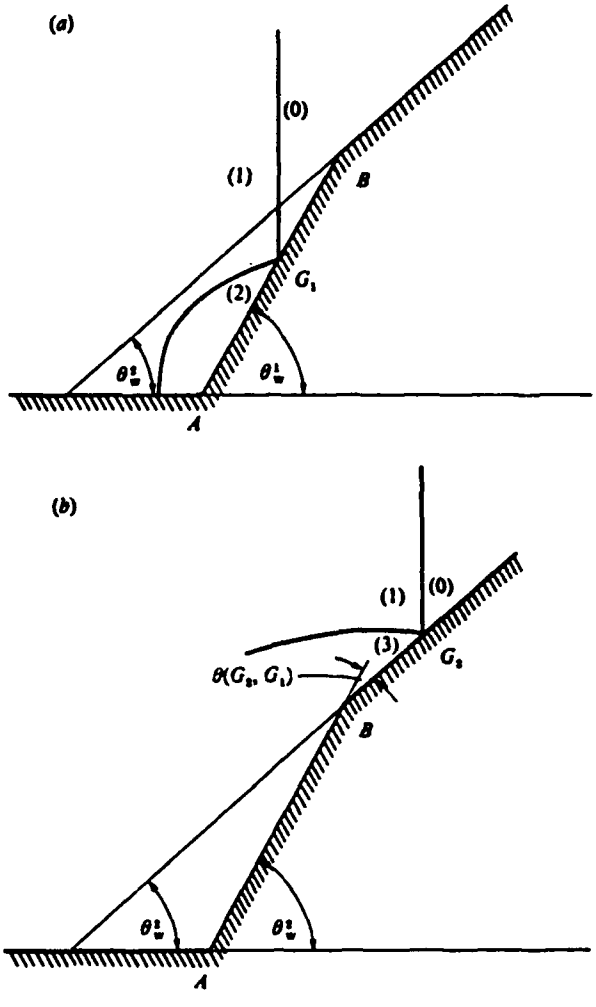

FIGURE 9. Schematic illustration of the shock-wave reflections over (*a*) the first and (*b*) the second wedge for region 2.

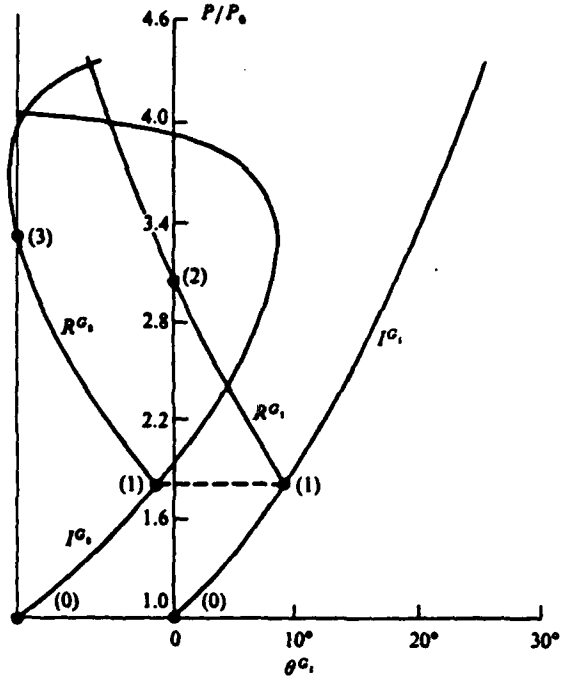

FIGURE 10. The shock-polar solution of the shock-wave reflection process for region 2. The polars are drawn accurately for an incident shock with Mach number $M_1 = 1.3$, and a double convex wedge with inclinations $\theta_w^1 = 60°$ and $\theta_w^2 = 47°$. I^{G_1}, R^{G_1} and I^{G_2}, R^{G_2} are the incident and reflected shock polars for the pseudo-steady regular reflections over the first and second wedges, respectively.

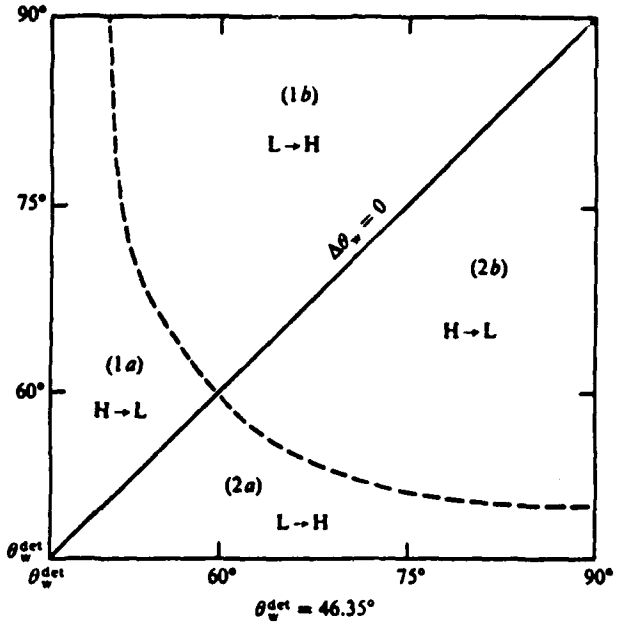

FIGURE 11. Subregions of the different regular to regular reflection processes in regions 1 and 2. In subregions $1a$ and $2b$ there will be a transition from high to low pressure behind the reflected shock (H → L), and in subregions $1b$ and $2a$, a transition from low to high pressure (L → H).

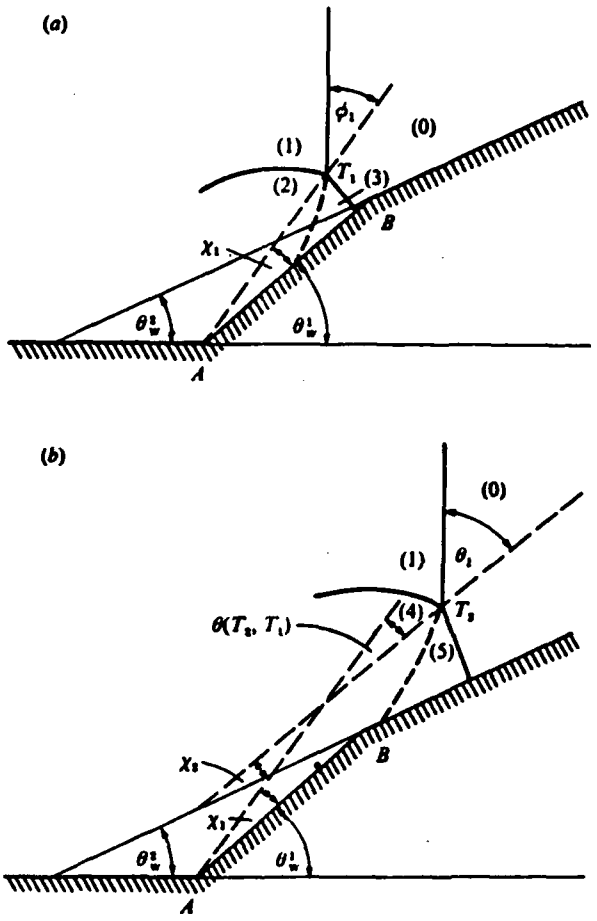

FIGURE 12. Schematic illustration of the shock-wave reflection process for region 3. (*a*) Mach reflection over the first wedge and (*b*) Mach reflection over the second wedge.

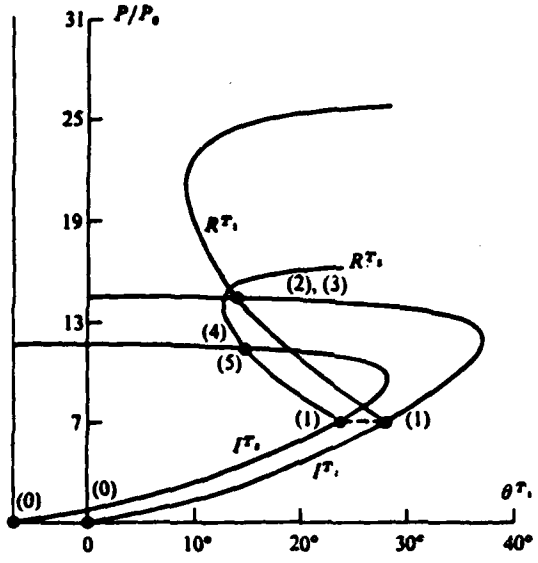

FIGURE 13. The shock-polar solution of the shock-wave reflection process in region 3. The polars are drawn accurately for an incident shock with Mach number $M_1 = 2.5$, and a double convex wedge with inclinations $\theta_w^1 = 60°$ and $\theta_w^2 = 47°$. I^{G_1}, R^{G_1} and I^{G_2}, R^{G_2} are the incident and reflected shock $\chi_2 = 8.27°$. I^{T_1}, R^{T_1} and I^{T_2}, R^{T_2} are the incident and reflected shock polars for the pseudo-steady Mach reflections over the first and second wedges, respectively. The polars are linked by a dashed line representing the constant pressure of state (1) behind the incident shock.

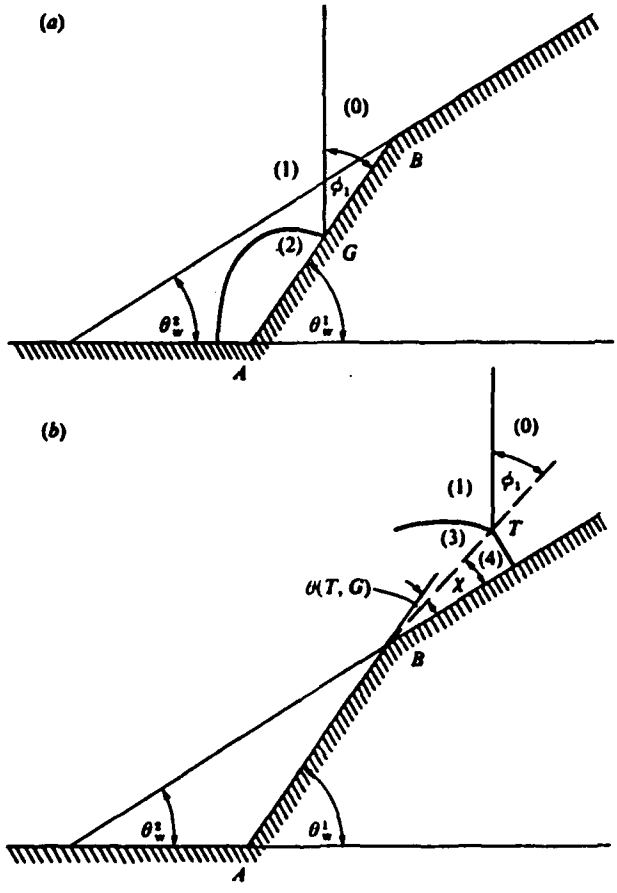

FIGURE 14. Schematic illustration of the shock-wave reflection process for region 4. (*a*) Regular reflection over the first wedge and (*b*) Mach reflection over the second wedge.

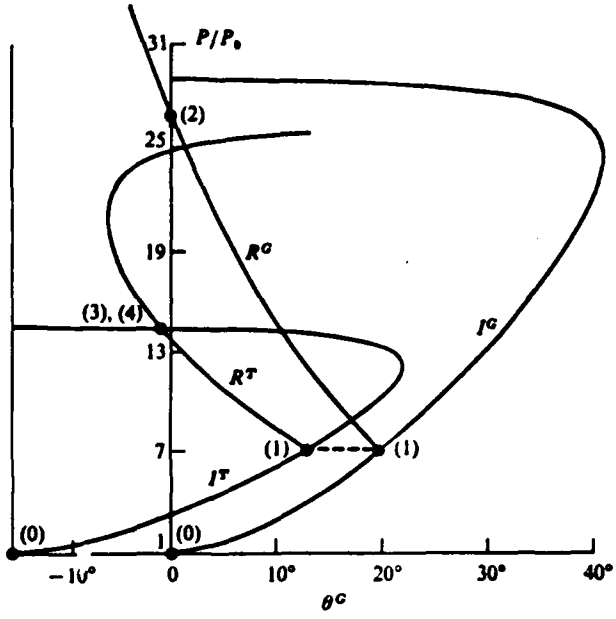

FIGURE 15. The shock-polar solution of the shock-wave reflection process in region 4. The polars are drawn accurately for an incident shock with Mach number $M_1 = 2.5$, and a double convex wedge with inclinations $\theta_w^1 = 60°$ and $\theta_w^2 = 40°$. The triple-point trajectory angle over the second wedge is $\chi = 5.29°$. I^G, R^G and I^T, R^T are the incident and reflected shock polars for pseudo-steady regular and Mach reflections respectively over the first and second wedges.

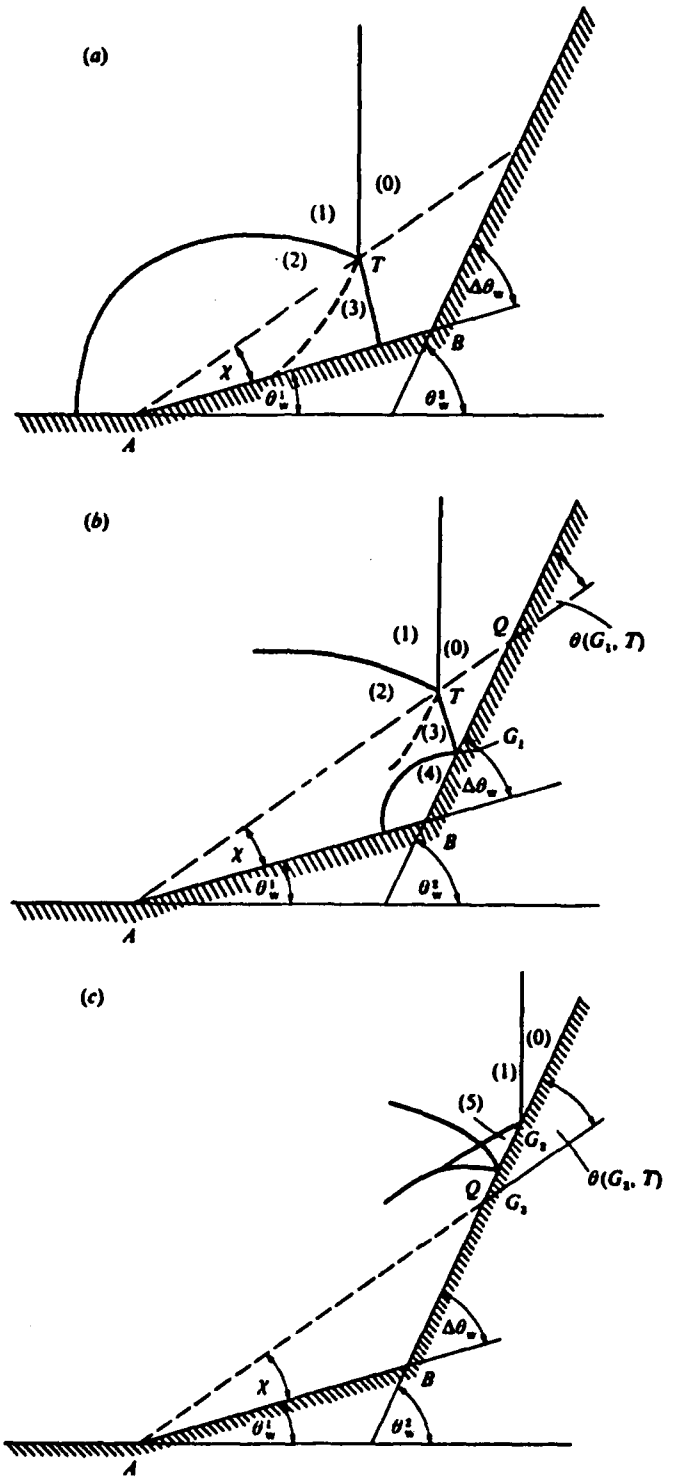

FIGURE 16. Schematic illustration of the shock-wave reflection process for region 5. Q is the intersection of the triple-point trajectory with the second wedge. (*a*) Mach reflection over the first wedge, (*b*) regular reflection over the second wedge and (*c*) the shock configurations after the incident shock has passed Q.

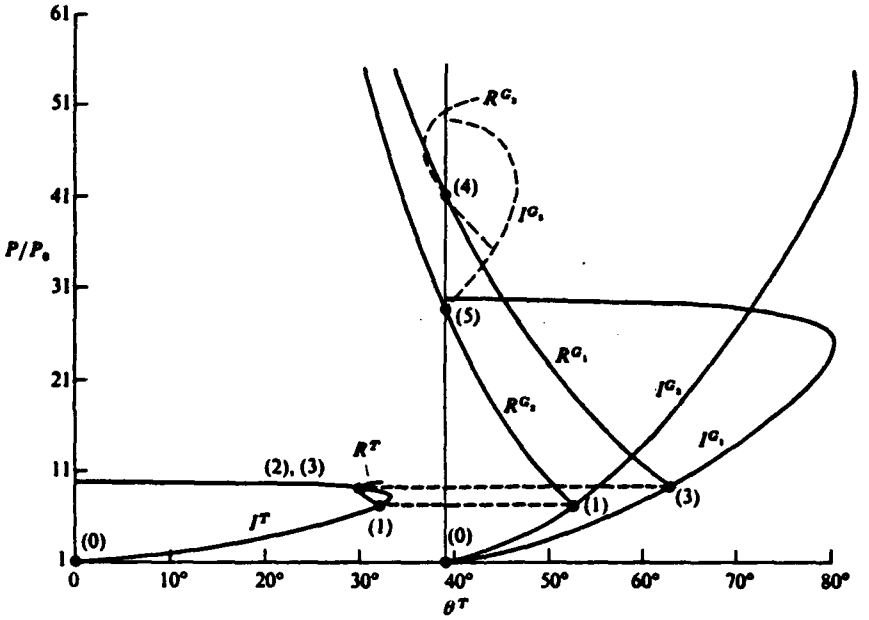

FIGURE 17. The shock-polar solution of the shock-wave reflection process in region 5. The polars are drawn acurately for an incident shock with Mach number $M_1 = 2.5$, and a double concave wedge with inclinations $\theta_w^1 = 15°$ and $\theta_w^2 = 70°$. The triple-point trajectory angle is $\chi = 15.72°$, and the Mach number of the Mach stem shock is $M_m = 2.8$. I^T and R^T are the incident and reflected shock polars for the pseudo-steady Mach reflection over the first wedge. I^{G_1}, R^{G_1} and I^{G_2}, R^{G_2} are the incident and reflected shock polars of the pseudo-steady regular reflections over the second wedge, before and after the intersection of the triple-point trajectory with the second wedge, respectively. The dashed I^{G_2}, R^{G_2} polars indicate the probable solution for the regular reflection which permits the pressure jump from state (4) to state (5) in figure 16. The polars are linked by the dashed lines representing the constant pressure in states (3) and (1) of figure 16.

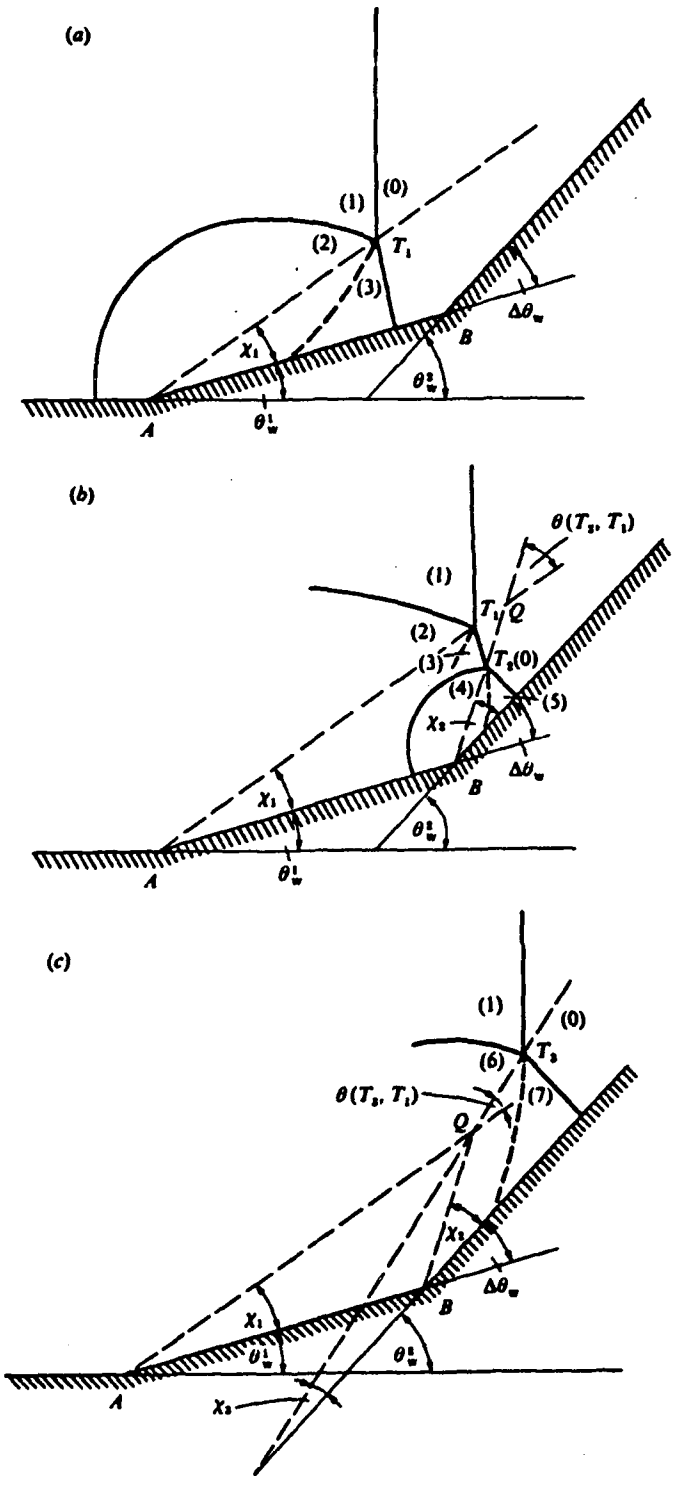

FIGURE 18. Schematic illustration of the shock-wave reflection process for region 6. (*a*) Mach reflection over the first wedge, (*b*) Mach reflection over the second wedge and (*c*) Mach reflection over the second wedge after the incident shock has passed Q, the point of intersection of the two triple-point trajectories.

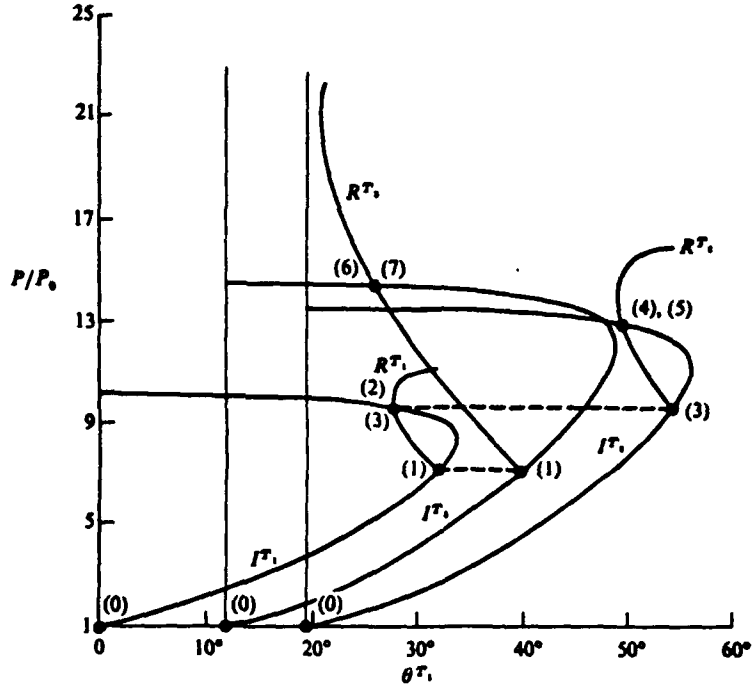

FIGURE 19. The shock-polar solution of the shock-wave reflection process in region 6. The polars are drawn accurately for an incident shock with Mach number $M_1 = 2.5$, and for a double concave wedge with inclinations $\theta_w^1 = 20°$ and $\theta_w^2 = 40°$. The Mach number of the Mach-stem shock over the first wedge is $M_m = 2.9$, and the triple-point trajectory angles are $\chi_1 = 12.85°$, $\chi_2 = 12.49°$ and $\chi_3 = 5.29°$. I^{T_1} and R^{T_1} are the incident and reflected shock polars of the pseudo-steady Mach reflection over the first wedge. I^{T_2}, R^{T_2} and I^{T_3}, R^{T_3} are the incident and reflected shock polars of the pseudo-steady Mach reflections over the second wedge, before and after the intersection of the triple-point trajectories, respectively. The polars are linked by the dashed lines representing the constant pressures in states (3) and (1) of figure 18.

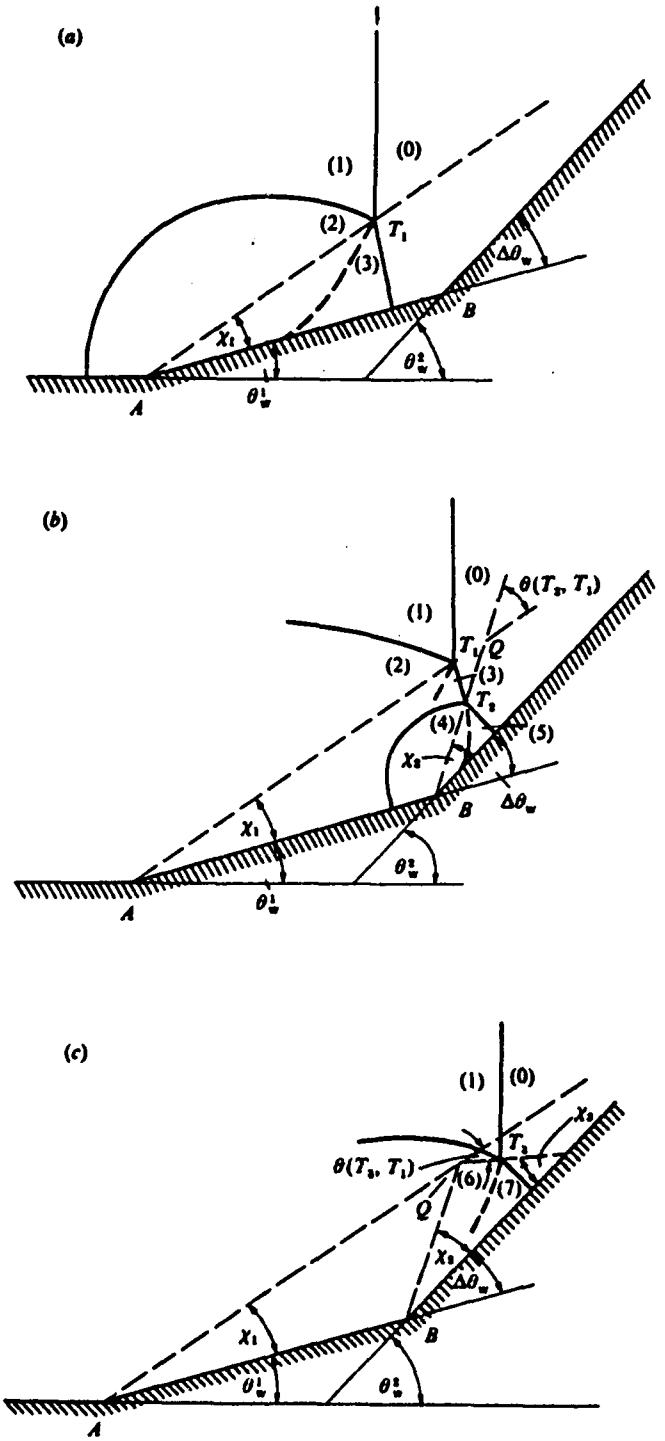

FIGURE 20(a–c). For caption see facing page.

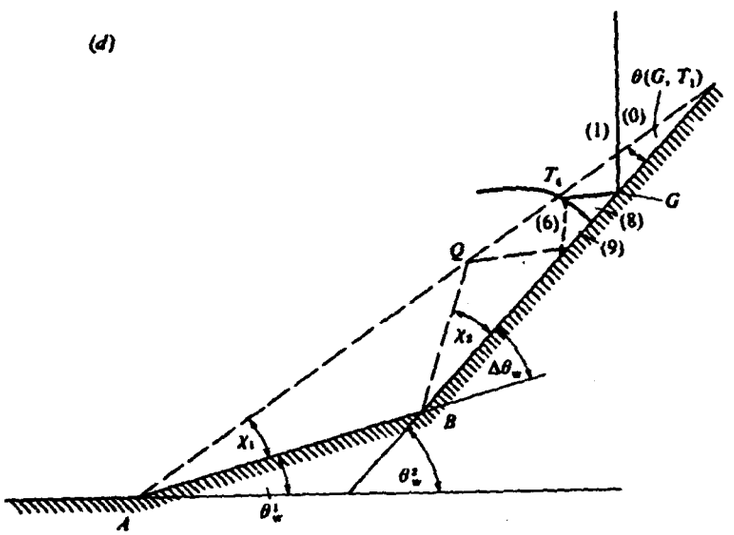

FIGURE 20. Schematic illustration of the shock-wave reflection process for region 7. (*a*) Mach reflection over the first wedge. (*b*) Mach reflection over the second wedge. Q is the intersection of the triple-point trajectories. (*c*) Inverse-Mach reflection over the second wedge after the incident shock has passed Q. (*d*) Regular reflection over the second wedge after the third triple point T_3 has reached the wedge surface.

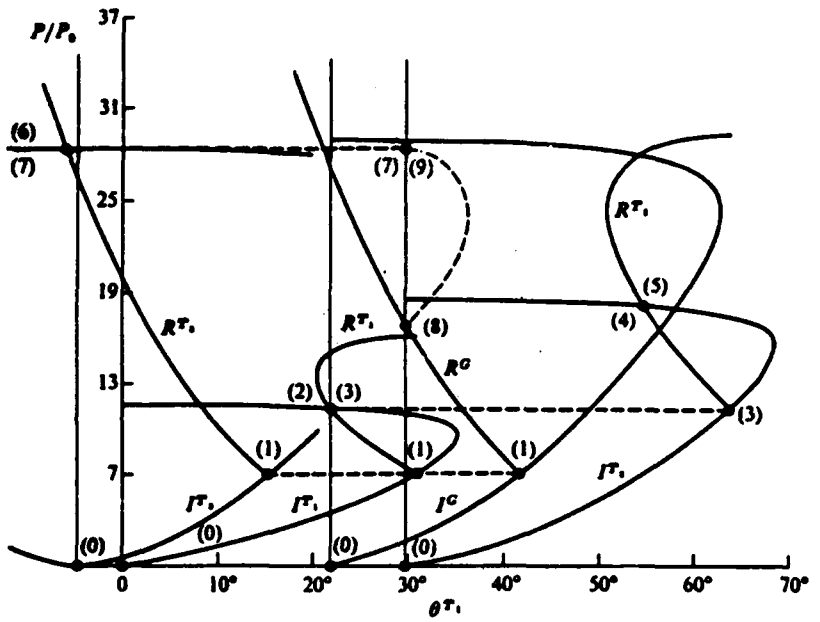

FIGURE 21. The shock-polar solution of the shock-wave reflection process in region 7. The polars are drawn accurately for an incident shock with Mach numbers $M_1 = 2.5$, and a concave double wedge with inclinations $\theta_w^1 = 30°$, and $\theta_w^2 = 60°$. The Mach number of the Mach-stem shock over the first wedge is $M_m = 3.15$, and the triple-point trajectory angles are $\chi_1 = 8.27$, $\chi_2 = 8.09°$ and $\chi_3 = -1.12°$. I^{T_1} and R^{T_1} are the shock polars for the pseudo-stationary Mach reflection over the first wedge. I^{T_2}, R^{T_2} and I^{T_3}, R^{T_3} are the shock polars for the pseudo-steady Mach reflections over the second wedge, before (direct-Mach) and after (inverse-Mach) the intersection of the triple-point trajectories, respectively. I^G and R^G are the shock polars for the ultimate pseudo-steady regular reflection over the second wedge. The dashed polar represents the probable solution for the normal shock which permits the pressure jump from state (8) to (9) in figure 20(*d*). The polars are linked by the dashed lines representing the constant pressures in states (1), (3) and (7) of figure 20.

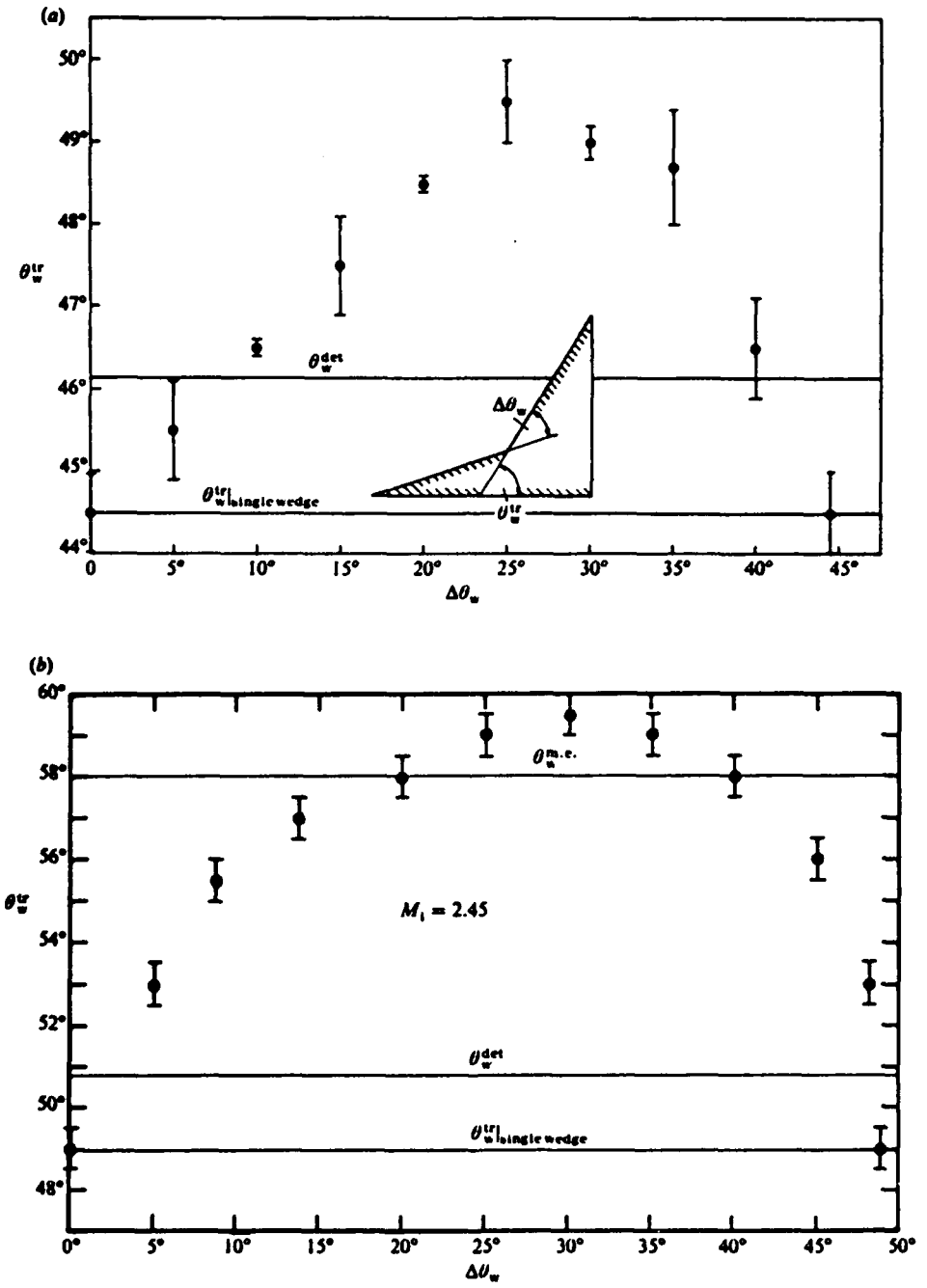

FIGURE 22. The angle of the second wedge at which transition from regular to Mach reflection was observed, θ_w^{tr}, as a function of $\Delta\theta_w$ for a concave double wedge: (*a*) weak shock wave $M_1 = 1.29 \pm 0.01$. (*b*) strong shock wave $M_1 = 2.45 \pm 0.01$.

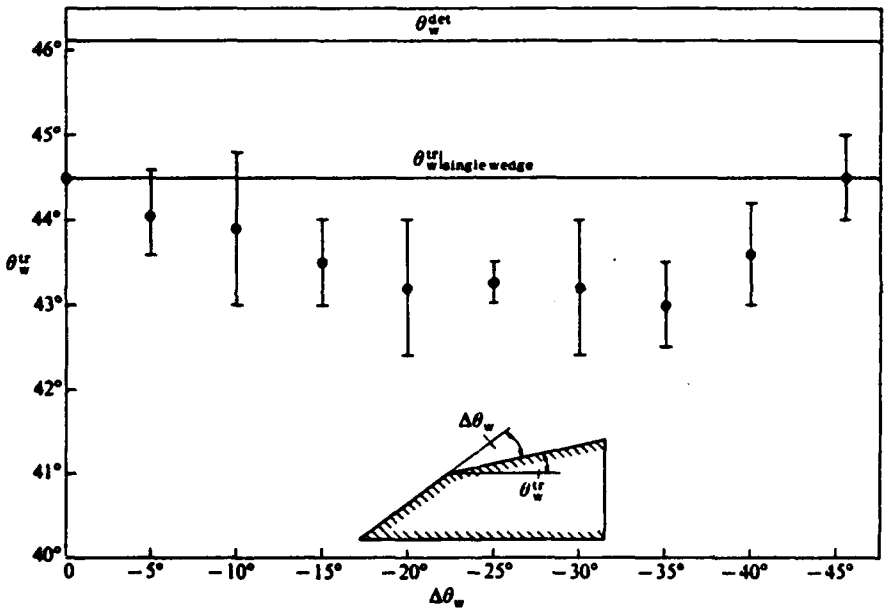

FIGURE 23. The angle of the second wedge at which transition from regular to Mach reflection was observed, θ_w^{tr}, as a function of $\Delta\theta_w$ for a convex double wedge and $M_1 = 1.29 \pm 0.01$.

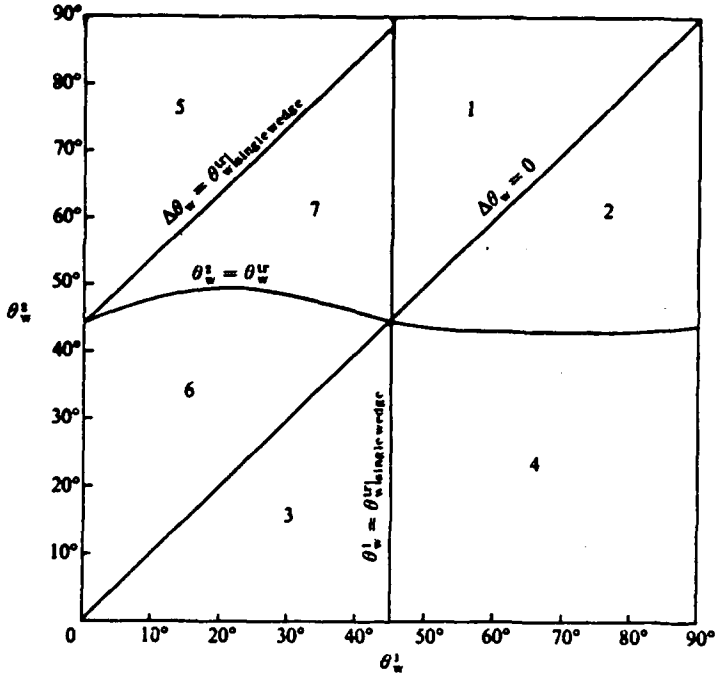

FIGURE 24. Actual regions and transition boundaries of the seven different reflection processes for an incident shock wave with $M_1 = 1.29 \pm 0.01$ over a double wedge.

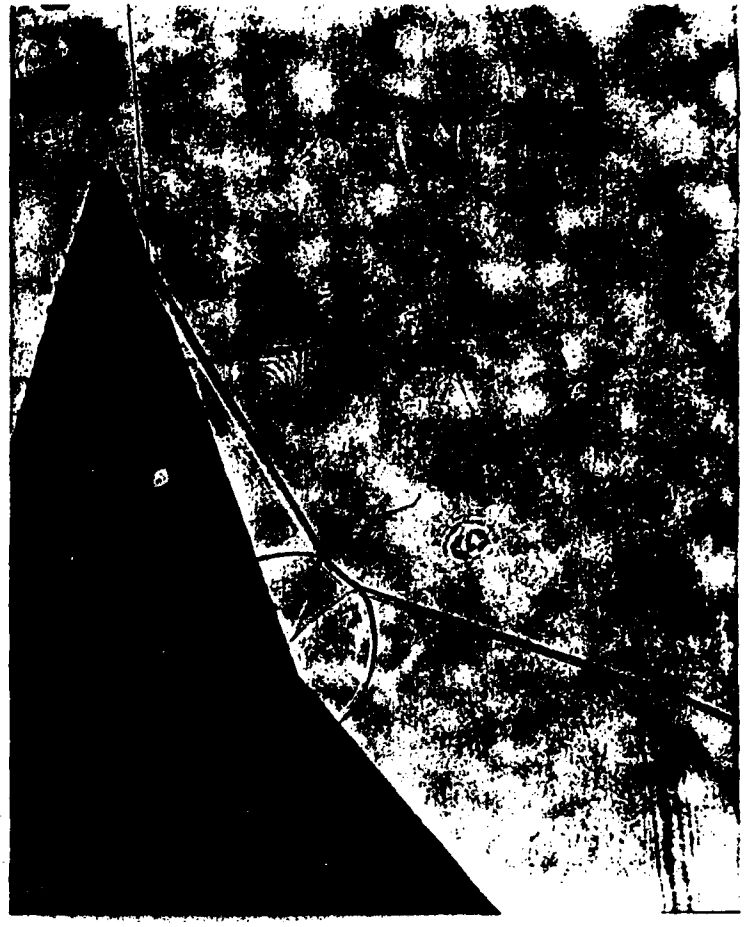

FIGURE 25. Shadowgraph illustrating the reflection on the second wedge, following a regular reflection on the first wedge for a double wedge in region I, $\theta_w^1 = 55°$ and $\theta_w^2 = 75°$.

FIGURE 26. Schlieren photograph illustrating the reflection on the second wedge following a regular reflection on the first wedge for a double wedge in region 2. $\theta_w^1 = 65°$ and $\theta_w^2 = 50°$. Details of the wave structure behind the second regular reflection can be seen.

FIGURE 27. Schlieren photograph illustrating the Mach reflection on the second wedge following a Mach reflection on the first wedge for a double wedge in region 3. $\theta_w^1 = 35°$ and $\theta_w^2 = 15°$. The effects of the expansion wave generated when the Mach reflection moves from the first to the second wedge can be seen.

FIGURE 28. Shadowgraph of the Mach reflection on the second wedge, following a regular reflection on the first wedge for a double wedge in region 4: $\theta_w^1 = 60°$ and $\theta_w^2 = 30°$.

FIGURE 29(*a*,*b*). For caption see facing page.

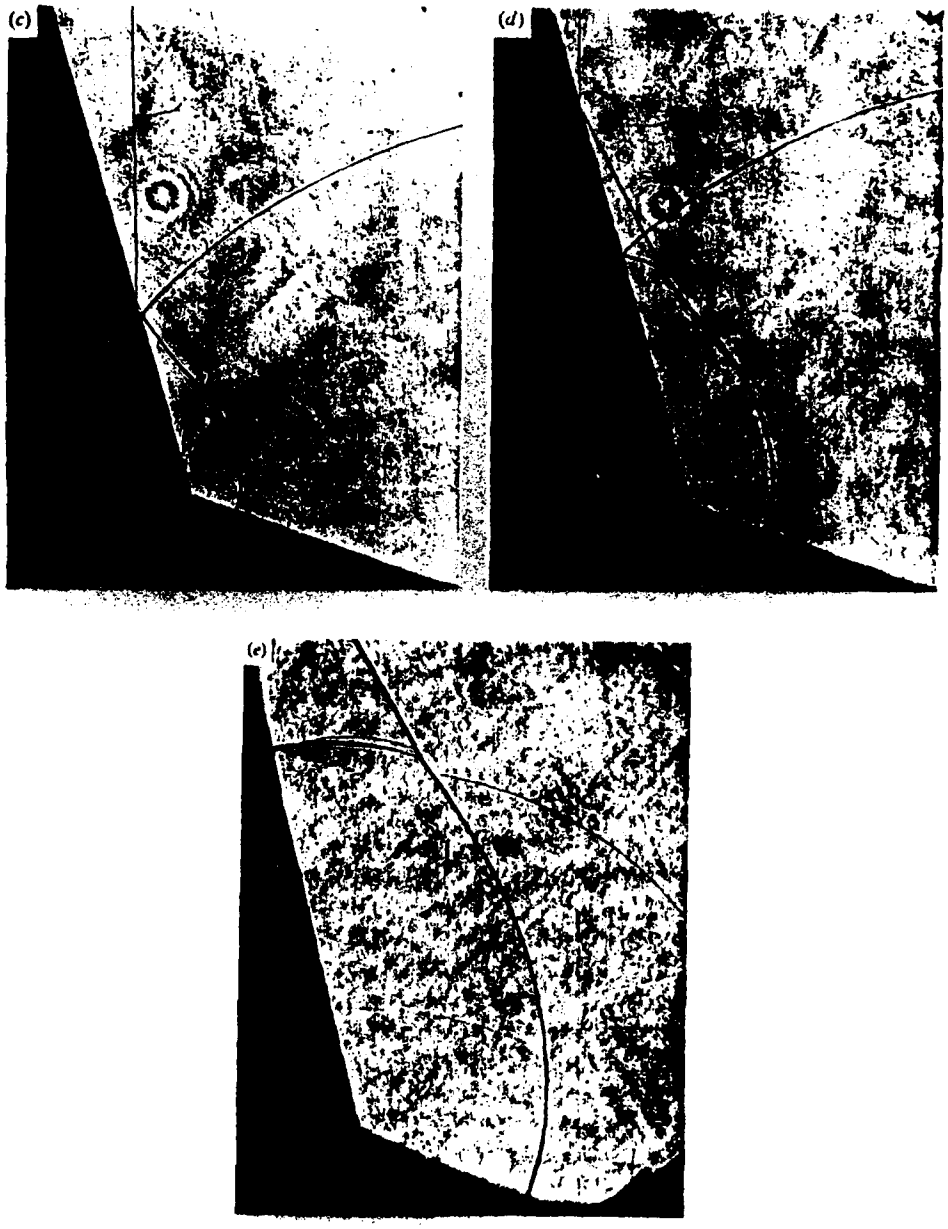

FIGURE 29. Shadowgraphs illustrating the reflection process over a double wedge in region 5. $\theta_w^1 = 20°$ and $\theta_w^2 = 75°$. (*a*) Mach reflection over the first surface. (*b*) The reflection of the Mach stem as a regular reflection from the second surface. (*c*) The wave structure immediately after the interaction between the triple point of the Mach reflection and the reflection point of the regular reflection. (*d*) The final regular reflection over the second surface followed by a regular reflection of the reflected shock of the Mach reflection which was terminated earlier. (*e*) The degeneration of the secondary regular reflection into a normal shock wave.

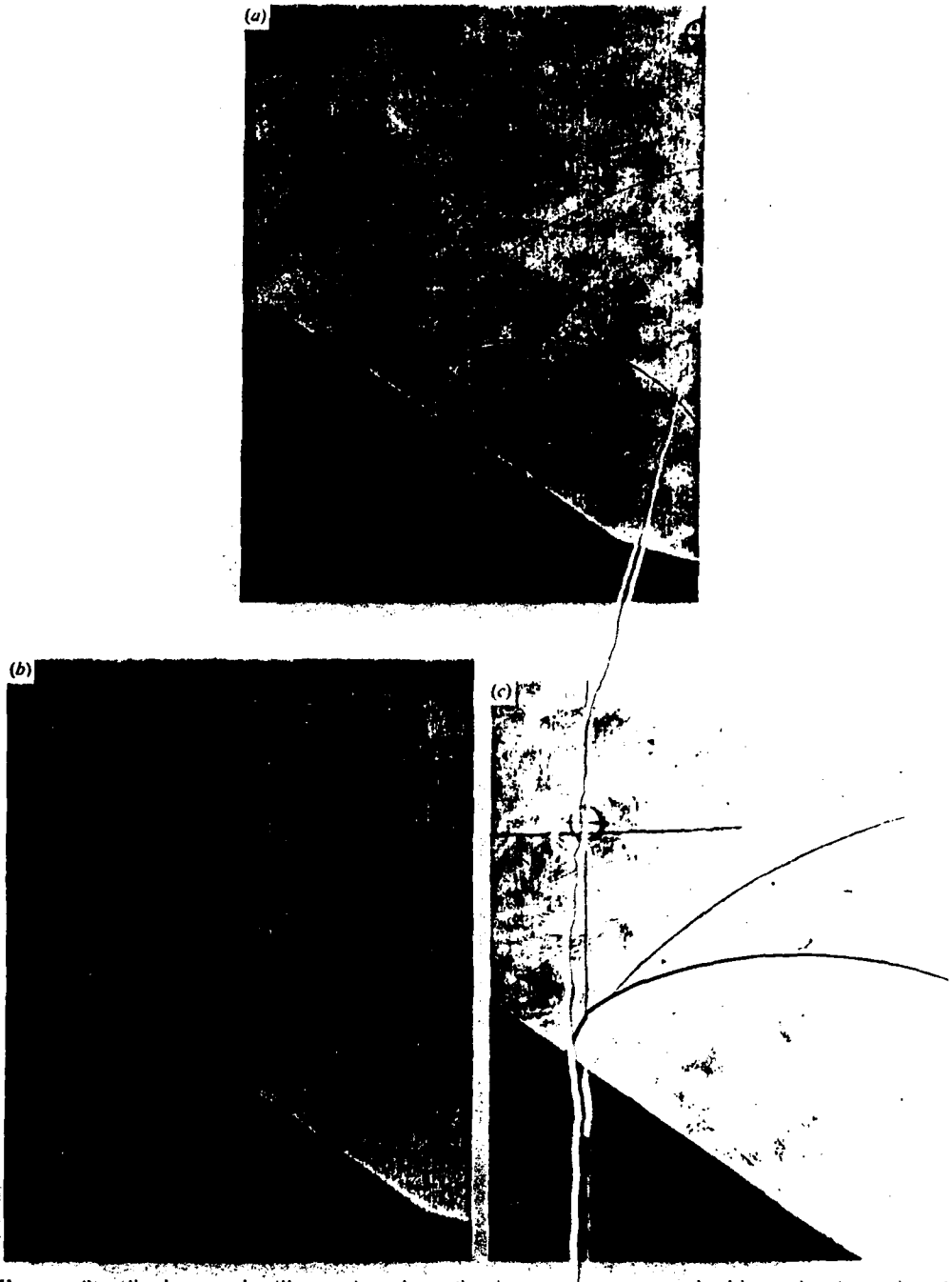

FIGURE 30. Shadowgraphs illustrating the reflection process over a double wedge in region 6. $\theta_w^1 = 15°$ and $\theta_w^2 = 35°$. (*a*) The reflection of the Mach stem from the first wedge over the second surface as a Mach reflection. (*b*) The interaction of the two triple points. (*c*) The final Mach reflection over the second wedge surface.

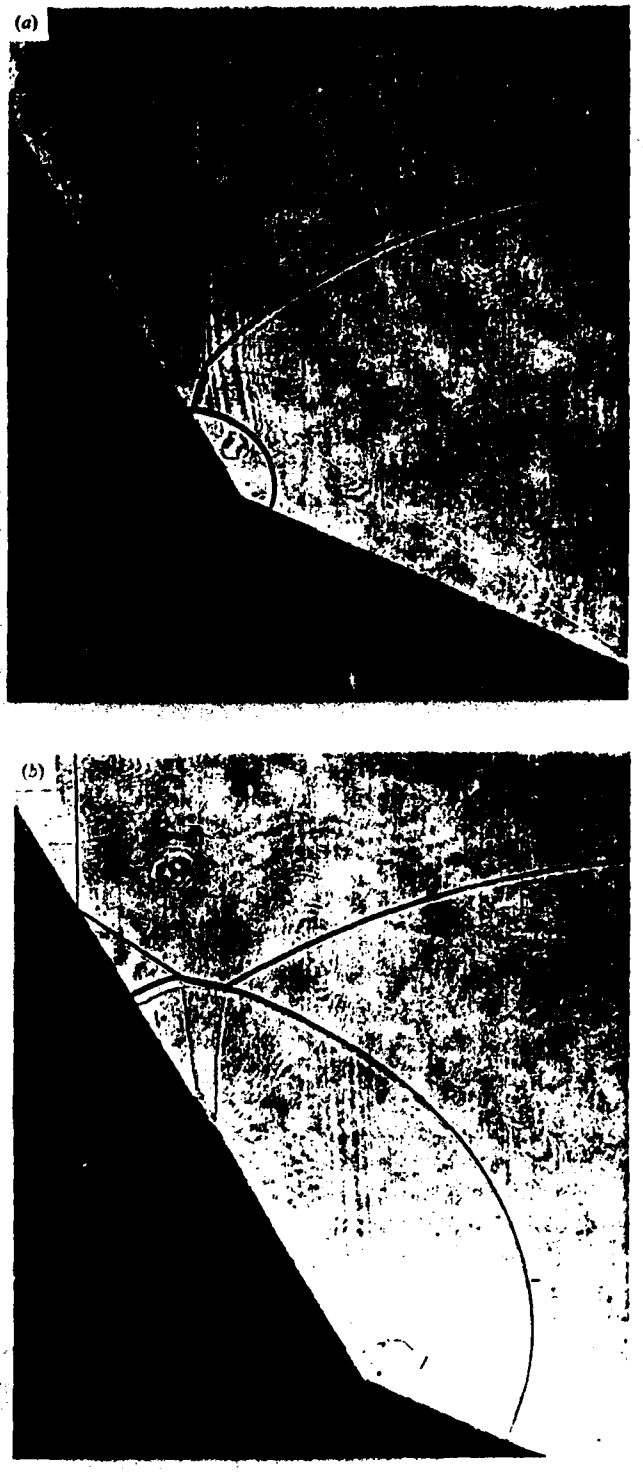

FIGURE 31. Shadowgraphs illustrating the reflection process over a double wedge in region 7. $\theta_w^1 = 25°$ and $\theta_w^2 = 60°$. (*a*) The reflection of the Mach stem from the first wedge over the second surface as a Mach reflection. (*b*) The final reflection over the second surface followed by a normal shock wave.

Part 2

The Wave Configuration Approached Asymptotically Following a Reflection of a Plane Shock Wave Over a Double Wedge

Experimental Investigation

INTRODUCTION

When a planar shock wave encounters a sharp compressive corner, such as the leading edge of a wedge, two different types of reflection may occur: regular reflection RR (figure 1a) or Mach reflection MR (figure 1b). Regular reflection consists of two shock waves, the incident shock i and the reflected shock r, which coincide on the wedge at the reflection point G. Mach reflection consists of four discontinuities, the incident shock i, the reflected shock r, the Mach stem m and the slipstream s, which coincide at the triple point T. Over a plane wedge the triple point moves along a straight line making an angle χ with the wedge surface. The Mach stem is usually curved.

For a given gas, the type of reflection which will occur depends on the strength of the incident shock, defined by the Mach number M_1, and on the wedge angle θ_w.

If a frame of reference is attached to the reflection point of a regular reflection or the triple point of a Mach reflection, then the nonstationary regular or Mach reflection becomes pseudo-steady (Jones, Martin & Thornhill 1951), and the shock waves i, r and m can be treated using steady flow theory. By considering these shock waves separately and using oblique shock wave relations with appropriate boundary conditions the equations of motion for regular and Mach reflection can be derived (Ben-Dor, 1978).

In the case of an inviscid regular reflection (figure 1a) when the frame of reference is attached to the reflection point, the flow in state (0) moves

towards the reflection in a direction parallel to the wedge surface and at an angle of incidence ϕ_1 to the incident shock. On passing through the incident shock wave the flow is deflected towards the wedge surface by an angle θ_1. The flow then passes through the reflected shock wave which deflects it back by an angle θ_2 to become again parallel to the wedge surface. Therefore, the boundary condition for a regular reflection is:

$$\theta_1 - \theta_2 = 0 \tag{1}$$

Thus the flow directions in states (0), (1) and (2) with respect to the trajectory of the reflection point, G, are:

$$\theta_0^G = 0,\ \theta_1^G = \theta_1, \text{ and } \theta_2^G = \theta_1 - \theta_2 = 0, \tag{2}$$

respectively, where superscript G designates that θ is measured with respect to the direction defined by the trajectory of G.

In the case of Mach reflection (figure 1b) when the frame of reference is attached to the triple point T, the flow in state (0) moves towards the reflection in a direction parallel to the triple point trajectory. The flow above the triple point trajectory approaches the incident shock wave at an angle of incidence ϕ_1. On passing through the incident shock the flow is deflected towards the wedge by an angle θ_1. It then passes through the reflected shock which deflects it back by an angle θ_2, parallel to the slipstream. Below the triple point trajectory the flow approaches the Mach stem at an angle of incidence ϕ_3, and is deflected towards the wedge by an angle θ_3, also parallel to the slipstream. Since the flows in states (2) and (3) are parallel and separated by a slipstream across which there is no change of static pressure, the boundary conditions for the Mach reflection are:

$$\theta_1 - \theta_2 = \theta_3, \text{ and } P_2 = P_3, \tag{3}$$

where P is the static pressure. Thus the flow directions in states (0), (1), (2), and (3) with respect to the trajectory of the triple point, T, are:

$$\theta_0^T = 0;\ \theta_1^T = \theta_1; \tag{4}$$
$$\theta_2^T = \theta_1 - \theta_2, \text{ and } \theta_3^T = \theta_3.$$

Equations (3) and (4) give;

$$\theta_2^T = \theta_3^T. \tag{5}$$

Kawamura & Saito (1956) suggested that, since the boundary conditions (1) and (3) are in terms of the flow deflection angles, θ, and pressures, P, the relationship between P and θ may be of importance in understanding shock reflection phenomena. The graphical representation of the relationship between the pressure ratio, P/P_0, across an oblique shock and the angle, θ, through which the flow is deflected by the shock for a fixed value of the Mach number of the incident flow, M_0, is called a pressure-deflection shock polar.

Figure 2a represents the (P, θ) polar solution of a regular reflection. All the flow deflection angles, θ^G, are measured with respect to the trajectory of the reflection point G (see figure 1a). State (0) is represented by the origin, where $P = P_0$ and $\theta_0^G = 0$. The locus of all the flow states which can be obtained from state (0) by passing through any oblique shock wave is represented by the I polar. Consequently, state (1) of a regular reflection is represented on the I polar by the point $P = P_1$ and $\theta^G = \theta_1^G$. The R polar is the locus of all the flow states which can be obtained from state (1) by passing through any oblique shock. Consequently, state (2) which is obtained from state (1) by passing through the reflected shock wave is on the R polar. The boundary condition (2) implies that $\theta_2^G = 0$, therefore, state (2) is represented by the point where the R polar intersects the P axis (i.e. $\theta^G = 0$) as illustrated in figure 2a.

Figure 2b represents the (P, θ) polar solution of a Mach reflection. All the deflection angles are measured with respect to the trajectory of the triple point (see figure 1b). Again, state (1) behind the incident shock lies on the I polar and is the origin of the R polar, and state (2), behind the reflected shock lies on the R polar. State (3) behind the Mach stem also lies on the I polar. Since the pressures and the flow directions with respect to the triple point trajectory in states (2) and (3) are equal, states (2) and (3) are represented by the intersection of the I and R polars.

Figure 3 illustrates the regions in the (M_1, θ_w) plane in which the different types of reflection are possible or impossible. The regions are separated by curves A and B. Curve A describes the "detachment" criterion of von Neumann (1963), and curve B the "mechanical equilibrium" criterion of Henderson & Lozzi (1975). Hornung, Oertel and Sandeman (1979) used a "corner signal" concept to show that transition from regular to Mach reflection is best defined by the "sonic" criterion, namely the condition when the signal speed behind the reflected shock equals that of the reflection point. The "sonic" criterion is very close to the detachment criterion, particularly for strong shocks.

For a given gas (i.e., value of the specific heat ratio, γ) there is a certain value of incident shock Mach number, M_1^*, below which the "mechanical equilibrium" criterion does not exist. Henderson & Woolmington (1983) have shown that for a diatomic gas, $\gamma = 7/5$, $M_1^* = 1.4565$ and for a monatomic gas, $\gamma = 5/3$, $M_1^* = 1.5487$. Incident shock waves with Mach numbers in the range $M_1 < M_1^*$ are called weak shocks and those in the range $M_1 > M_1^*$ are called strong shocks. Figure 3 indicates that for weak shocks there is one region in which regular

reflection is theoretically impossible ($\theta_w < \theta_w^{det}$) and another region in which Mach reflection is theoretically impossible ($\theta_w > \theta_w^{det}$). The regions are separated by the detachment transition line $\theta_w = \theta_w^{det}$. However, for the strong shocks there is a region, $\theta_w < \theta_w^{det}$, in which regular reflection is theoretically impossible; a region , $\theta_w > \theta_w^{m.e.}$, in which Mach reflection is theoretically impossible, and an additional region, $\theta_w^{det} < \theta_w < \theta_w^{m.e.}$, in which both regular and Mach reflection are theoretically possible. Dewey and McMillin (1985) have shown that the assumption of pseudo-stationarity may not be valid for weak Mach reflections and that realistic shock polars cannot be drawn for this region.

In the case of truly unsteady flows, i.e., flows which cannot be made pseudo-steady by a simple co-ordinate transformation, the wedge angle at which transition from regular to Mach reflection occurs depends on the geometry of the process itself. For example, the MR→RR transition over concave cylinders occurs at wedge angles greater than those predicted by the "mechanical equilibrium" transition line, and the RR→MR transition over convex cylinders occurs at wedge angles smaller than those predicted by the "detachment" transition line. For both cases the transition angle also depends on the initial angle of incidence and the radius of curvature of the cylindrical wedges. Details of these reflection phenomena are described by Heilig (1969), Ben-Dor, Takayama & Kawauchi (1980), Itoh, Okazaki & Itaya (1981) and Dewey, Walker, Lock & Scotten (1983). To the best of our knowledge, no shock wave phenomenon has been recorded yet, in which the RR$\overset{\rightarrow}{\leftarrow}$MR transition occurs at wedge angles in the range $\theta_w^{det} < \theta_w^{tr} < \theta_w^{m.e.}$.

A suggested approach to the study of shock wave reflections from concave and convex cylindrical surfaces is a consideration of the reflection from a double

wedge with a single increase or decrease of the wedge angle. In the present paper, seven different shock configurations resulting from the reflection of a planar shock wave over a concave or a convex double wedge are identified and investigated analytically and experimentally.

A study of the reflection process over three of the seven possible double wedge combinations was conducted by Ginzburg & Markov (1975). However, it will be shown that some of the schematic drawings in their paper, illustrating the wave configurations, are incorrect. This is probably due to the poor resolution of their photographic method. Some of their schematic drawings show confluence points of four shocks, which are known to be theoretically impossible (Courant & Friedrichs, 1948), and others fail to observe the details of the waves structure.

Two of the possible Mach configurations over a concave double wedge have been studied by Matsuo et al (1985) and their observations appear to be in agreement with the results presented here.

Analysis

The analysis presented below establishes all the reflection processes and final shock configurations that are possible over any double plane wedge combination. A compressive and an expansive double wedge are illustrated in figures 4(a) and 4(b), respectively. The slopes of the first and second wedges are θ_w^1 & θ_w^2, respectively, and the slope of the second wedge with respect to the first is

$$\Delta\theta_w = \theta_w^2 - \theta_w^1 . \qquad (6)$$

The reflection over a double wedge depends on three parameters: the incident shock wave Mach number M_1, and the first and second wedge angles θ_w^1 and θ_w^2.

In the following analysis it will be assumed that:

1) the flow is two dimensional;
2) the gas is perfect ($p = \rho RT$) and ideal ($\mu = 0$, $k = 0$);
3) the flow over the first wedge is pseudo-steady;

4) the flow over the second wedge aymptotically approaches a pseudo-steady situation;

5) the regular $\overset{\rightarrow}{\leftarrow}$ Mach reflection transition follows the "detachment" criterion, and

6) the incident shock waves are weak enough so that if the reflection over the first wedge is a Mach type reflection, it is a single-Mach reflection.

Further assumptions concerning the Mach stems are given subsequently.

For a given shock wave Mach number there is an appropriate "detachment" wedge angle, θ_w^{det}. If $\theta_w^1 < \theta_w^{det}$ the shock wave reflects from the first wedge as a Mach reflection, and if $\theta_w^1 > \theta_w^{det}$ it reflects over the first wedge as a regular reflection. The Mach or the regular reflection propagates up the wedge until it encounters the leading edge of the second wedge. If the incident shock wave has reflected as a Mach reflection over the first wedge, then the Mach stem of this reflection encounters the second wedge and reflects from it either as a Mach or as a regular reflection depending upon the size of the differential wedge angle, $\Delta\theta_w$, and the Mach number of the Mach stem, M_m.

In the following analysis it will be assumed that the Mach stem is straight and perpendicular to the wedge surface so that

$$M_m = M_i \frac{\cos \chi_1}{\cos\left(\theta_w^1 + \chi_1\right)} \tag{7}$$

where χ_1 is the first triple point trajectory angle [Ben-Dor 1980].

Thus $M_m > M_i$, but the difference in Mach number is not large and it will therefore be assumed that

$$\theta_w^{det}\Big|_{M_m} \simeq \theta_w^{det}\Big|_{M_i} \tag{8}$$

For example, for $M_i = 2.5$ and $\theta_w^1 = 20°$ the Mach reflection solution results in

$\chi_1 = 12.88°$, thus $M_m = 2.902$. The corresponding detachment wedge angles for M_i and M_m are 50.77° and 50.72°, respectively. Similarly, for $M_i = 1.775$ and $\theta_w^1 = 20°$, one obtains $\chi_1 = 16.17°$ and $M_m = 2.112$. For this case the corresponding detachment wedge angles are 50.22 and 50.68. These two examples indicate that although the difference between the incident shock wave Mach number and the Mach stem Mach number is about 15%, the difference in the detachment angle for these shocks is only a fraction of a degree. Using the assumption of (8), it may be concluded that the Mach stem of the first Mach reflection reflects from the second wedge as a Mach reflection if, $\Delta\theta_w < \theta_w^{det}$, and as a regular reflection if $\Delta\theta_w > \theta_w^{det}$.

The lines $\theta_w^1 = \theta_w^{det}$, $\theta_w^2 = \theta_w^{det}$, $\Delta\theta_w = 0$ and $\Delta\theta_w = \theta_w^{det}$ are all drawn in the (θ_w^1, θ_w^2) plane shown in figure 5. These boundary lines define seven regions with different reflection processes. Those regions above the diagonal, $\Delta\theta_w = 0$, are for a concave double wedge, and those below the diagonal are for a convex wedge. The reflection process in each region and a shock polar solution which gives information about the pressure changes produced by the reflection process are presented, beginning with the simplest case and ending with the most complicated.

The input data for the analysis were the incident shock wave Mach number, M_i and the double wedge geometry, θ_w^1 and $\Delta\theta_w$. The analysis used the two-shock and the three-shock theories of von Neumann (1963) to determine the shock wave angles and the thermodynamic properties behind the shocks for each reflection. The flow properties obtained from the solution were used to draw the shock-polars shown subsequently, which are accurately drawn to scale.

Region 1

In this region $\Delta\theta_w > 0$; $\theta_w^1 > \theta_w^{det}$, and $\theta_w^2 > \theta_w^{det}$, and the reflection process is shown schematically in figure 6, with regular reflection over both wedges, but with different wave angles. The regular reflections can be considered by attaching frames of reference to the reflection points G_1 or G_2, as appropriate.

In order to combine the shock polars of the two regular reflections on a single plot in the (P, θ^{G1}) plane it is necessary to know the direction of G_2 with respect to G_1, namely:

$$\theta(G_2, G_1) = \theta_w^2 - \theta_w^1 = \Delta\theta_w \qquad (9)$$

A shock polar solution for a typical reflection process in region 1 is shown in figure 7 for initial conditions of $M_i = 1.3$, $\theta_w^1 = 47°$ and $\Delta\theta_w = 13°$.

The I^{G1} and R^{G1} polars represent the regular reflection over the first wedge. Since the solution of the reflection over the second wedge is in a frame of reference rotated by the angle $\theta(G_2, G_1)$ with respect to the original frame of reference, the origin of the I^{G2} and R^{G2} shock polars combination is located at $\theta^{G1} = \theta(G_2, G_1) = \Delta\theta_w$. Since $\theta_w^2 > \theta_w^1$, the velocity of G_2 is greater than that of G_1, and so the I^{G2} polar is larger than the I^{G1} polar. The pressure behind the incident shock is the same for both reflections and so the points representing state (1), i.e., the origins of the R^{G1} and R^{G2} polars, have the same ordinates in the (P, θ^{G1}) plane.

The pressure P_2 in state (2) behind the reflected shock over the first wedge is given by the intersection of the R^{G1} polar with the pressure axis, i.e. point (2) in figure 7, and the pressure P_3 in state (3) behind the reflected shock over the second wedge is given by the intersection of the R^{G2} polar with the $\Delta\theta_w$ ordinate, i.e., point (3). In general $P_2 \neq P_3$, and as the incident shock moves from the first to the second wedge there will be a sudden change of pressure.

According to Henderson & Lozzi (1975), "If a pressure discontinuity occurs during transition then an unsteady wave of finite amplitude or a finite amplitude band of waves will be generated in the flow". We may therefore expect that the reflection point on the second wedge will be followed by either compression waves (or a shock wave) or expansion waves depending upon whether the transition causes a sudden pressure decrease or increase.

Figure 8 shows the theoretical pressure ratio behind the reflection point of a regular reflection as a function of the reflecting wedge angle θ_w for a given incident shock Mach number $M_i = 1.3$. The pressure ratio P_2/P_0 goes through a minimum at about $\theta_w = 60°$. Consequently, in the double wedge reflection process now being considered three pressure change behaviours are possible. If, in the example for $M_i = 1.3$, $\theta_w^1 = 50°$ and $\theta_w^2 = 60°$ then at transition from the first to the second wedge the pressure behind the reflection point suddenly drops. However, if $\theta_w^1 = 60°$ and $\theta_w^2 = 85°$ then at transition the pressure behind the reflection point suddenly increases. There could also be a case for which there is no pressure change at transition e.g., $\theta_w^1 = 55°$ and $\theta_w^2 = 65.775°$. Thus, different flow patterns are to be expected behind the second reflection point according to these different pressure changes.

Region 2

In this region $\Delta\theta_w < 0$; $\theta_w^1 > \theta_w^{det}$, and $\theta_w^2 > \theta_w^{det}$, and the reflection process is shown schematically in figure 9. The reflection is regular over both wedges, and can be made pseudo-stationary by attaching frames of reference to the points of reflection G_1 and G_2. The direction of the second reflection point G_2 with respect to that of the first, G_1, is given by

$$\theta\,(G_2,\, G_1) = \Delta\theta_w\,, \qquad (10)$$

and for a convex double wedge $\Delta\theta_w$ is negative.

A shock polar solution for a typical reflection process in region 2 is shown in figure 10, for $M_1 = 1.3$, $\theta_w^1 = 60°$ and $\Delta\theta_w = -13°$.

The I^{G1}, R^{G1} and I^{G2}, R^{G2} polars represent the solutions of the regular reflections over the first and second wedges, respectively, with the origin of I^{G2} shifted by $\Delta\theta_w$ in the (P, θ^{G1}) plane so that the I^{G2} and R^{G2} polars are now to the left of the I^{G1} and R^{G1} polars. The pressure in state (1), behind the incident shock is identical for both frames of reference, and the two-shock-polar combinations are bridged by the constant pressure line P_1 which is dashed in figure 10.

The velocity of G_1 is greater than that of G_2 and so in the pseudo-steady frames of reference the velocity of the incident flow over the first wedge, M_0^{G1}, is greater than that over the second, M_0^{G2}. Therefore, the I^{G1} polar is larger than the I^{G2} polar. The polars again indicate that, in general, the pressure behind the reflected shock over the first wedge, P_2, will be different from the pressure behind the reflected shock over the second wedge, P_3, which should therefore be followed by either compression or expansion waves depending upon whether the pressure suddenly decreases or increases at transition from the first to the second wedge.

Figure 11 is an enlarged drawing of regions 1 and 2 of figure 5. The added dashed line divides each region into two subregions 1 a&b and 2 a&b. In subregions 1a and 2b the reflection process involves a transition from a high pressure regular reflection to a low pressure regular reflection (H → L) while in 1b and 2a, the transition is from a low pressure regular to a high pressure regular reflection (L → H). Therefore in subregions 1a and 2b it is expected that the reflection over the second wedge will be followed by a shock or compression wave, while in subregions 1b and 2a the second reflection is expected

to be followed by an expansion wave. It is of interest to note that in region 1a the pressure behind the reflected shock may be expected to drop as the shock passes a compressive corner and in region 2a the pressure may be expected to increase around an expansive corner.

Region 3

In this region $\Delta\theta_w < 0$; $\theta_w^1 < \theta_w^{det}$, and $\theta_w^2 < \theta_w^{det}$, and the reflection process is shown schematically in figure 12. There is a Mach reflection over both wedges, but with different wave angles, and a non-stationary transition region. The initial and final Mach reflections can be made pseudo-stationary by attaching frames of reference to the triple points T_1 and T_2. The direction of T_2 with respect to the direction of the T_1, is given by

$$\theta\,(T_2,\, T_1) = -\,(-\,\Delta\theta_w + \chi_1 - \chi_2), \qquad (11)$$

where χ_1 and χ_2 are the triple point trajectory angles with respect to the two wedges.

A shock polar solution for a typical reflection process in region 3 is shown in figure 13. The incident shock wave Mach number is $M_1 = 2.5$. It initially reflects as a Mach reflection over the first wedge for which $\theta_w^1 = 40°$ and $\chi_1 = 5.29°$. $\Delta\theta_w = -10°$ and the Mach reflection over the second wedge for which $\theta_w^2 = 30°$, has a triple point trajectory angle $\chi_2 = 8.27°$.

The I^{T2} and R^{T2} polars are plotted in the (P, θ^{T1}) plane, with the origin of the I^{T2} polar displaced by $(\Delta\theta_w - \chi_1 + \chi_2)$. Since the inclination of the second triple point trajectory is less than that of the first, the velocity of T_2 is less than that of T_1 and the Mach number of the incident flow in the pseudo-steady frame of reference, M_0^{T2} will be less than that over the first wedge, M_0^{T1}. The I^{T2} polar is therefore smaller than the I^{T1} polar. The two polars are again related by the pressure P_1 behind the incident shock, shown as a dashed line in the figure. It can be seen that the pressure behind the Mach stem

over the second wedge, P_5, will be less than the pressure behind the Mach stem over the first wedge, P_3. Because the signal speed, i.e. the sound speed plus the particle velocity behind the Mach stem is greater than the speed of the Mach stem, any compression waves will overtake the Mach stem. It is expected, therefore, that after transition from the first to the second wedge, the Mach stem shock initially will be stronger than that produced by an incident shock reflection from a single wedge with an inclination θ_w^2, but will asymptotically approach that value.

Region 4

In this region $\Delta\theta_w < 0$; $\theta_w^1 > \theta_w^{det}$, and $\theta_w^2 < \theta_w^{det}$, and the reflection process is shown schematically in figure 14. The incident shock reflects over the first wedge as a regular reflection (figure 14a) and upon encountering the second wedge there is a transition to a Mach reflection (figure 14b). The initial and final reflections can be made pseudo-stationary by attaching a frame of reference respectively to the reflection point G, or the triple point T.

The direction of the triple point T with respect to that of the reflection point G is given by

$$\theta\,(T,\ G) = -\left(-\Delta\theta_w - \chi\right) \tag{12}$$

A shock polar solution for a typical reflection process in region 4 is shown in figure 15. The incident shock wave ($M_1 = 2.5$) reflects over the first wedge ($\theta_w^1 = 60°$) as a regular reflection. However, since $\Delta\theta_w = -20°$, the second wedge, $\theta_w^2 = 40°$, cannot support a regular reflection, and a Mach reflection with $\chi = 5.29°$ is finally established over it.

The I^G and R^G shock polars represent the regular reflection over the first wedge, and the origin of the I^T and R^T shock polars, which represent the Mach reflection over the second wedge, are displaced by $(\Delta\theta_w + \chi)$, which is negative.

The constant pressure P_1 behind the incident shock again bridges the two sets of polars. For this case the velocity of G is greater than that of T so that M_0^G is greater than M_0^T and the I^G polar is larger than I^T polar.

In general the pressure P_2 behind the reflected shock over the first wedge will be different from the pressure P_4 behind the Mach stem over the second wedge. A transition period is expected after the incident shock moves from the first to the second wedge with expansion or compression waves which will dissipate through the flow. It is not expected that these waves will persist as is predicted for the reflections in regions 1 and 2, and the Mach reflection over the second wedge will asymptotically approach that which would be produced if the incident shock had reflected from a single wedge with an inclination θ_w^2.

Region 5

In this region $\Delta\theta_w > 0$; $\theta_w^1 < \theta_w^{det}$; $\Delta\theta_w > \theta_w^{det}$, and $\theta_w^2 > \theta_w^{det}$, and the reflection process is shown schematically in figure 16. The incident shock reflects over the first wedge as a Mach reflection (figure 16a). The Mach stem of this reflection reflects from the second wedge as a regular reflection (figure 16b). The triple point T and the reflection point G_1 of the Mach and regular reflections interact at point Q on the second wedge surface to form a new regular reflection, with reflection point G_2 (figure 16c).

The reflections can be made pseudo-stationary by attaching frames of reference to the triple point T, or the points of reflection G_1 and G_2, as appropriate. The direction of the reflection points G_1 and G_2 with respect to the direction of the triple point T are given by

$$\theta\,(G_1, T) = \Delta\theta_w - \chi\ , \text{ and} \tag{13}$$

$$\theta\,(G_2, T) = \Delta\theta_w - \chi \tag{14}$$

A shock polar solution for a typcial reflection process in region 5 is shown in figure 17. The incident shock wave ($M_1 = 2.5$) reflects over the first wedge ($\theta_w^1 = 15°$) as a Mach reflection with $\chi = 15.72°$. The Mach number of the Mach stem of this reflection is $M_m = 2.8$. Since $\Delta\theta_w = 55°$, the Mach stem reflects over the second wedge as a regular reflection. Finally, the incident shock wave ($M_1 = 2.5$) encounters the second wedge ($\theta_w^2 = 70°$) from which it reflects regularly.

The I^T and R^T shock-polars represent the Mach reflection solution over the first wedge. Since the solutions of the two regular reflections over the second wedge are made from a frame of reference which is displaced by the angle $\theta\ (G_1, T)$ or $\theta\ (G_2, T)$ with respect to the original frame of reference, the origins of the I^{G_1}, $R^{G_1}$and the I^{G_2}, R^{G_2} shock polars, which represent the regular reflections over the second wedge are located at $\theta^T = \theta(G_1,T) = \theta(G_2,T) = \Delta\theta_w - \chi$. Since the pressures in states (1) and (3) are independent of the frame of reference from which the solution is carried out, the I^T, R^T and I^{G_1}, R^{G_1} shock polars are bridged by the constant P_3 line, and the I^T, R^T and I^{G_2}, R^{G_2} shock polars are bridged by the constant P_1 line, which are dashed in figure 17.

The shock polars in Figure 17 indicate that the transition on the second wedge at point Q is associated with a sudden decrease in the pressure from P_4 behind G_1 to P_5 behind G_2. It will be shown subsequently that this sudden pressure drop is supported by an additional regular reflection, that of the reflected shock wave of the Mach reflection over the first wedge. This secondary regular reflections follows the main regular reflection over the second wedge. This additional regular reflection is drawn schematically in figure 16c with reflection point G_3. It is expected that the overall pressure jump across this additional regular reflection should be close to P_4/P_5. A dashed I^{G_3}, R^{G_3} polar

combination representing this regular reflection is added to figure 17.

It will be shown subsequently that as this secondary regular reflection propagates up the wedge its reflected shock catches up with its incident shock to finally form a single shock wave normal to the wedge surface.

Region 6

In this region $\Delta\theta_w > 0$; $\theta_w^1 < \theta_w^{det}$; $\Delta\theta_w < \theta_w^{det}$, and $\theta_w^2 < \theta_w^{det}$, and the reflection process is shown schematically in figure 18. The incident shock reflects over the first wedge as a Mach reflection (figure 18a), and the Mach stem of this reflection reflects from the second wedge also as a Mach reflection (figure 18b). The triple points T_1 and T_2 of these two Mach reflections, intersect at Q to form a direct Mach reflection (figure 18c), for which the triple point moves away from the second wedge surface. Therefore, the Mach reflection is maintained. It is assumed that these three Mach reflections can be made pseudo-stationary by attaching frames of reference to their appropriate triple points. The directions of T_2 and T_3 with respect to the direction of T_1 are given by

$$\theta\,(T_2,\ T_1) = \Delta\theta_w + \chi_2 - \chi_1 \tag{15}$$

and,

$$\theta\,(T_3,\ T_1) = \Delta\theta_w + \chi_3 - \chi_1 \tag{16}$$

A shock polar solution for a typical reflection process in region 6 is shown in figure 19. The incident shock wave ($M_i = 2.5$) reflects over the first wedge ($\theta_w^1 = 20°$) as a Mach reflection with $\chi_1 = 12.85°$. The Mach number of the Mach stem of this reflection is $M_m = 2.9$. Since $\Delta\theta_w = 20°$, the Mach stem r flects

over the second wedge as a Mach reflection with $\chi_2 = 12.42°$. Finally, after the interaction between the two triple points, at Q, the incident shock wave ($M_1 = 2.5$) forms a Mach reflection over the second wedge ($\theta_w^2 = 40°$) with $\chi_3 = 5.29°$.

The I^{T1} and R^{T1} polars represent the Mach reflection over the first wedge and the origins of the I^{T2}, R^{T2} and I^{T3}, R^{T3} polars, for the second and third Mach reflections are located at $\theta^{T1} = \theta\ (T_2, T_1)$ and $\theta^{T1} = \theta(T_3, T_1)$ respectively. Since the pressures in states (1) and (3) are independent of the frame of reference, the I^{T1}, R^{T1} and I^{T2}, R^{T2} polars are bridged by the constant P_3 line, and the I^{T1}, R^{T1} and I^{T3}, R^{T3} polars are bridged by the constant P_1 line, which are dashed in figure 19.

The changes of pressure along the wedge from P_5 to P_7 at the time when the triple points T_1 and T_2 interact at Q and form the third Mach reflection with a different Mach stem, will result in the generation of compression or expansion waves but these are expected to dissipate in the flow and not to persist as in regions 1 and 2.

Region 7

In this region $\Delta\theta_w > 0$; $\theta_w^1 < \theta_w^{det}$; $\Delta\theta_w < \theta_w^{det}$, and $\theta_w^2 > \theta_w^{det}$, and the reflection process is shown schematically in figure 20. The incident shock reflects over the first wedge as a Mach reflection (figure 20a), and the Mach stem reflects from the second wedge also as a Mach reflection (figure 20b). The triple points T_1 and T_2 intersect at Q to form a third Mach reflection (figure 20c). Unlike the reflection in region 6, the new triple point T_3 moves towards the second wedge surface, i.e., the Mach reflection is an inverse-Mach reflection

(Takayama & Ben-Dor (1985)). Upon colliding with the wedge surface, the inverse-Mach reflection transitions to a regular reflection, which continues to propagate up the wedge (figure 20d).

It is assumed that the three Mach reflections and the final regular reflection can be made pseudo-stationary by attaching a frame of reference to the appropriate triple points T_1, T_2 or T_3, or the reflection point G. The directions of T_2, T_3 and G with respect to the direction of T_1 are given by

$$\theta\,(T_2,\, T_1) = \Delta\theta_w + \chi_2 - \chi_1; \tag{17}$$

$$\theta\,(T_3,\, T_1) = -\left(-\Delta\theta_w + \chi_3 + \chi_1\right), \tag{18}$$

$$\theta\,(G,\, T_1) = \Delta\theta_w - \chi_1 \tag{19}$$

A shock polar solution for a typical reflection process in region 7 is shown in figure 21. The incident shock ($M_1 = 2.5$) reflects over the first wedge ($\theta_w^1 = 30°$) as a Mach reflection with $\chi_1 = 8.27°$. Since $\Delta\theta_w = 30°$, the Mach stem ($M_m = 3.15$) reflects over the second wedge as a Mach reflection with $\chi_2 = 8.09°$. Eventually, the two triple points intersect at Q and the incident shock ($M_1 = 2.5$) propagates over the secondary wedge ($\theta_w^2 = 60°$) from which it reflects regularly.

The I^{T1}, R^{T1} shock polars represent the Mach reflection solution over the first wedge, and the origins of the I^{T2}, R^{T2} and I^{T3}, R^{T3} shock polars, which represent the second and the third Mach reflections are located at $\theta^{T1} = \theta\,(T_2,\, T_1)$ and $\theta^{T1} = \theta(T_3,\, T_1)$, respectively. Since the pressures in states (1) and (3) are independent of the frames of reference, the I^{T1}, R^{T1} and I^{T2}, R^{T2} shock polars are bridged by the constant P_3 line, and the I^{T1}, R^{T1} and I^{T3}, R^{T3} shock polars are bridged by the constant P_1 line. Since the third Mach reflection is an inverse-Mach reflection, its polar solution (states 6 & 7) takes place on the left part of the I^{T3} polar (for details see Takayama & Ben-Dor 1985). For clarity, parts of the I^{T3} polar have been omitted from figure 21.

The origin for the final regular reflection is at $\theta^{T_1} = \theta\ (G, T_1)$. The I^G, R^G polar combination which represents the regular reflection is also bridged to the I^{T_1}, R^{T_1} polars through the constant P_1 line.

The shock polars in figure 21 suggest that a sudden pressure drop will occur from P_7 just before the termination of the inverse-Mach reflection, to P_8, just after the formation of the regular reflection. It was found experimentally that, unlike the case, in region 5, where the sudden pressure drop is supported by a secondary regular reflection (figure 16c), here it is supported by a normal shock wave which follows the regular reflection. This normal shock wave is shown in figure 20d. It is expected that the pressure jump across this normal shock wave should be close to P_6/P_8. A dashed polar representing this normal shock wave is added to figure 21. In figure 20 the state behind the normal shock wave is labled as state (9), and hence the pressure jump across it is P_9/P_8, however states (9) and (6) and states (6) and (7) are separated by slip-streams and hence $P_7 = P_9$.

Experimental Investigations

The reflection of plane shock waves from concave and convex double wedges was studied experimentally using the 7.6 cm×25.4 cm shock tube of the Department of Physics at the University of Victoria, Canada, and the 7.6 cm×12.7 cm shock tube of the Institute of High Speed Mechanics, Tohoku University, Japan. The objectives of the experimental studies were to establish the conditions for transition from regular to Mach reflection or Mach to regular reflection (RR $\rightleftharpoons$ MR) for concave and convex double wedges; to verify the existence of the seven reflection processes predicted in the foregoing analysis, and to verify the predictions of the shock polar analysis concerning the wave configurations

following the major reflections. These objectives were achieved using various high speed photographic techniques such as contact shadowgraphs, multi-frame schlieren and holographic interferometry.

RR $\overset{\rightarrow}{\leftarrow}$ MR transition wedge angle

Using nominal incident shock Mach numbers of 1.3 and 2.45, the angle of the second wedge at which RR $\overset{\rightarrow}{\leftarrow}$ MR occured, was determined. Experiments were conducted using double wedges, similar to those shown in figure 4. Depending upon the final reflection which was observed over the second surface, the second wedge angle, θ_w^2, was increased or decreased by tilting the double wedge until the reflection over the second surface changed from MR to RR or from RR to MR.

The lowest value of θ_w^2 for which RR was observed, and the highest value of θ_w^2 for which MR was observed were averaged to give an estimate of θ_w^{tr} and the associated uncertainty.

In the "weak" shock experiments there were small variations in the incident shock Mach number from experiment to experiment but all were in the range $1.28 < M_1 < 1.30$. The theoretical detachment transition wedge angle for this range of Mach numbers is $45.899° < \theta_w^{det} < 46.347°$. The wedge angles, θ_w^{tr}, at which transition was observed on the second wedge are plotted as a function of $\Delta\theta_w$ for a concave double wedge in figure 22a. At $\Delta\theta_w = 0$, i.e., the case of a straight single wedge, the measured value of θ_w^{tr} is about 1.5° smaller than the theoretical detachment value. This observation is in accordance with experimental results of many other investigators and is probably due to boundary layer effects. The same value is obtained at $\Delta\theta_w = 44.5°$ which again represents the case of single straight wedge, since for this case $\theta_w^1 = 0$.

For the specific incident shock Mach number of these experiments,

$M_1 = 1.29 \pm 0.01$, the transition angle, θ_w^{tr} reaches a maximum of approximately 49.5° for a double wedge with $\Delta\theta_w = 25°$. It is interesting to note that in the range $0 < \Delta\theta_w < 25°$ there appears to be a linear relationship between θ_w^{tr} and $\Delta\theta_w$. The overall relationship between θ_w^{tr} and $\Delta\theta_w$ for a concave double wedge may be compared with that between θ_w^{tr} and R, the radius of curvature of a concave cylindrical wedge for which the transition angle is also greater than that over a single plane wedge (Ben-Dor, Takayama & Kawauchi 1980).

The measured transition wedge angles for a strong shock wave $(M_1 > M_1^*)$ over a concave double wedge are shown in figure 22b. For these cases $M_1 = 2.45 \pm 0.01$. The transition wedge angles for $\Delta\theta_w = 0$ and $\Delta\theta_w = 49°$ which correspond to a single straight wedge are about 1.7° below the value predicted by the "detachment" criterion ($\theta_w^{det} = 50.77°$). This persistence is probably due to boundary layer effects. As $\Delta\theta_w$ increases the transition wedge angle becomes higher until it reaches a maximum of $\theta_w^{tr} = 59.5°$ at $\Delta\theta_w = 30°$. This value of θ_w^{tr} is greater than the "mechanical-equilibrium" transition wedge angle for this Mach number ($\theta_w^{m.e.} = 58°$). For $\Delta\theta_w > 30°$ the transition wedge angle decreases until it reaches the value appropriate to a single wedge at $\Delta\theta_w = 49°$. It should be noted that for this case of a strong incident shock wave the transition wedge angles lie between the "detachment" and the "mechanical-equilibrium" transition wedge angles. To the best of our knowledge this is the first time that the RR $\rightleftarrows$ MR transition has been observed in this range of wedge angle.

Figure 23 shows the observed transition wedge angles, θ_w^{tr}, as a function of $\Delta\theta_w$ for a convex double wedge and an incident shock Mach number of $1.29 \pm .01$. In this case $\Delta\theta_w = 0$ corresponds to the single wedge case with $\theta_w^{tr} = 44.5°$. For decreasing values of $\Delta\theta_w$ the transition angle decreased to a minimum of about 43.25° for $\Delta\theta_w$ in the range from -20° to -35°, and then returned to 44.5° at

$\Delta\theta_w = -45.5°$, which also corresponds to a single straight wedge. The variation of θ_w^{tr} with $\Delta\theta_w$ over a convex double wedge may be compared with the variation of θ_w^{tr} with the radius of curvature of a convex cylinder for which the observed transition angle is also less than the theoretical detachment angle, θ_w^{det}, and the observed transition angle on a straight wedge (Ben-Dor, Takayama & Kawauchi 1980).

The observed transition wedge angles presented in figures 22a and 23 were used to modify the boundaries between regions 6 and 7, and 2 and 4 in figure 5, and the modification is presented as figure 24.

Experimental Verification of the Reflection Processes

Experiments were carried out using combinations of wedge angles representative of each of the seven regions defined by figure 24, using a nominal incident shock Mach number of 1.3. The shock reflections were observed using two photographic methods: multiple double-pass laser schlieren at a framing rate of approximately 20,000 pps., and single frame contact shadowgraphy. In each case the exposure time per frame was approximately 50 ns. The shadowgraphs produced very high quality distortionless pictures, but they did not reveal details of the density variations behind the shocks to the same degree as the schlieren photographs. The double-pass schlieren system has been described by Dewey and Walker (1975). The normally reflecting mirror in this system has a 1 cm grid of small holes through which smoke can be injected as a flow tracer. Smoke was not used in the experiments discussed here, but the holes served as a grid of fiducial markers.

Region 1

The final reflection process in this region is shown in figure 25 for $\theta_w^1 = 55°$ and $\theta_w^2 = 75°$. The regular reflection over the first wedge encounters the second compressive wedge, and the flow is compressed. The compression waves generated at the corner merge into two circular shock waves. One propagates upstream and follows the reflection point of the regular reflection and the other propagates downstream. They are both perpendicular to the wedge surface. These two circular shock waves interact which the reflected shock wave of the second and first regular reflections to form two triple points. The slipstreams of these triple points coincide at a point on the wedge. This point propagates upstream along the second wedge surface. The information about the change in the slope of the surface is probably bounded by these two shock waves.

Region 2

The final reflection process in this region is shown as a schlieren photograph in figure 26 for $\theta_w^1 = 65°$ and $\theta_w^2 = 50°$. The regular reflection over the first wedge encountered an expansive corner which generated expansion waves, which can be seen in the figure, one propagating downstream just behind the reflection point, and the other propagating upstream along the first wedge. the combination of θ_w^1 and θ_w^2 in this experiment lies in region 2a of figure 11 and it is expected that the pressure in the small region behind the reflected shock and the rarefaction is at a higher pressure than behind the reflected shock on the first wedge.

Region 3

The schlieren photograph of the unsteady wave system, generated when the first Mach stem encounters the sudden change in the slope of the surface is shown in figure 27 for $\theta_w^1 = 35°$ and $\theta_w^2 = 15°$. A rarefaction wave is seen to be travelling backwards carrying the information about the sudden change in the model geometry. This corner signal causes the readjustment of the wave angles of the second Mach reflection needed to negotiate the new slope of the second wedge. As the rarefaction produced at the corner advanced up the first Mach stem it produced a weaker shock over the second surface. The contact surface separating the gases behind the stronger and weaker shocks, until the rarefaction reached the triple point, can be clearly seen in figure 27.

Region 4

The final reflection process in this region is shown in figure 28 for $\theta_w^1 = 60°$ and $\theta_w^2 = 30°$. The regular reflection over the first surface encounters the sudden change in the slope and forms a Mach reflection over the second surface. The rarefaction wave generated at the corner, carries the information about the sudden change in the wedge geometry and causes the reflection to adjust its wave angles to negotiate the new slope of the second wedge.

Region 5

The reflection process in this region is shown in figures 29a to 29e for $\theta_w^1 = 20°$ and $\theta_w^2 = 75°$. The Mach reflection over the first wedge is shown in figure 29a. Its collision with the second wedge results in a regular reflection (figure 29b). The triple point of the Mach reflection over the first wedge and the reflection point of the regular reflection of the Mach stem over the second

wedge interact on the second wedge. Figure 29c was recorded shortly after this interaction. The reflected shock wave of the Mach reflection now lags behind the incident shock wave. A clearer configuration of the wave system at a later time is shown in figure 29d. The incident shock wave reflects from the second surface regularly. The reflected shock of the original Mach reflection reflects regularly from the second surface, and follows the major regular reflection. As this secondary regular reflection propagates along the wedge the wave angles of the incident and reflected shocks change until they merge together and form a single shock normal to the reflection surface, as shown in figure 29e.

Region 6

The reflection process in this region is shown in figures 30a to 30c for $\theta_w^1 = 15°$ and $\theta_w^2 = 35°$. The Mach stem of the Mach reflection over the first wedge reflects from the second wedge also as a Mach reflection (figure 30b). The two triple points later interact (figure 30b) resulting in a direct Mach reflection of the incident shock wave over the second wedge. A second triple point is formed at the intersection of the two reflected shock, as shown in figure 30c, but the slipstream from this triple point is not visible in the shadowgraph.

Region 7

The reflection process in this region is shown in figures 31a and 31b for $\theta_w^1 = 25°$ and $\theta_w^2 = 60°$. The Mach stem of the Mach reflection over the first wedge reflects over the second wedge as a Mach reflection (figure 31a). The two triple points interact to give an inverse-Mach reflection (Takayama & Ben-Dor, 1985), i.e., its triple point propagates towards the second wedge surface. When it meets the

second surface the inverse-Mach reflection terminates and a regular reflection is formed, as shown in figure 31b. The reflection is followed by a shock wave which is perpendicular to the second wedge surface, and which meets the reflected shock at a triple point. Another triple point is generated by the reflected shock waves of the two Mach reflections. The slipstreams of the two triple points can be seen in the shadowgraph of figure 31b.

The final wave configuration shown in figure 31b is similar to the one finally obtained through the reflection process of region 5. However, the normal shock wave in region 6 was established at the moment the inverse-Mach reflection terminated at the wedge surface, while in region 5 the initial reflection is a regular reflection which degenerates into a normal shock wave.

Conclusions

The reflection processes of a plane shock wave over a concave or convex double wedge, have been analyzed using the basic concepts of the reflection of a plane shock wave over a single wedge. It was found that there are seven different reflection processes, which are summarized in Table 1.

To simplify the analysis of the shock reflection processes a number of assumptions were made, namely, that transition between regular and Mach reflection would take place according to the theoretical "detachment" criterion; that all Mach stems would be straight, and that the same "detachment" transition angle could be used for both the incident and Mach stem shock waves. It is known that transition between regular and Mach reflection over a wedge does not occur at the angle predicted by theory; that for most shock strengths the Mach stem shock is curved, and that there will be a slight difference in the transition

angle for the incident and Mach stem shock waves. Nevertheless we believe that the shock reflection processes described here are qualitatively correct.

For each of the seven reflection processes a shock polar analysis was carried out. These analyses have provided information about the detailed wave structures following the main reflections along the wedge surfaces, and have made it possible to identify the sudden pressure changes as the reflections moved from the first to the second wedge. The different reflection pr cesses predicted by the analysis, and the shock structures predicted by the shock polars have all been verified experimentally using shadowgraph and schlieren photographs. The shock waves which support the sudden pressure changes produced by some of the transitions and predicted by the shock polar solutions, have been observed. In some cases these shocks are normal to the reflecting surface and in other cases they are regularly reflected shocks. The criteria to determine which of those configurations will occur, have not yet been established, but are the subject of continuing studies.

	θ_{w_1}	θ_{w_2}	$\Delta\theta_w$	First surface	Second surface	Region
Convex	> det	> det	-	Regular	Regular	2
	< det	< det	-	Mach	Mach	3
	> det	< det	-	Regular	Mach	4
Concave	> det	> det	-	Regular	Regular	1
	< det	> det	> det	Mach	Regular→Regular	5
	< det	< det	< det	Mach	Mach→Mach	6
	< det	> det	< det	Mach	Mach→Regular	7

Table 1

A summary of the seven different reflection processes which can occur over convex and concave double wedges depending on the magnitude of the wedge angles θ_w^1 , θ_w^2 and $\Delta\theta_w$ compared to the detachment wedge angle θ_w^{det}(referred to simply as 'det' above). The numbers in the final column refer to the regions in the θ_w^1, θ_w^2 plane of figure 5.

List of References

Ben-Dor, G. 1978, UTIAS Re. No. 232

Ben-Dor, G., 1980, Canadian Aeronautics & Space J., 26 (2), 98.

Ben-Dor, G., Takayama, K. & Kawauchi, T., 1980, J. Fluid Mech. 92, 735.

Courant, R. & Friedrichs, K.O., 1948, Hypersonic Flow and Shock Waves, Wiley-Interscience, New York.

Dewey, J.M. & McMillin, D.J., 1985, J. Fluid Mech. 152, 67.

Dewey, J.M. & Walker, D.K., 1975, J. Appl. Phys., 46, 8, 3454.

Dewey, J.M., Walker, D.K., Lock, G.C. & Scotten, L.N., 1983, Shock Tubes and Waves, Proc, 14th Int. Symp. Shock Tubes and Waves, Ed. Archer, R.D. & Milton, B.E., 144.

Ginzburg, I.P. & Markov, Y.S., 1975, Fluid Mech. Sov. Res. 4(3), 167.

Heilig, W.H., 1969, Phys. Fluids, Suppl. 12, I 154.

Henderson, L.F. & Lozzi, A., 1975, J. Fluid Mech. 68, 139.

Henderson, L.F. & Woolmington, J.P., 1983, Shock Tubes and Waves, Proc. 14th Int. Symp. Shock Tubes and Waves, Ed. Archer, R.D. & Milton, B.E., 160.

Hornung, H.G., Oertel, H. & Sandeman, R.J., 1979, J. Fluid Mech., 90, 541.

Itoh, S., Okazaki, N. & Itaya M., 1981, J. Fluid Mech., 108, 383.

Jones, D.M., Martin, P.M. & Thornhill, C.K., 1951, Proc. Roy. Soc., A209, 238.

Matsuo, K., Aoki, T., Hirahara, H. and Kondoh, N. 1985 (Private Communication).

Kawamura, R. & Saito, H., 1956, J. Phys. Soc. Japan, 11, 5, 584.

Neumann, J. von, 1963, Collected Works, vol. 6, Pergamon Press.

Takayama, K. & Ben-Dor, G., 1985, AIAA J. to be published.

Part 3

Numerical Investigation of the Reflection of a Plane Shock Wave Over a Double Wedge

As mentioned earlier a numerical code based on the TVD scheme was developed. In the following, twelve examples are illustrated. The initial conditions for each of the twelve cases are given in Table 1. Each example consists of 5 figures, and one table, namely;

- the actual interferogram of the experiment
- the values of the labelled isopycnics
- the numerical simulation
- the pressure distribution along the wedge
- the density distribution along the wedge.

The pressure and density distributions along the wedge were obtained using the numerical simulation.

Similar plots of the distribution of any flow property at any place and at any time can easily be obtained by the numerical code.

Table 1: The initial conditions of the 12 cases shown in the following

Case	Ms	Po[KPa]	θ_w^2[°]	θ_w^2[°]
1	1.95	50.7	55	20
2	1.96	50.7	25	35
3	2.16	30.4	20	35
4	1.96	50.7	15	20
5	2.16	50.7	15	20
6	2.16	30.4	60	-30
7	2.17	30.4	35	-20
8	1.49	66.9	35	-20
9	2.16	30.4	40	-15
10	1.50	66.9	40	-15
11	1.47	66.9	40	-15
12	1.47	66.9	65	-15

Ms = 1.95 at 50.7 kPa, 55°/75°

Case 1

fringe	ρ/ρ_0
a	4.1388
b	4.2214
c	4.3040
d	4.3866
e	4.4692
f	4.5518
g	4.6344
h	4.7170
i	4.7996
j	4.8822
k	4.9648
l	5.0474
m	5.1300
n	5.2126
o	5.2952

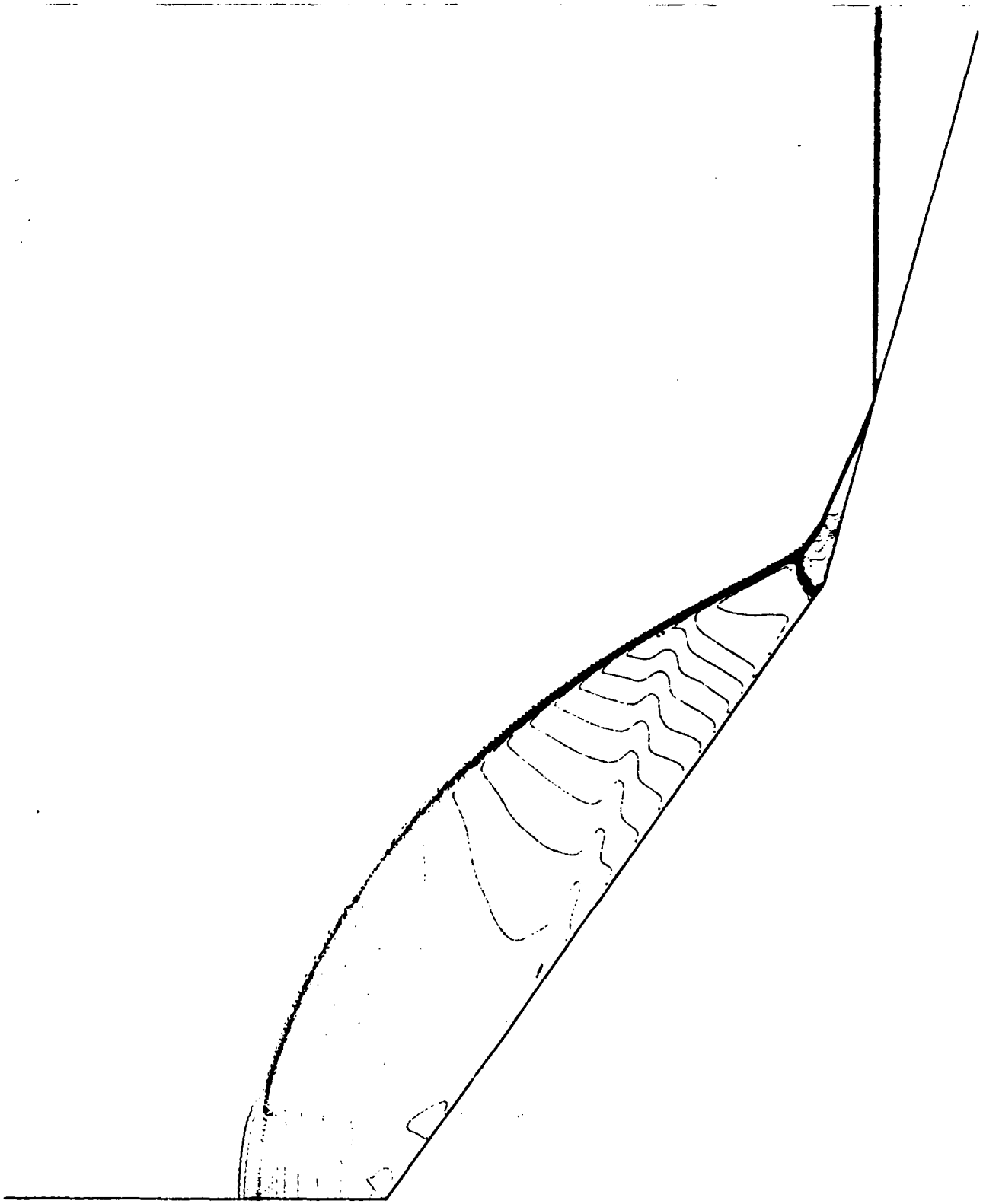

REVERT. 0 K

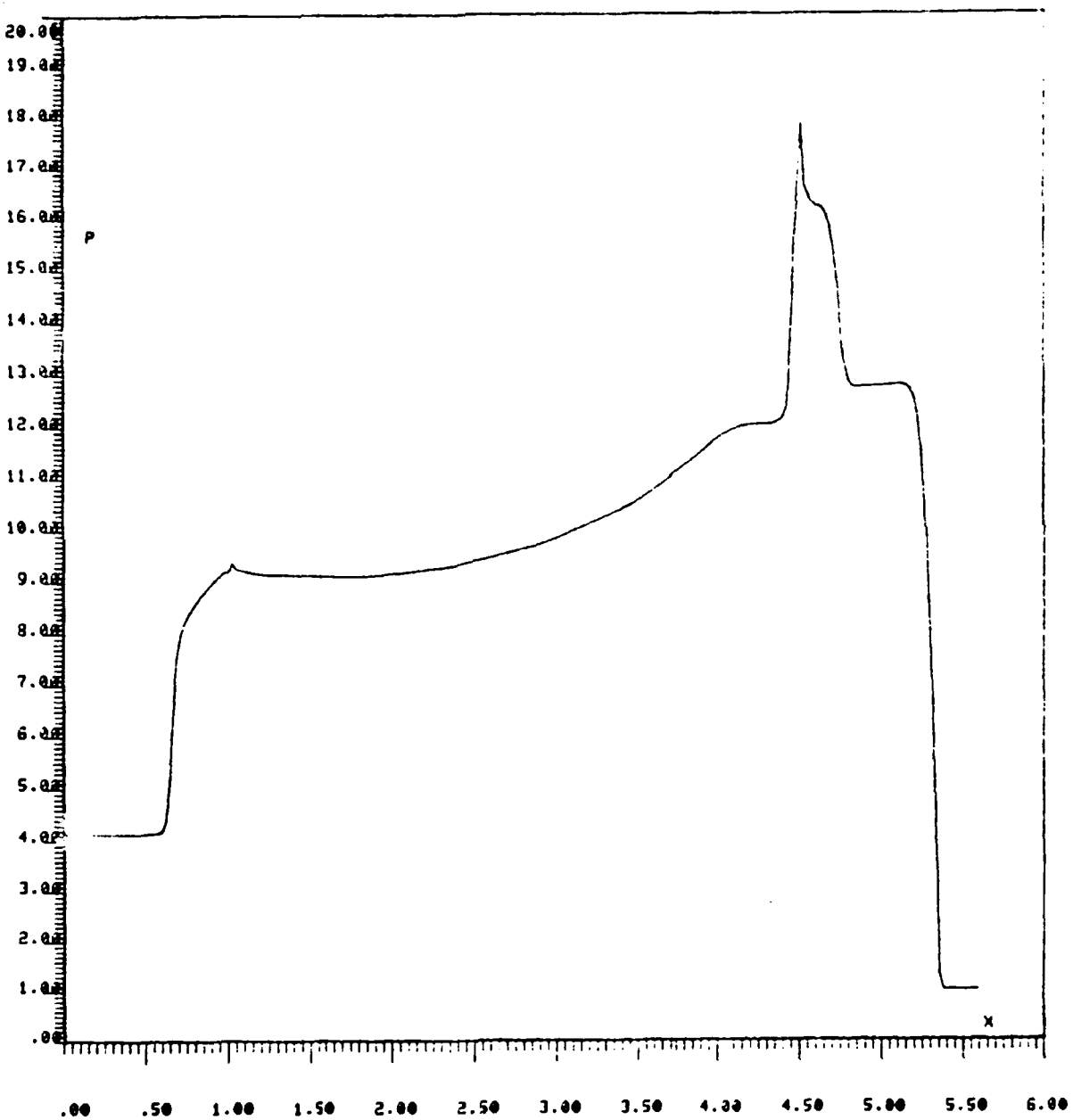

RELERT. 0 K
/
IDLE

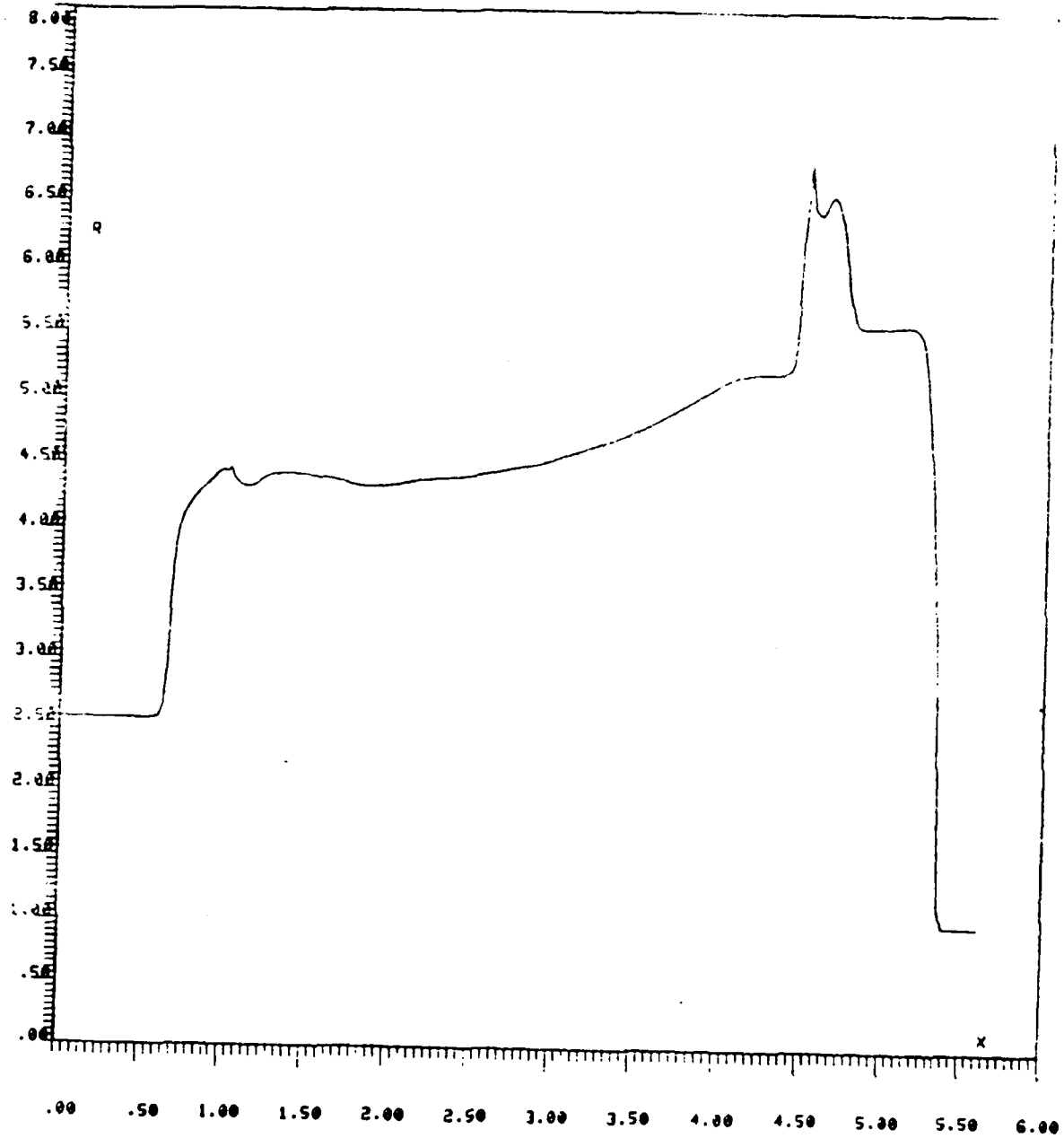

Ms = 1.96 at 50.7 kPa, 25°/60°

Case 2

fringe	ρ/ρ_0
a	3.0650
b	3.1476
c	3.2302
d	3.3128
e	3.3954
f	3.4780
g	3.5606
h	3.6432
i	3.7258
j	3.8084
k	3.8910
l	3.9736

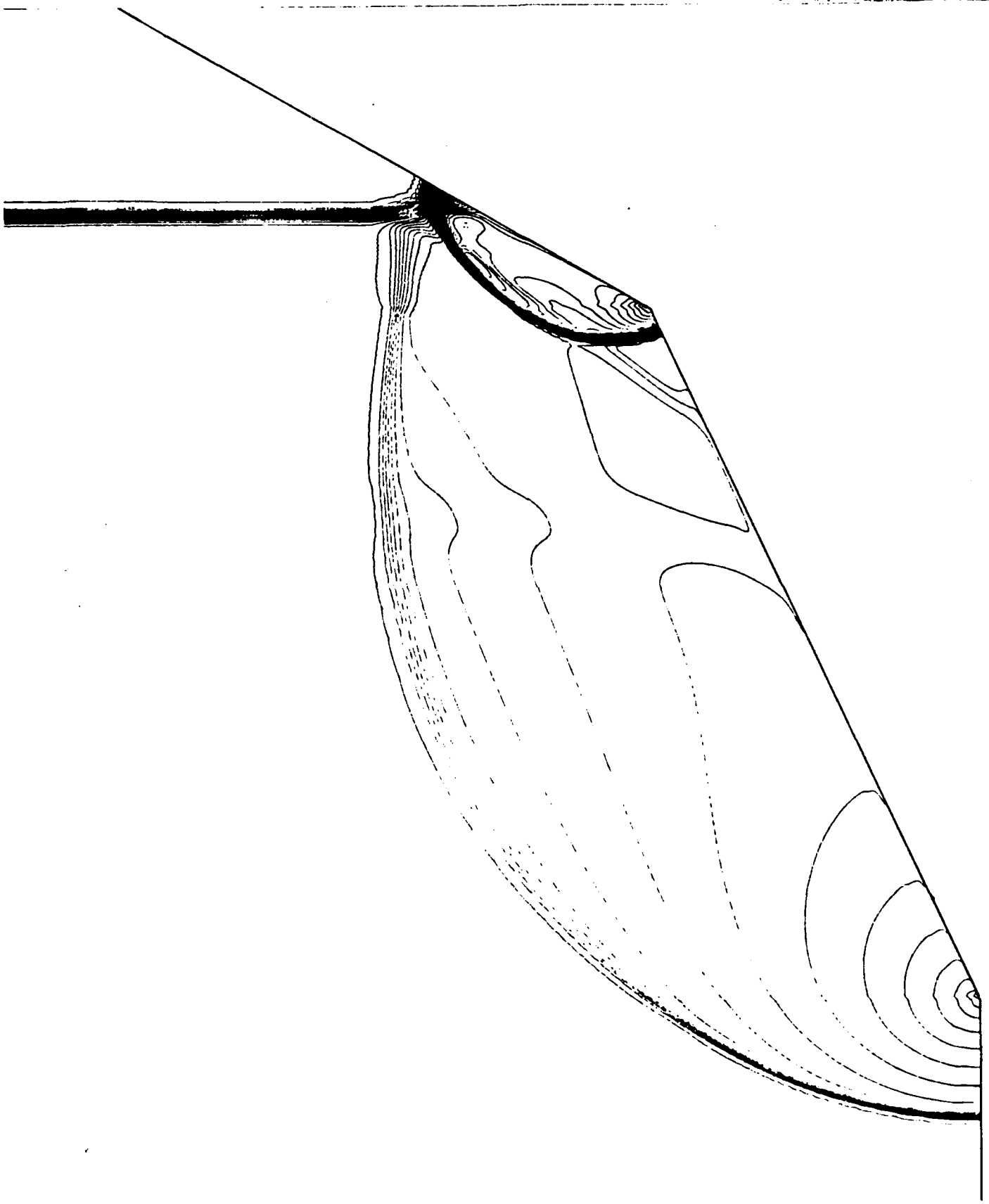

REVERT. O K

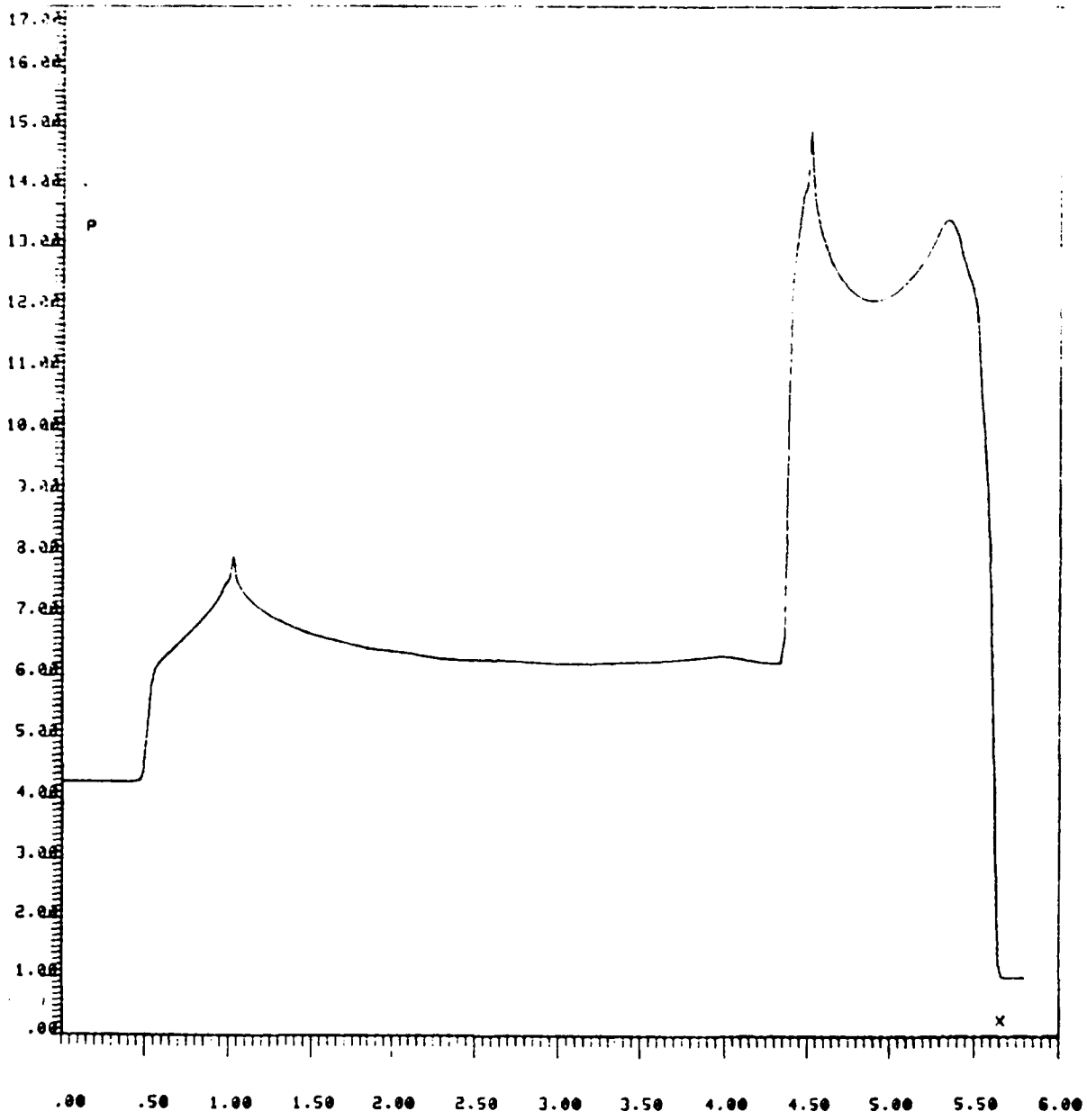

REVERT. O K

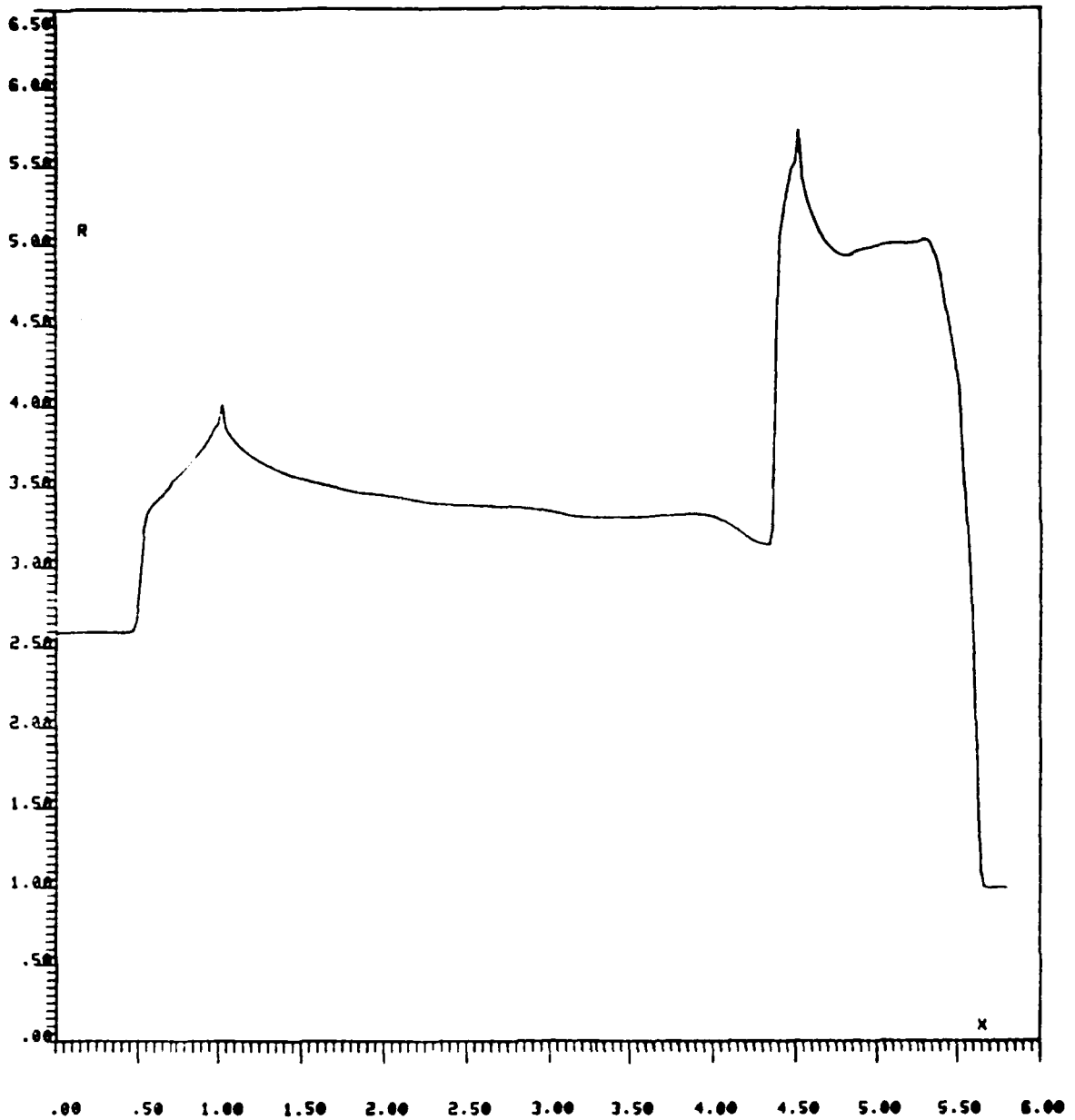
6.5R
6.0R
5.5R
5.0R
4.5R
4.0R
3.5R
3.0R
2.5R
2.0R
1.5R
1.0R
.5R
.0R
R
X
.00
.50
1.00
1.50
2.00
2.50
3.00
3.50
4.00
4.50
5.00
5.50
6.00

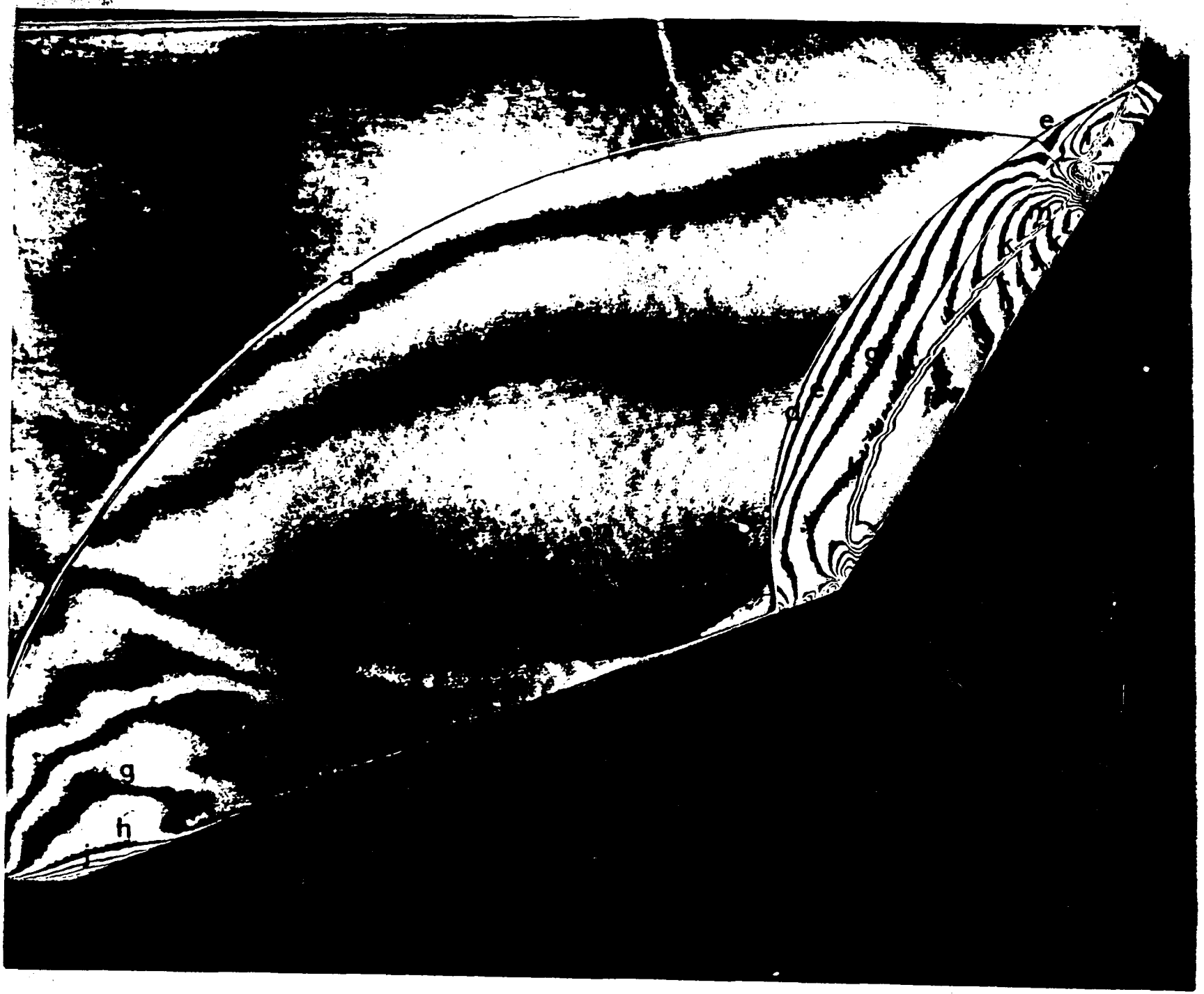

Ms=2.16 at 30.4 kPa, 20°/55°

Case 3

fringe	ρ/ρ_0
a	3.2048
b	3.3426
c	3.4804
d	7.4766
e	7.6144
f	7.7522
g	7.8900
h	8.0278
i	8.1656
j	8.3034
k	8.4412
l	8.5790
m	8.7168

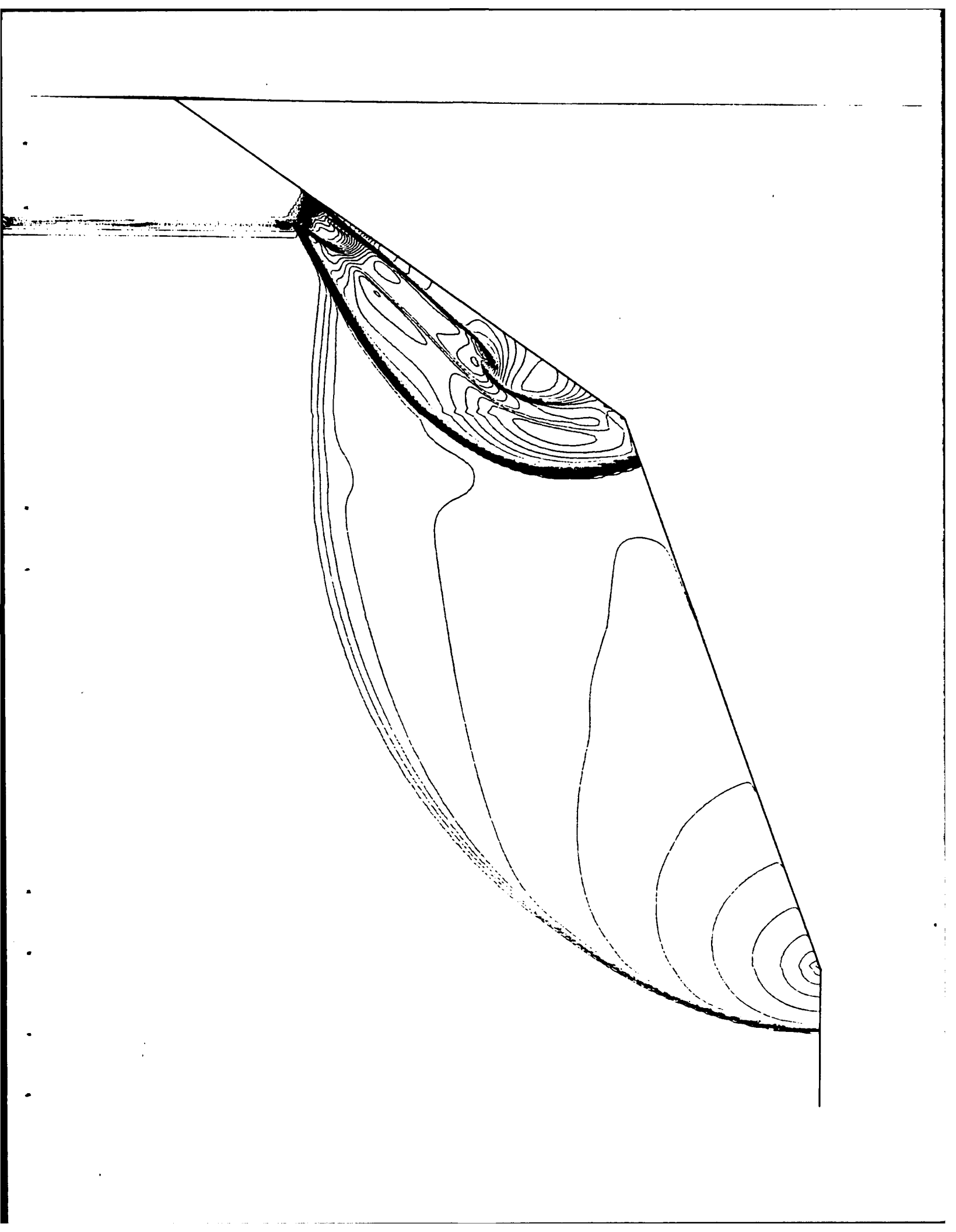

REVERT. 0 K

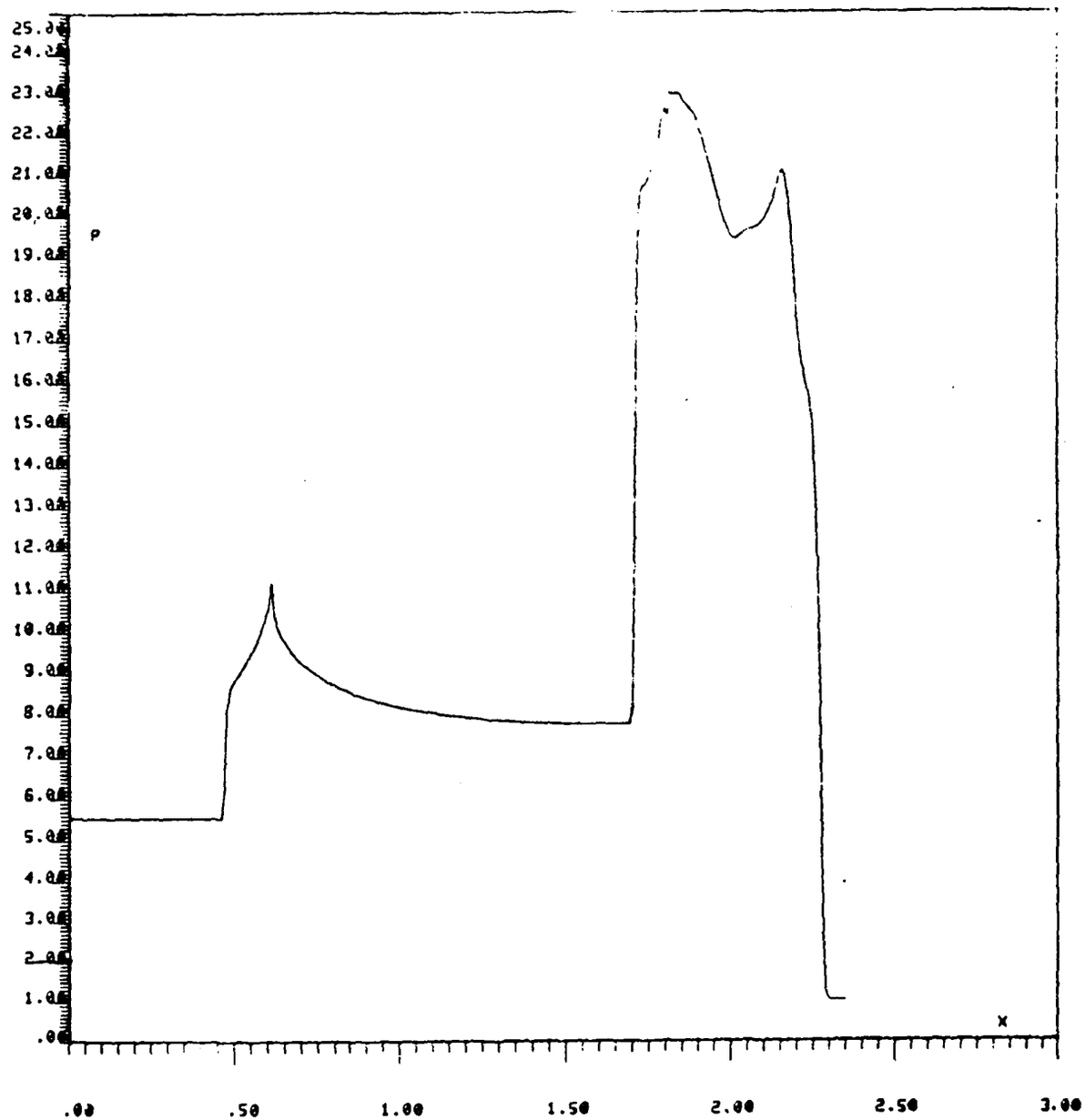

REVERT. 0 K

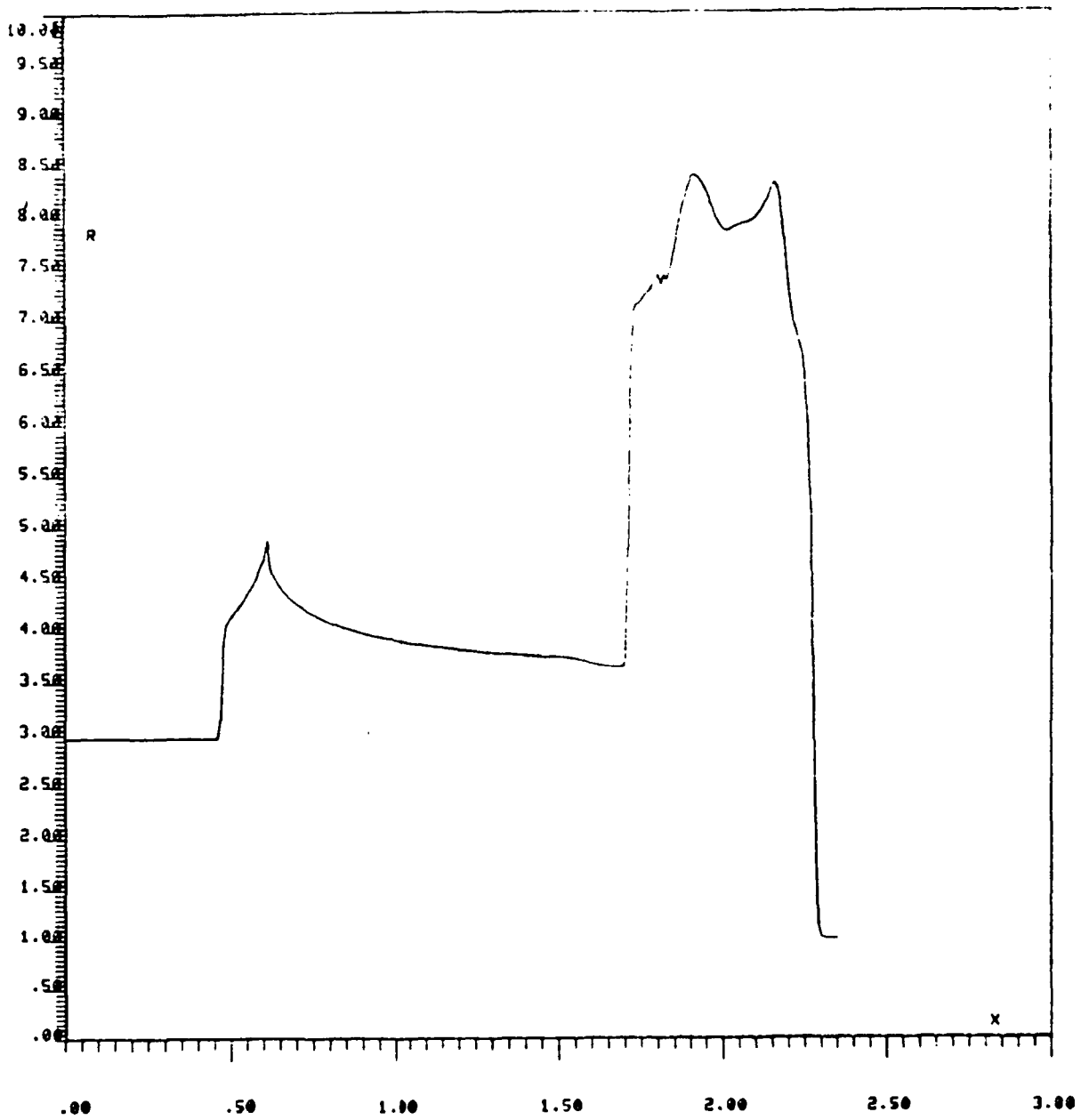

Ms=1.96 at 50.7 kPa, 15°/35°

Case 4

fringe	ρ/ρ_0
a	3.0650
b	3.1476
c	3.2302
d	3.3128
e	3.3954
f	3.4780
g	3.5606
h	3.6432
i	3.7258
j	3.8084
k	3.8910
l	3.9736
m	4.0562
y	3.6432
z	3.7258

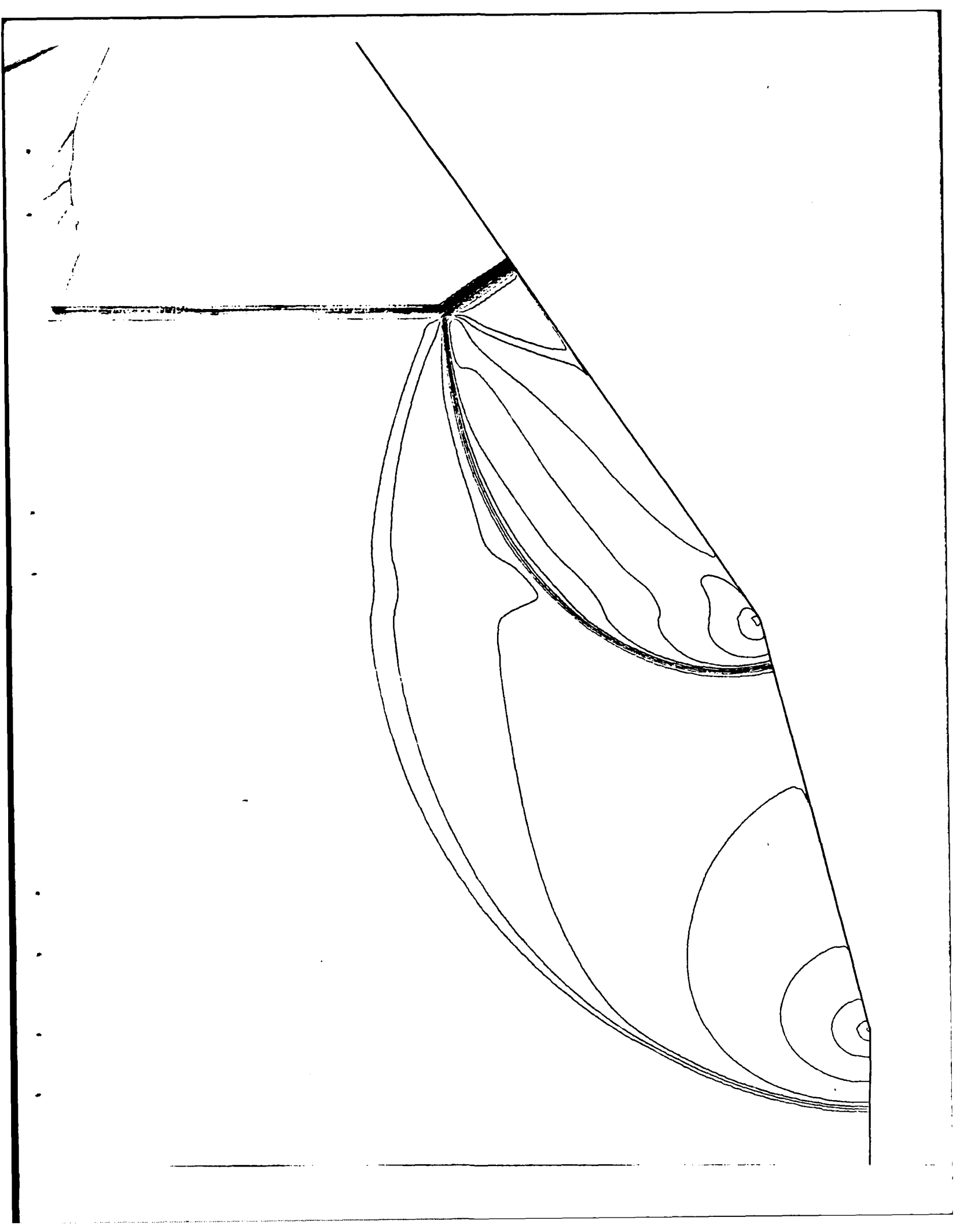

REVERT. 0 K

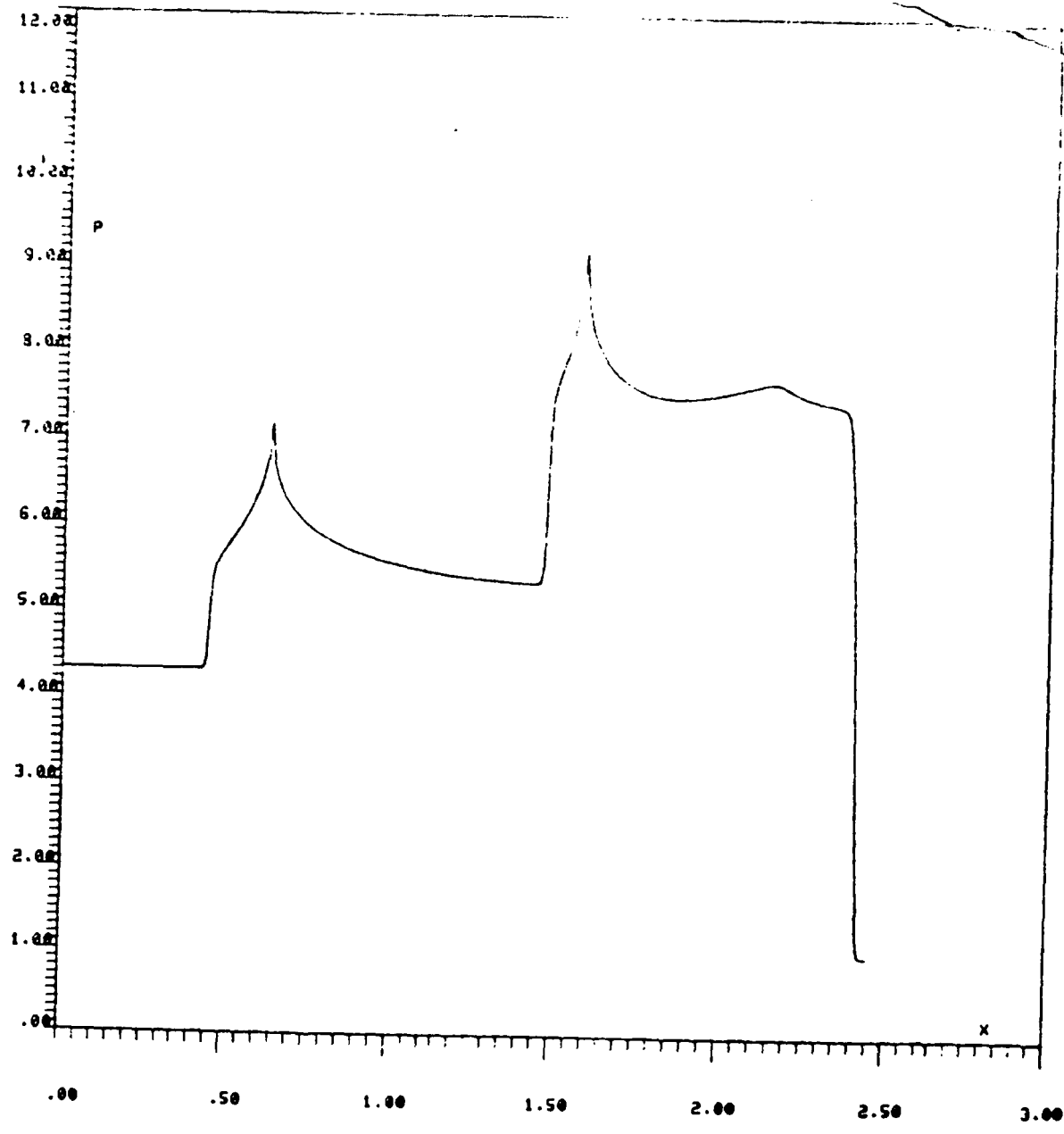

REVERT. O K

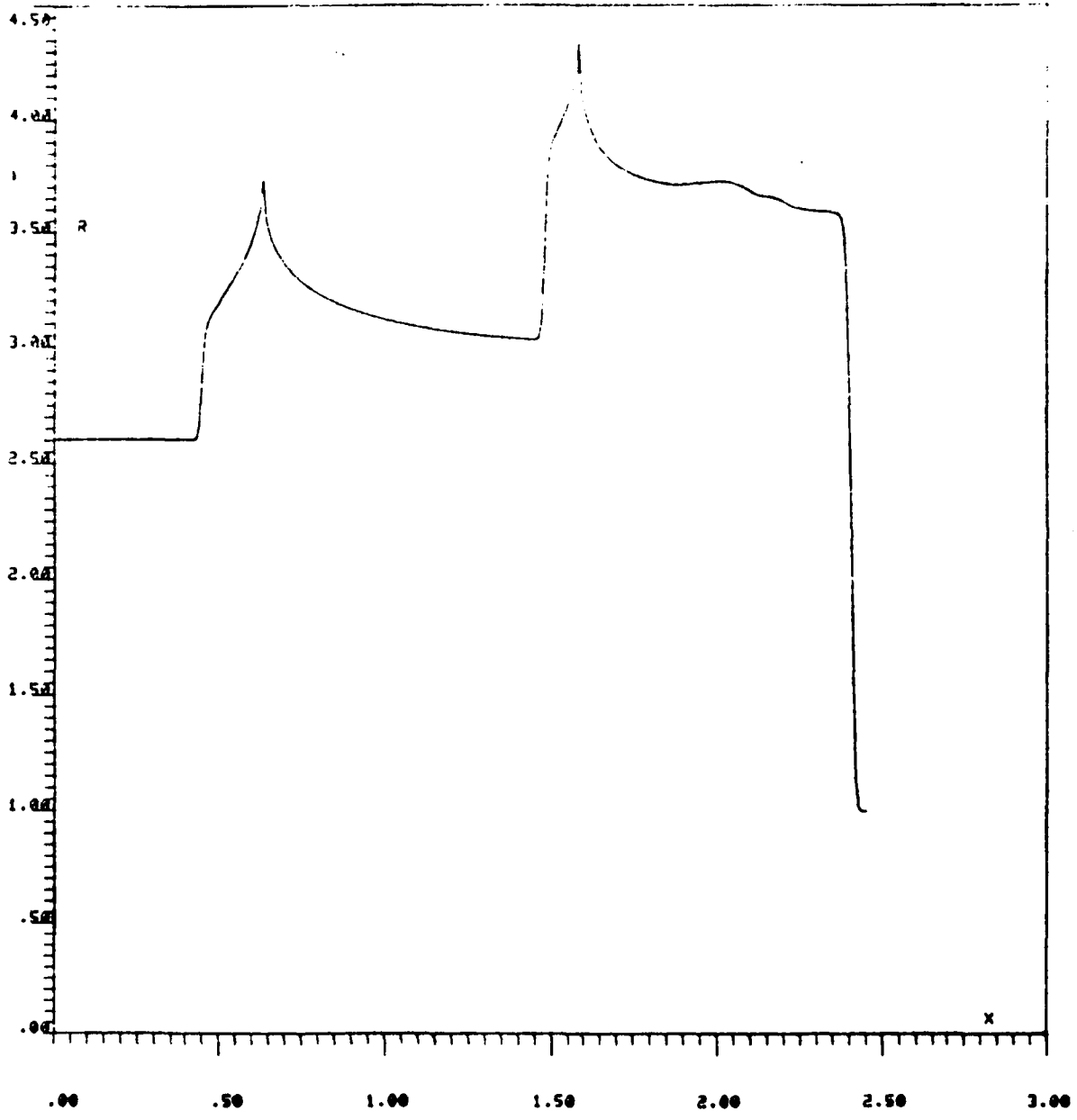

Ms=2.16 at 50.7 kPa, 15°/35°

Case 5

fringe	ρ/ρ_0
a	
b	4.223077
c	4.305720
d	4.388363
e	4.471006
f	4.553649
g	4.636292
h	4.718935
i	4.801578

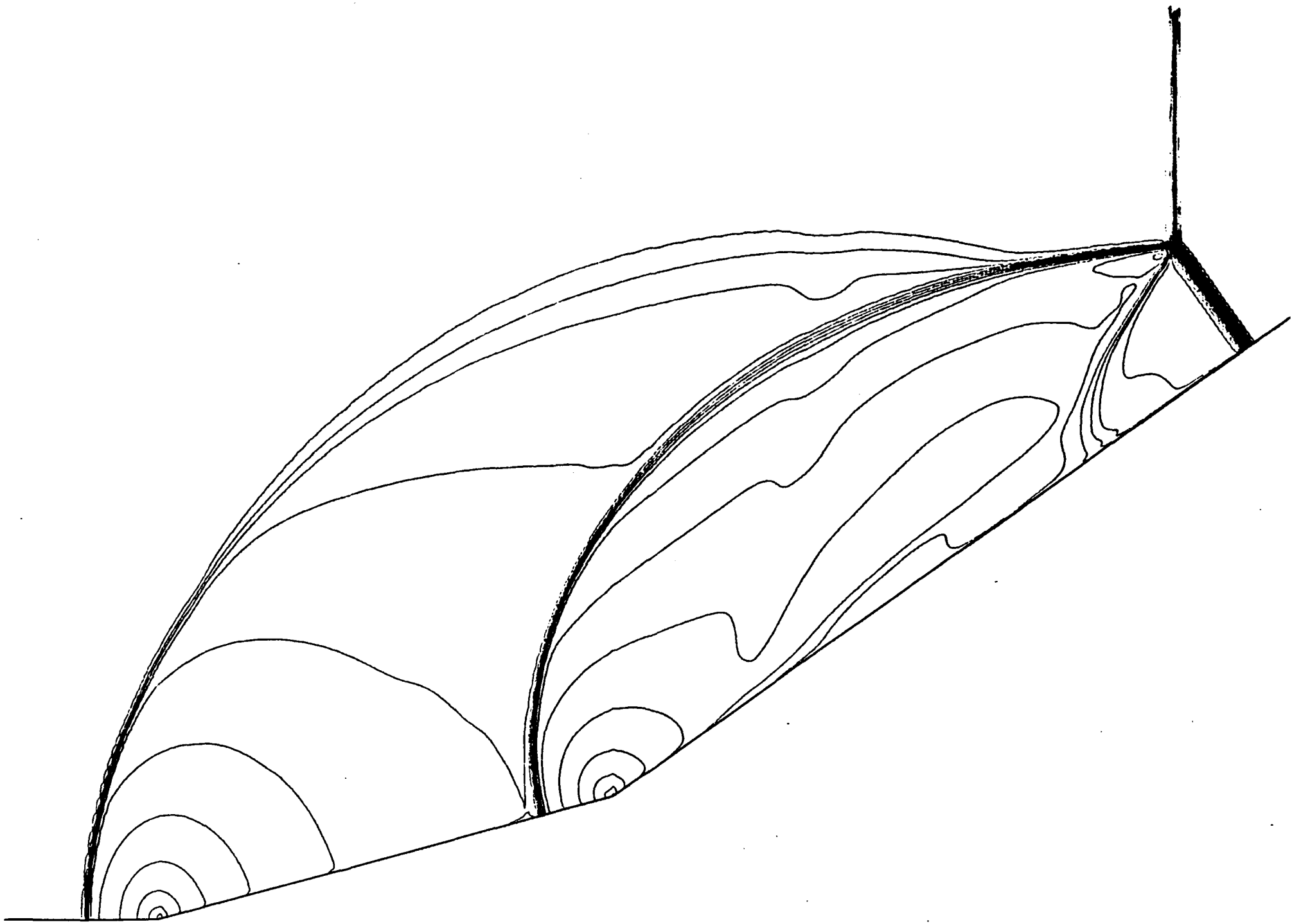

REVERT. 0 K

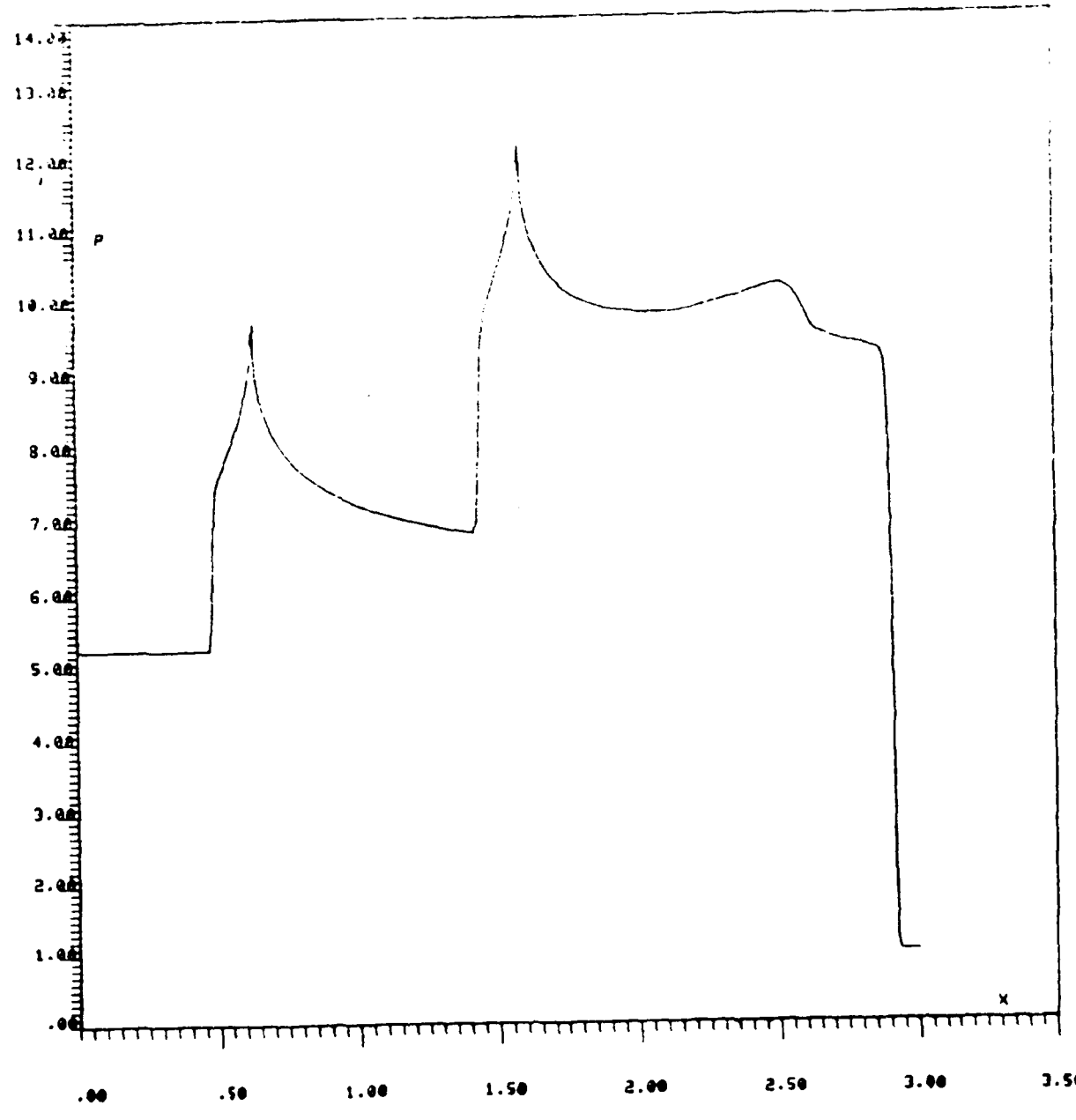

REVERT. 0 K

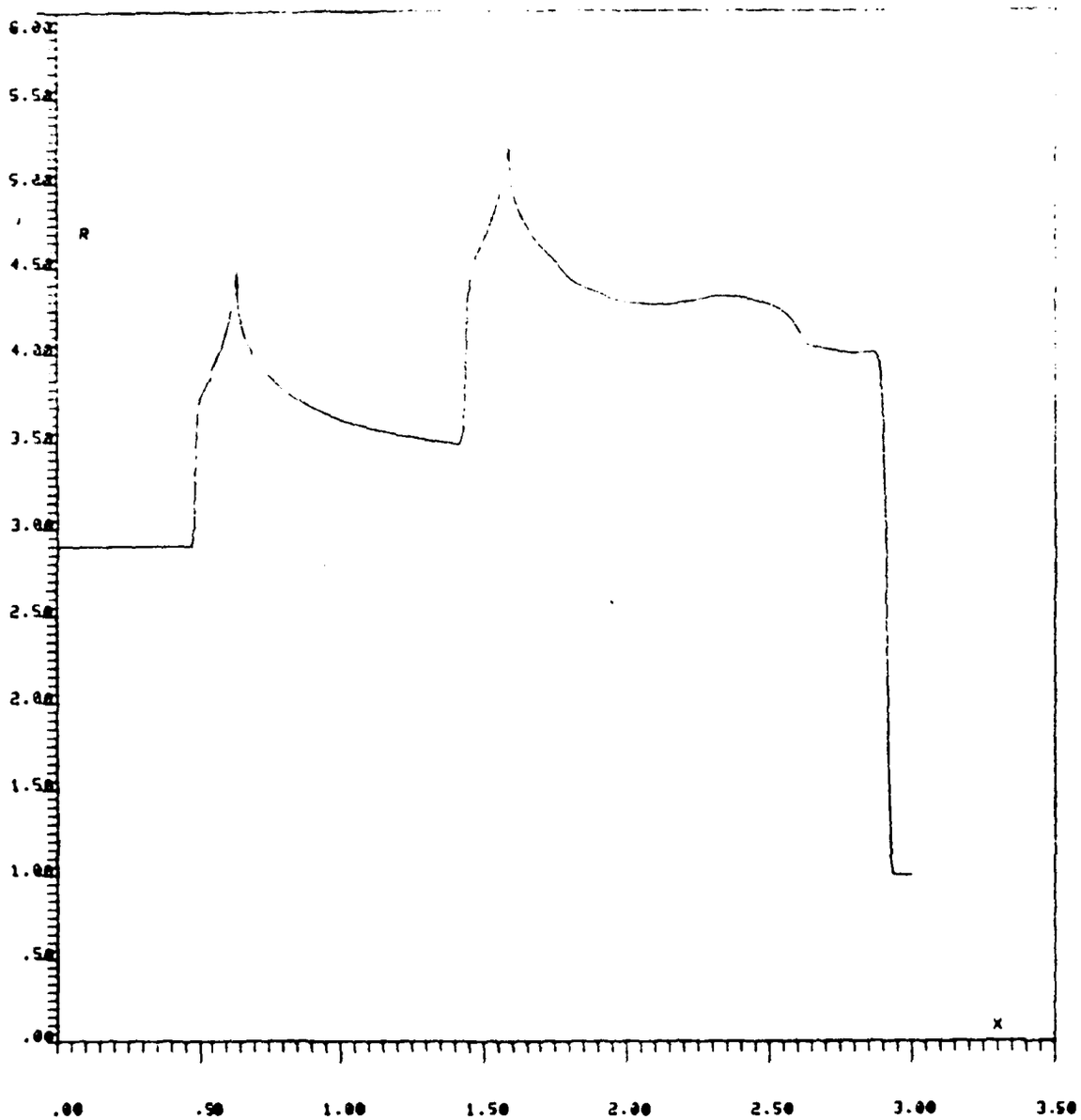

M_s = 2.16 at 30.4 kPa, 60°/30°

Case 6

fringe	ρ/ρ_0
a	4.307896
b	4.445725
c	4.583554
d	4.721383
e	4.859212
f	4.997041
g	5.134870
h	5.272699
i	5.410528
j	5.548357
k	5.686186
l	5.824015
m	5.961844
n	6.099673
o	6.237502
p	6.375331

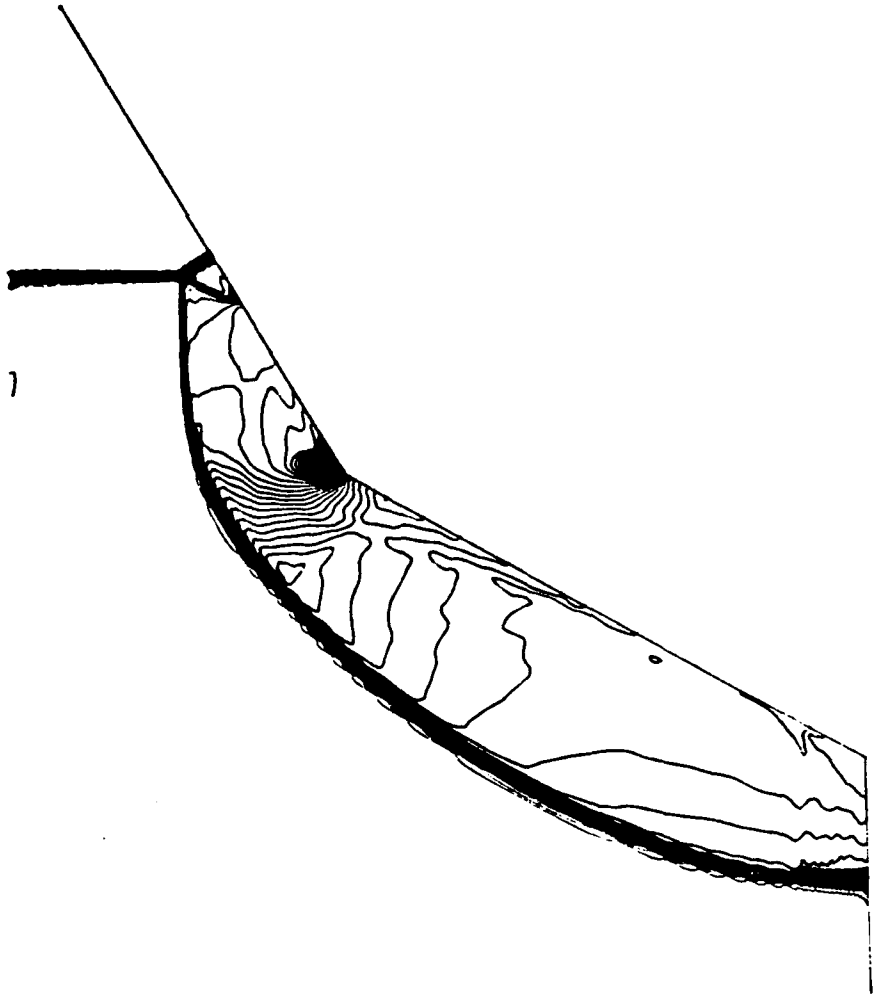

REVERT. 0 K

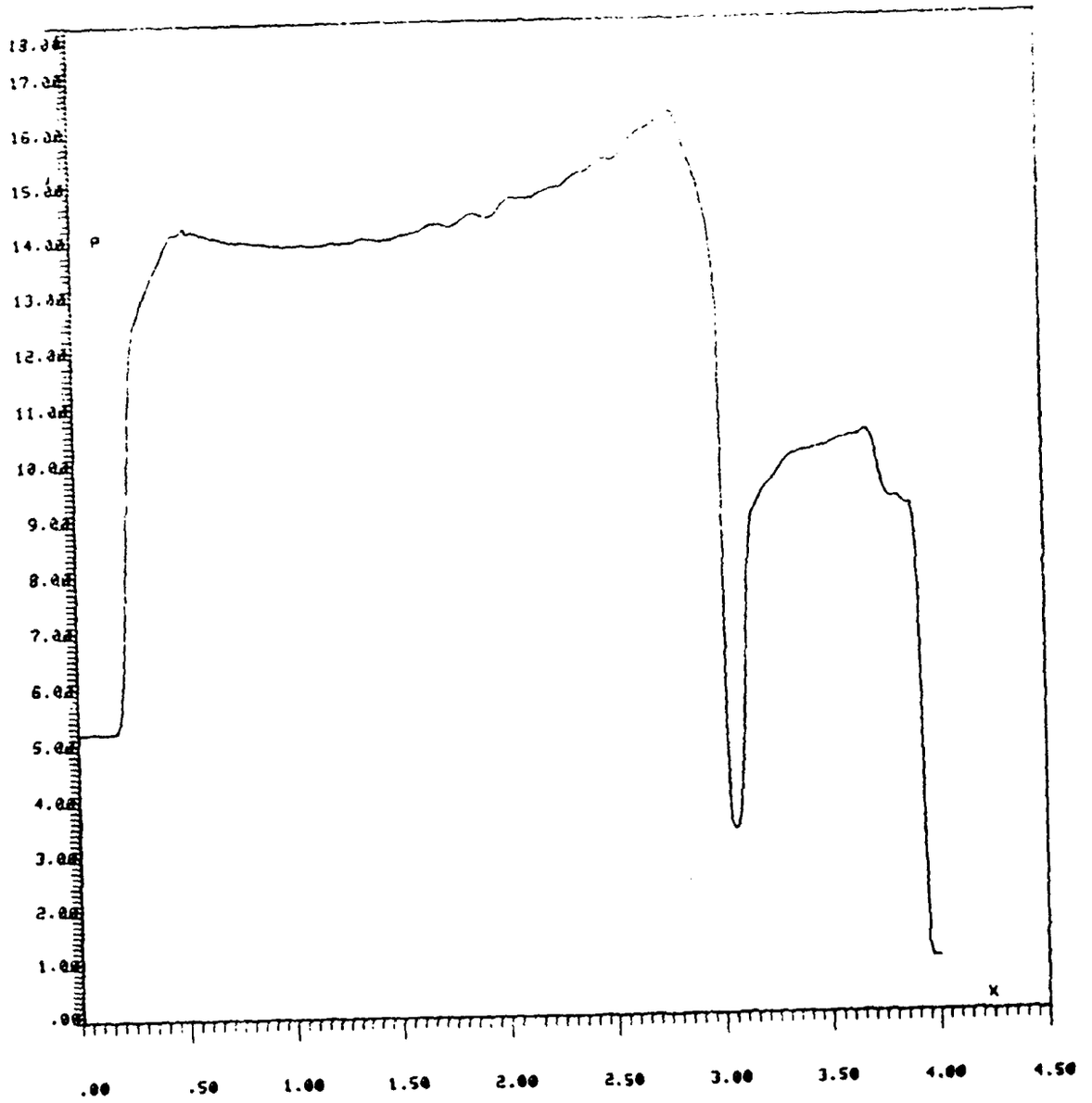

REVERT. O K

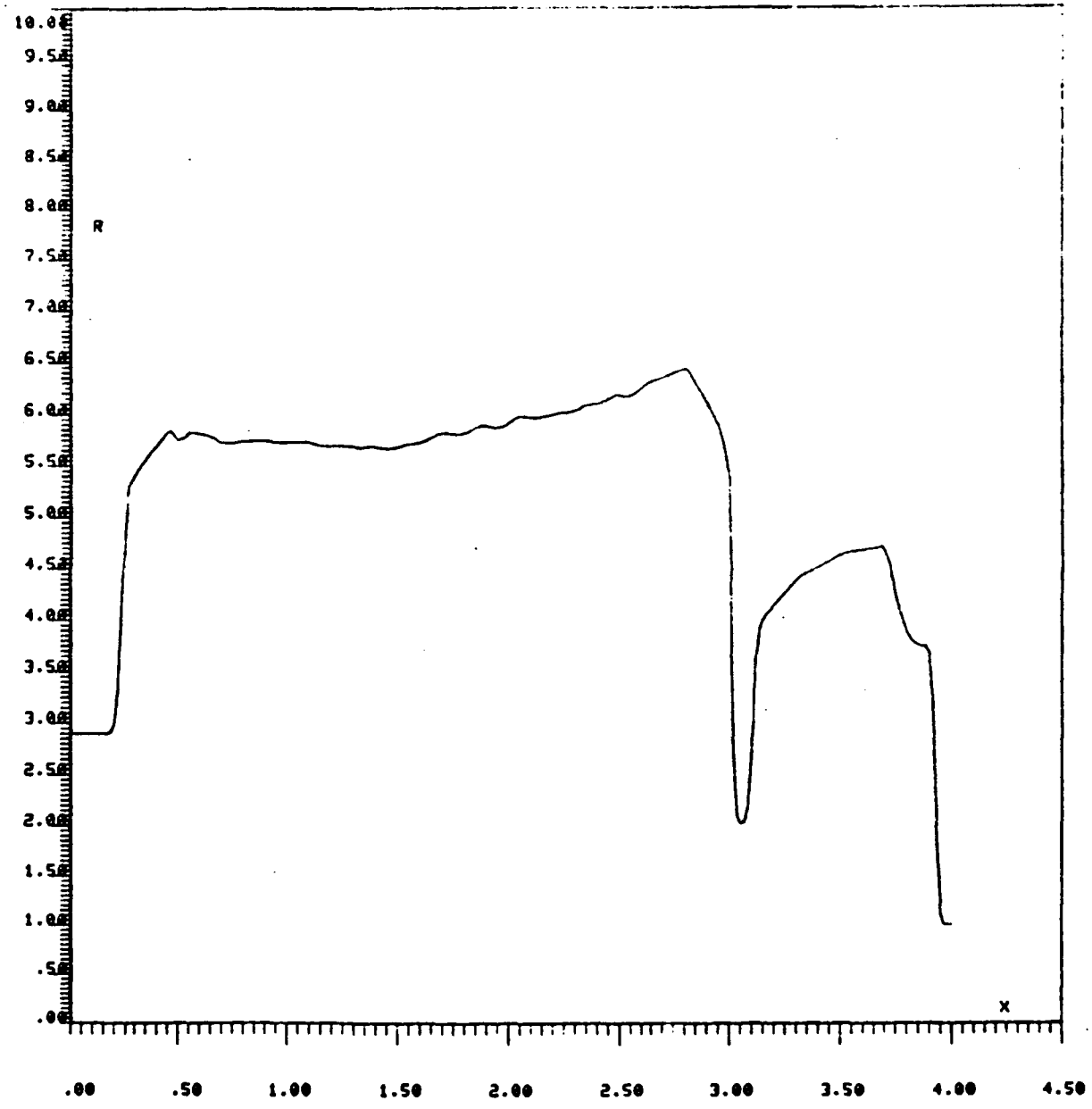
R
X
10.00
9.50
9.00
8.50
8.00
7.50
7.00
6.50
6.00
5.50
5.00
4.50
4.00
3.50
3.00
2.50
2.00
1.50
1.00
.50
.00
.00
.50
1.00
1.50
2.00
2.50
3.00
3.50
4.00
4.50

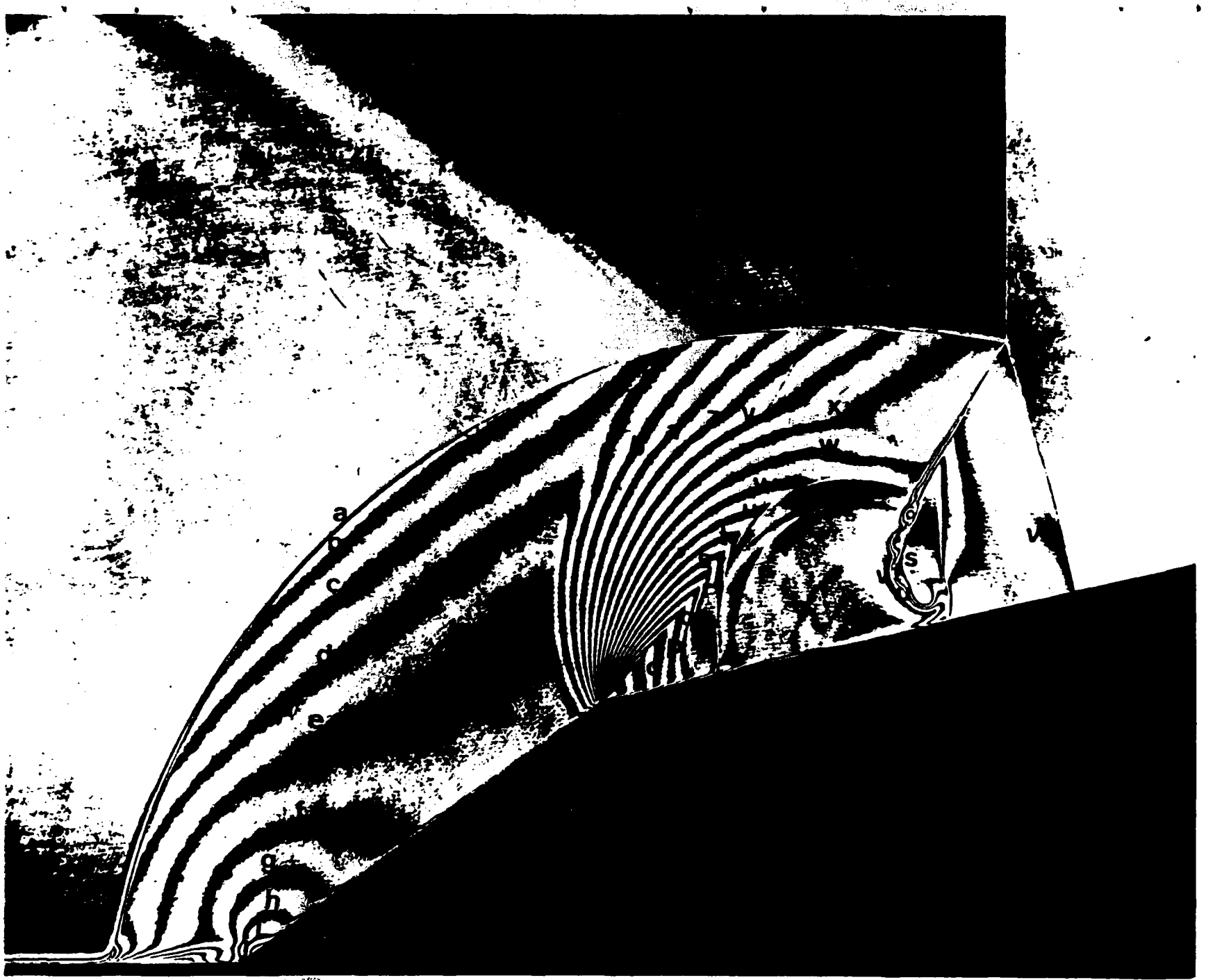

M_S = 2.17 at 30.4 kPa, 35°/15°

Case 7

fringe	ρ/ρ_0
a	3.6182
b	3.7560
c	3.8938
d	4.0316
e	4.1694
f	4.3072
g	4.4450
h	4.5828
i	4.7206
j	4.8584
n	1.8268
o	1.9646
p	2.1024
q	2.2402
r	2.3780
s	2.5158
t	2.6536
u	2.7914
v	2.9292
w	3.0670
x	3.2048
y	3.3426
z	3.4804

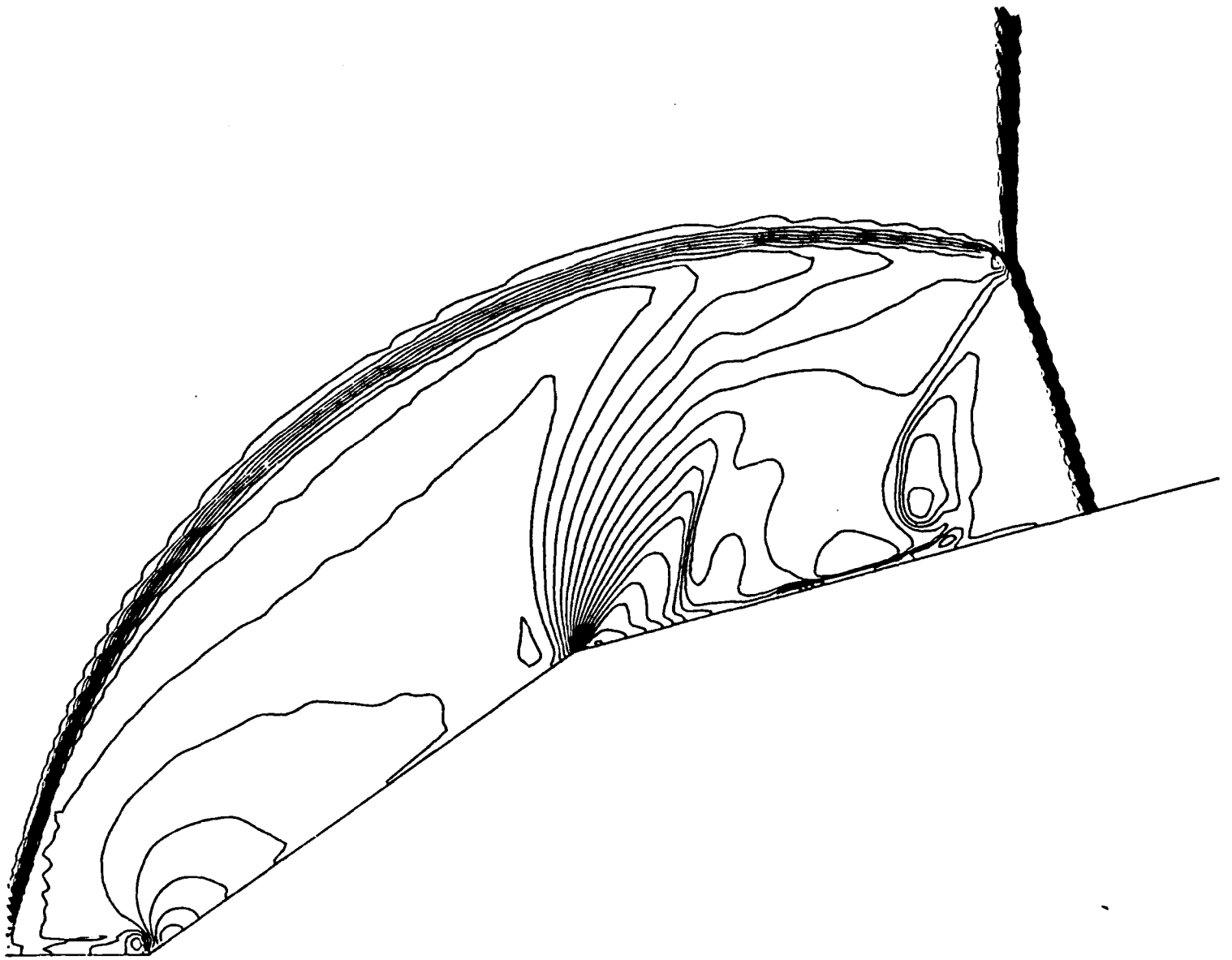

REVERT. O K

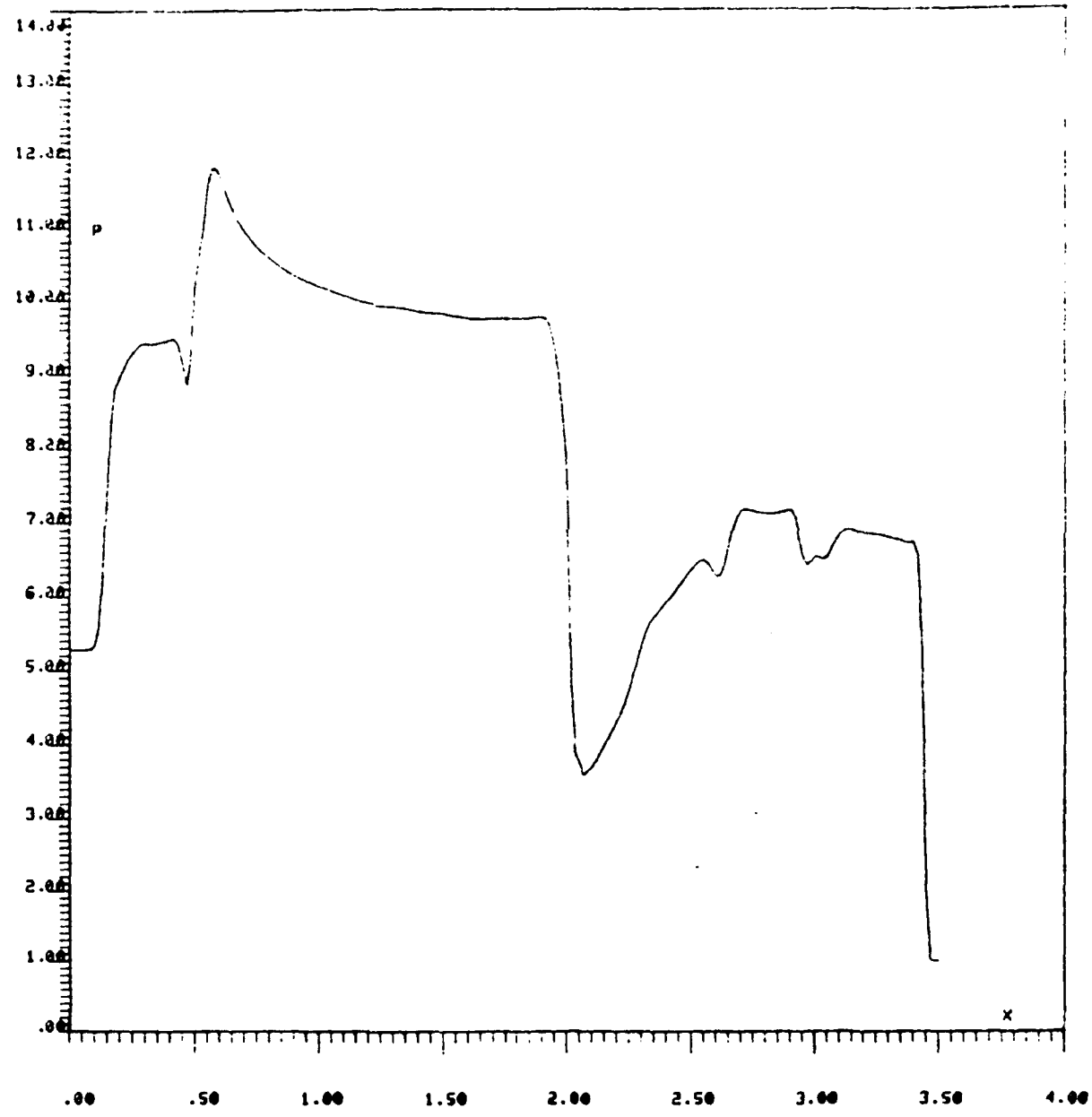

REVERT. 0 K

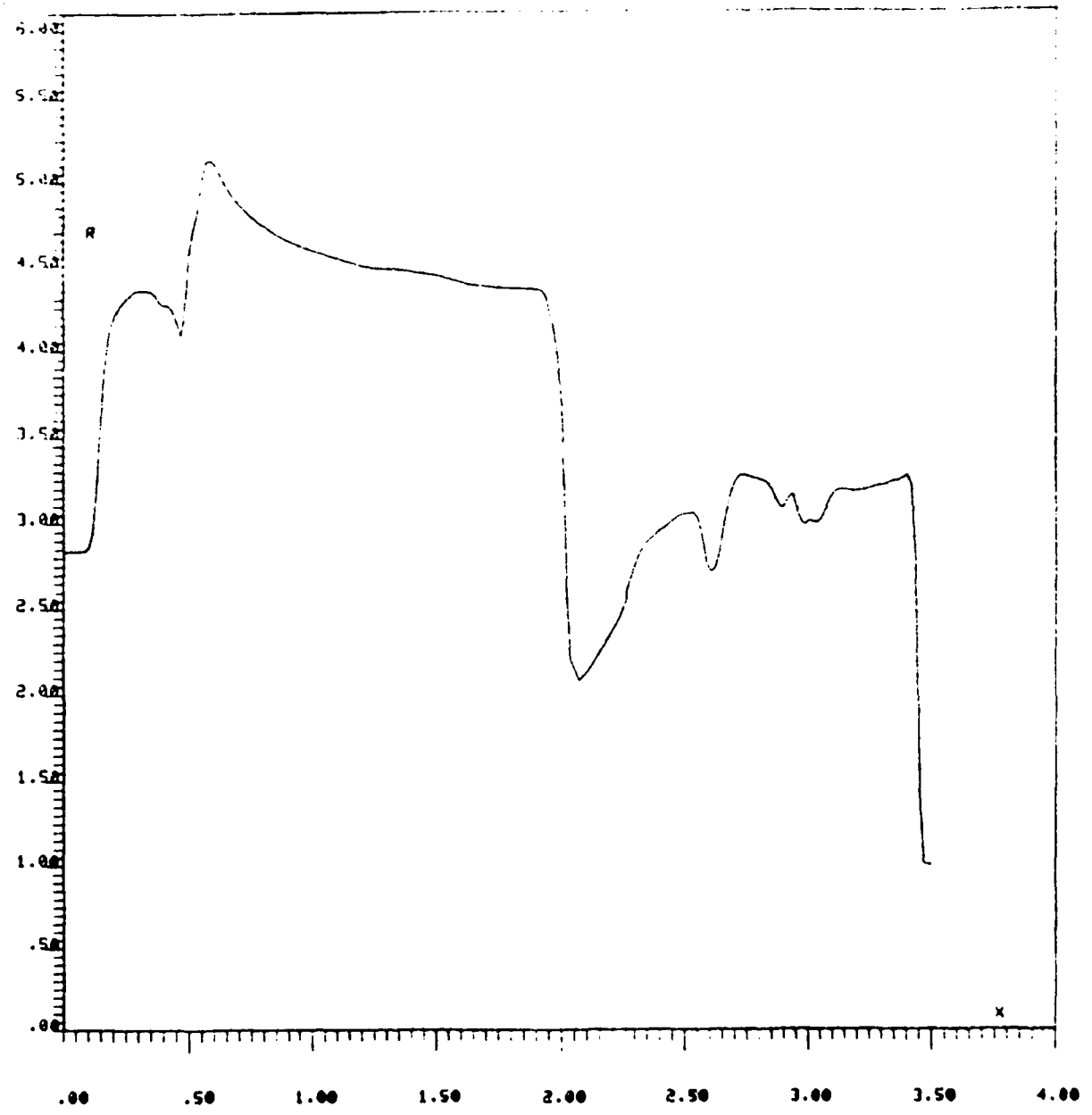

M_s = 1.49 at 66.9 kPa 35°/15°

Case 8

fringe	ρ/ρ_0
a	2.0744
b	2.1376
c	2.2008
d	2.2640
e	2.3272
f	2.3904
x	1.8848
y	1.9480
z	2.0112

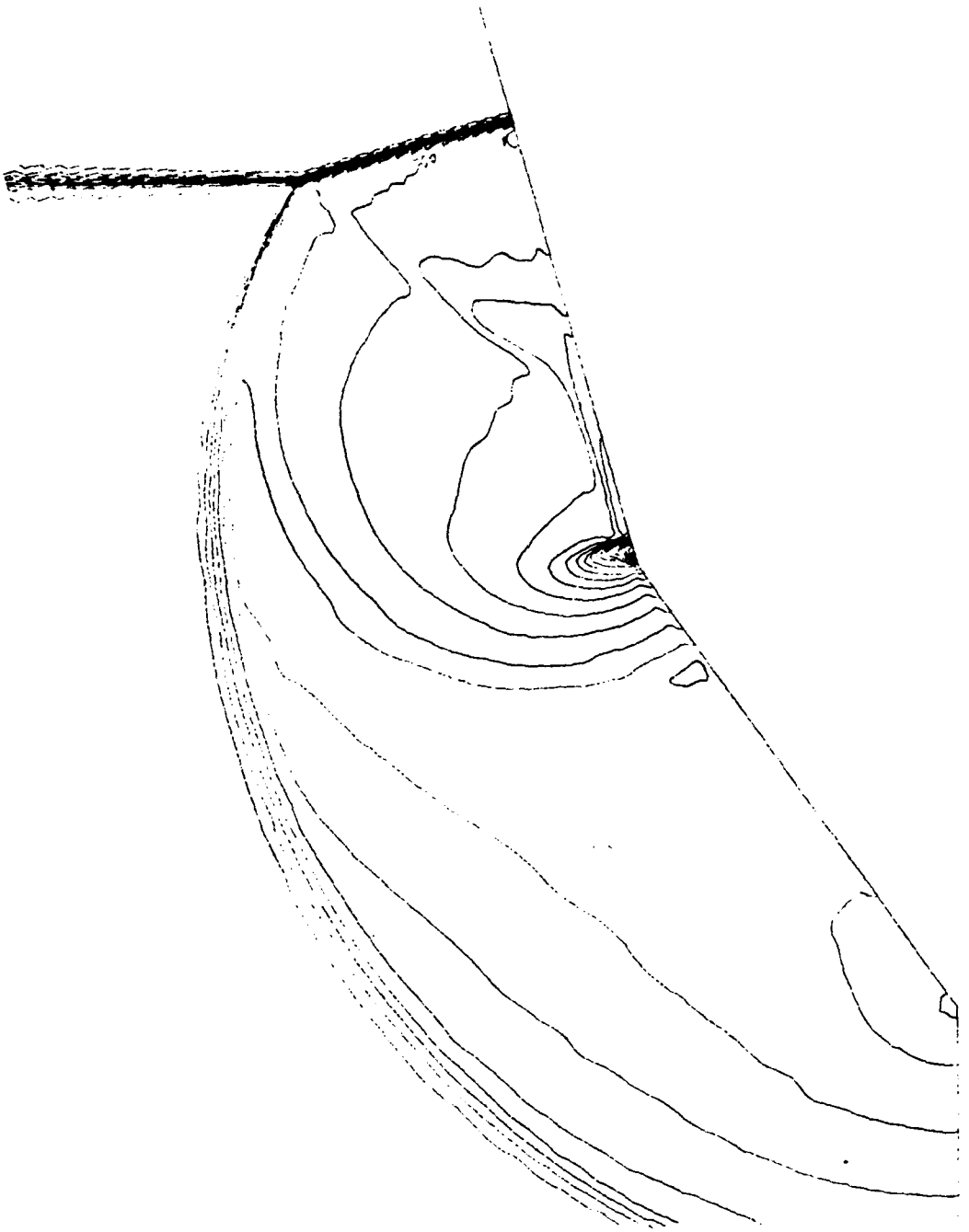

REVERT. O K

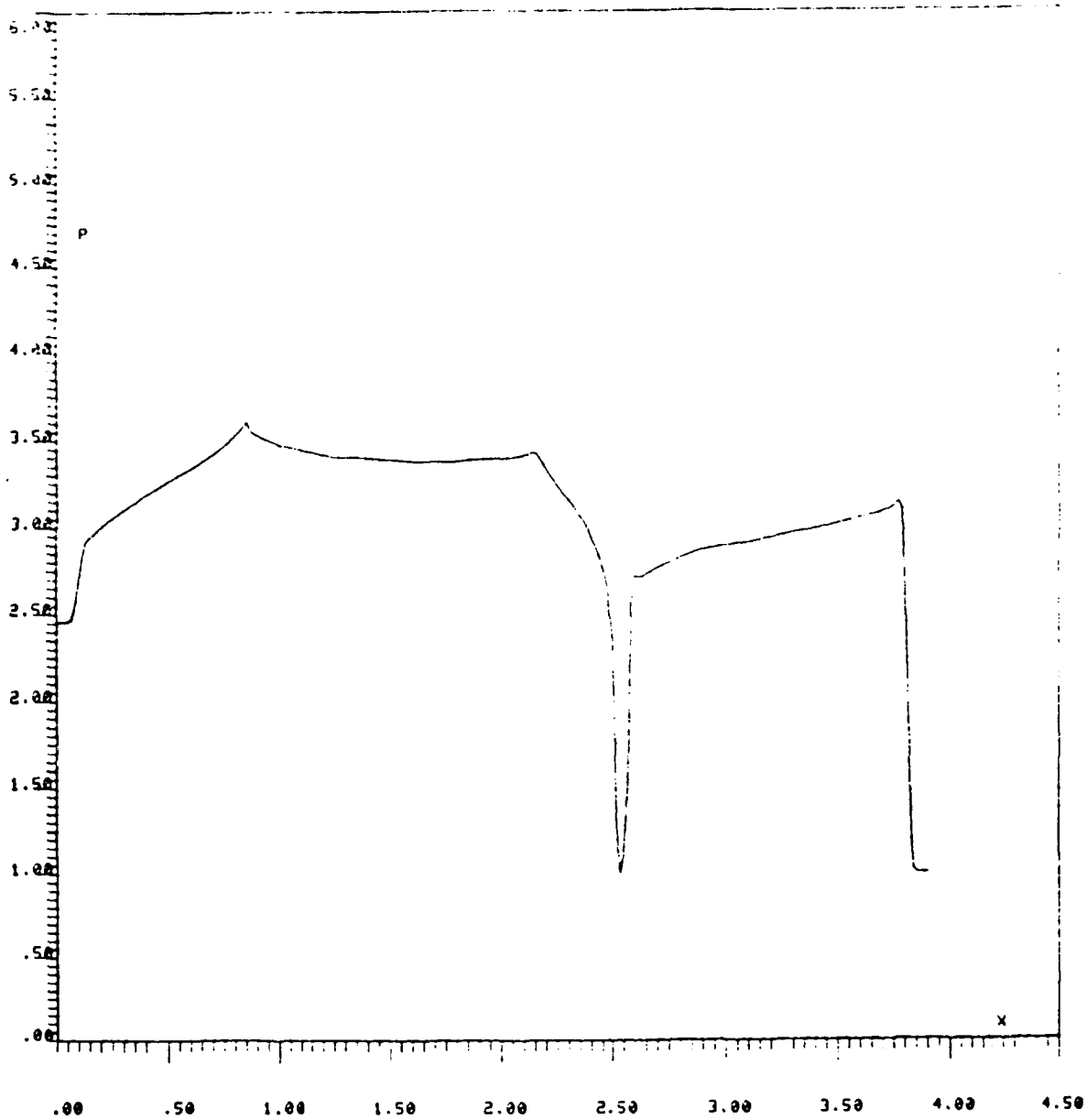

REVERT. O K

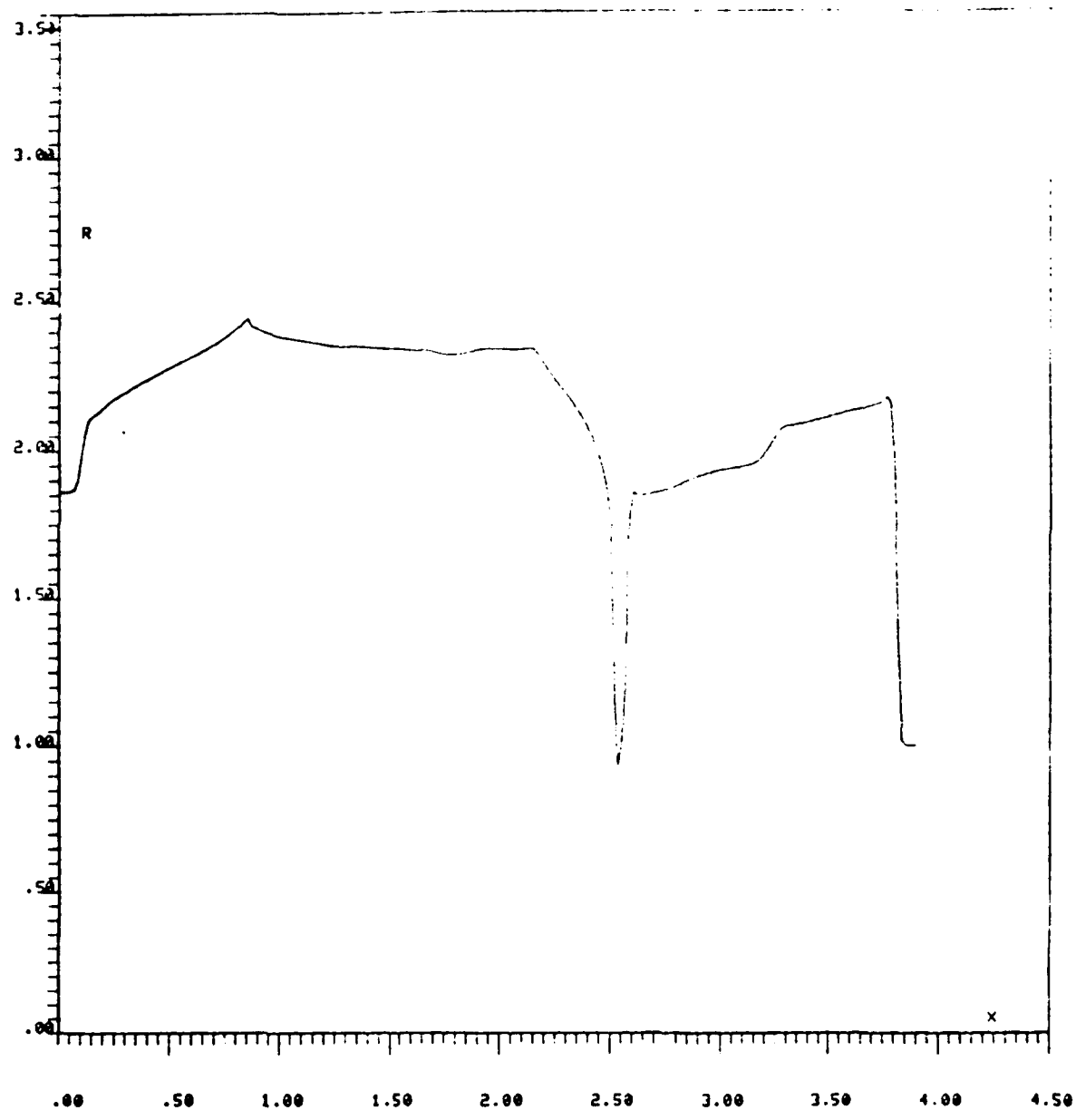

Ms = 2.16 at 30.4 kPa, 40°/25°

Case 9

fringe	ρ/ρ_0
a	3.067435
b	3.205264
c	3.343093
d	3.480922
e	3.618751
f	3.756580
g	3.894409
h	4.032238
i	4.170067
j	4.307896
k	4.445725
l	4.583554
m	4.721383
n	4.859212
o	4.997041

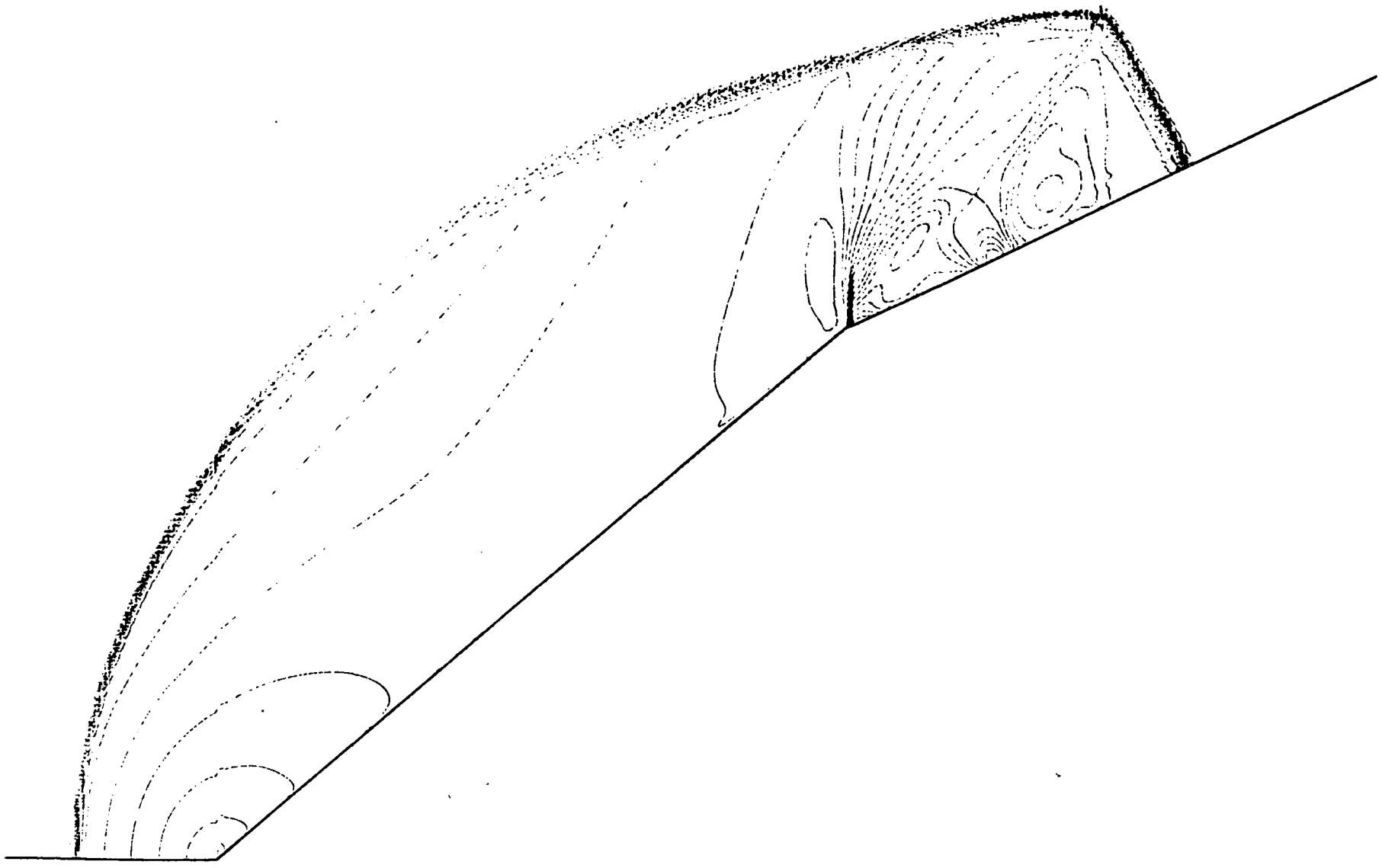

REVERT. O K

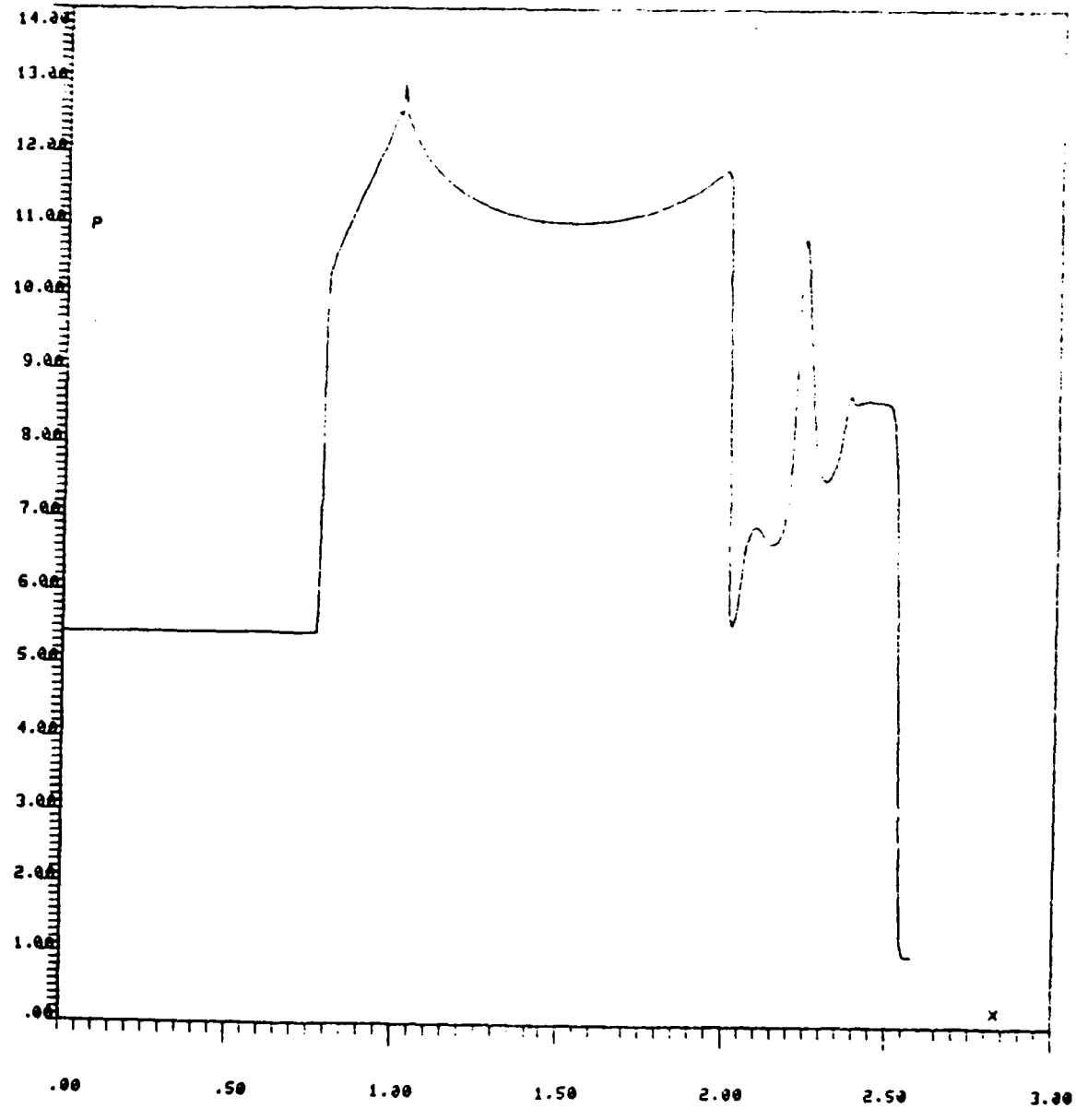

REVERT. 0 K

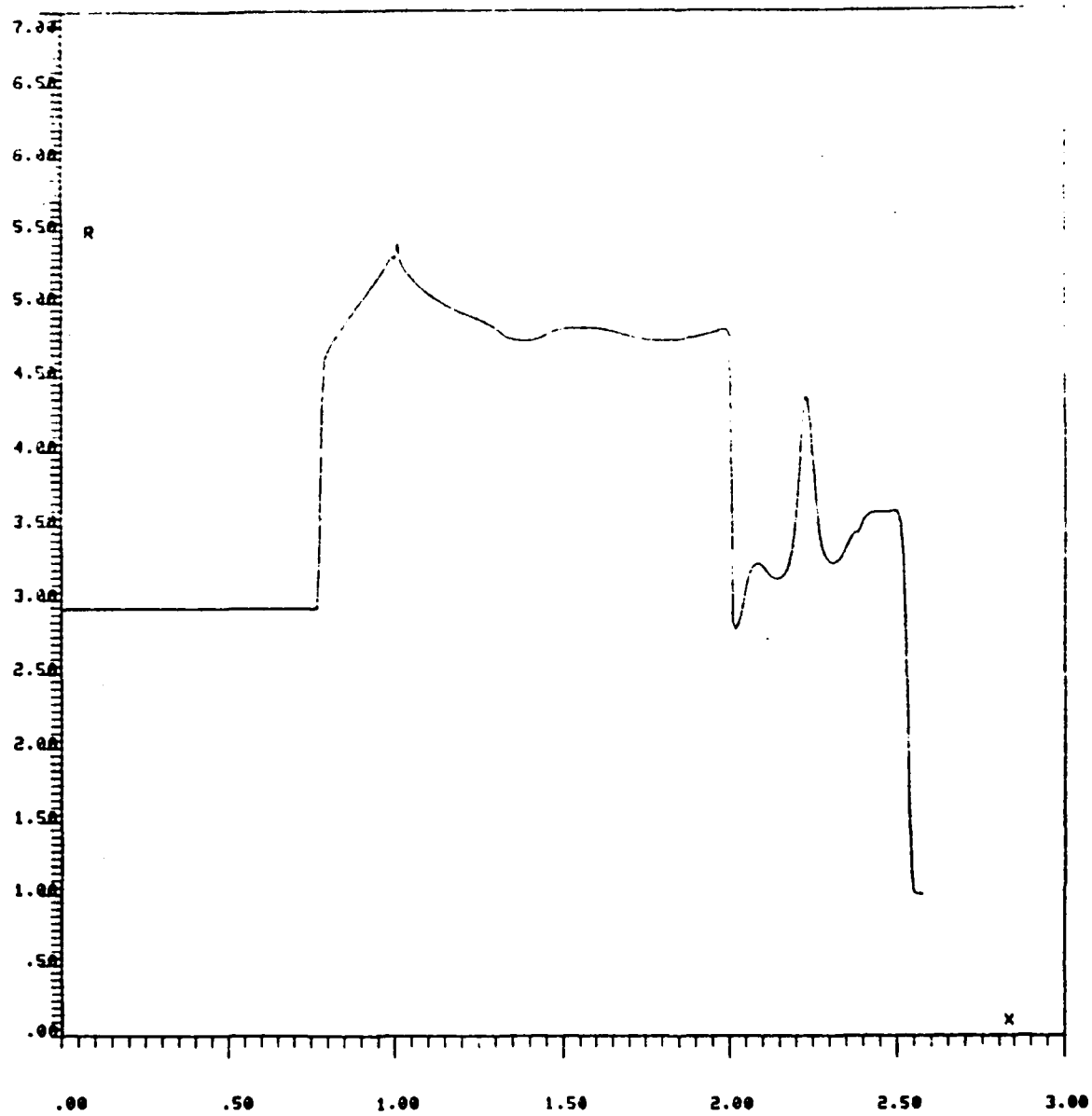

M_s = 1.50 at 66.9 kPa, 40°/25°

Case 10

fringe	ρ/ρ_0
z	1.939465
a	2.002096
b	2.064727
c	2.127358
d	2.189989
e	2.315251
f	2.377882
g	2.440513

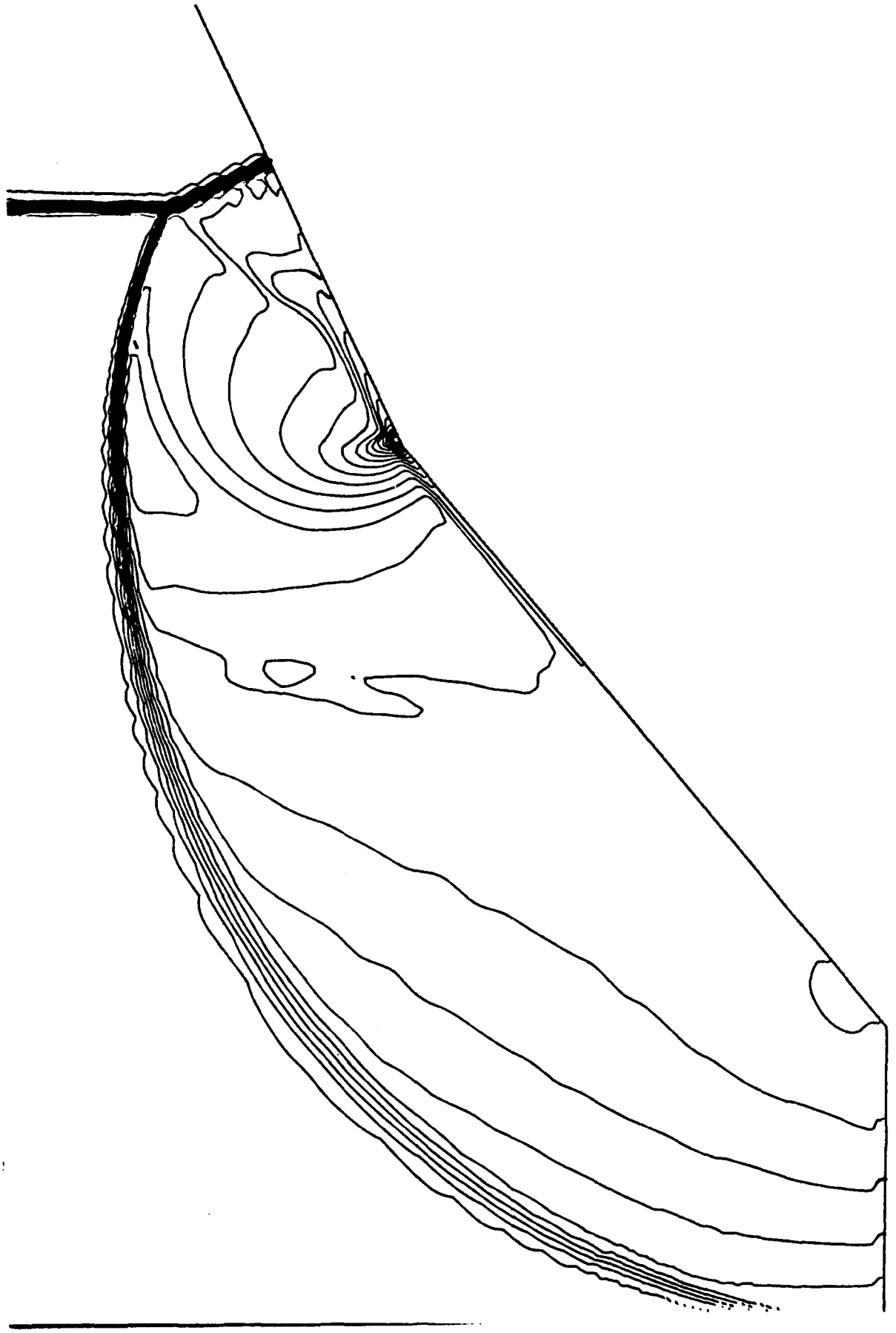

REVERT. 0 K

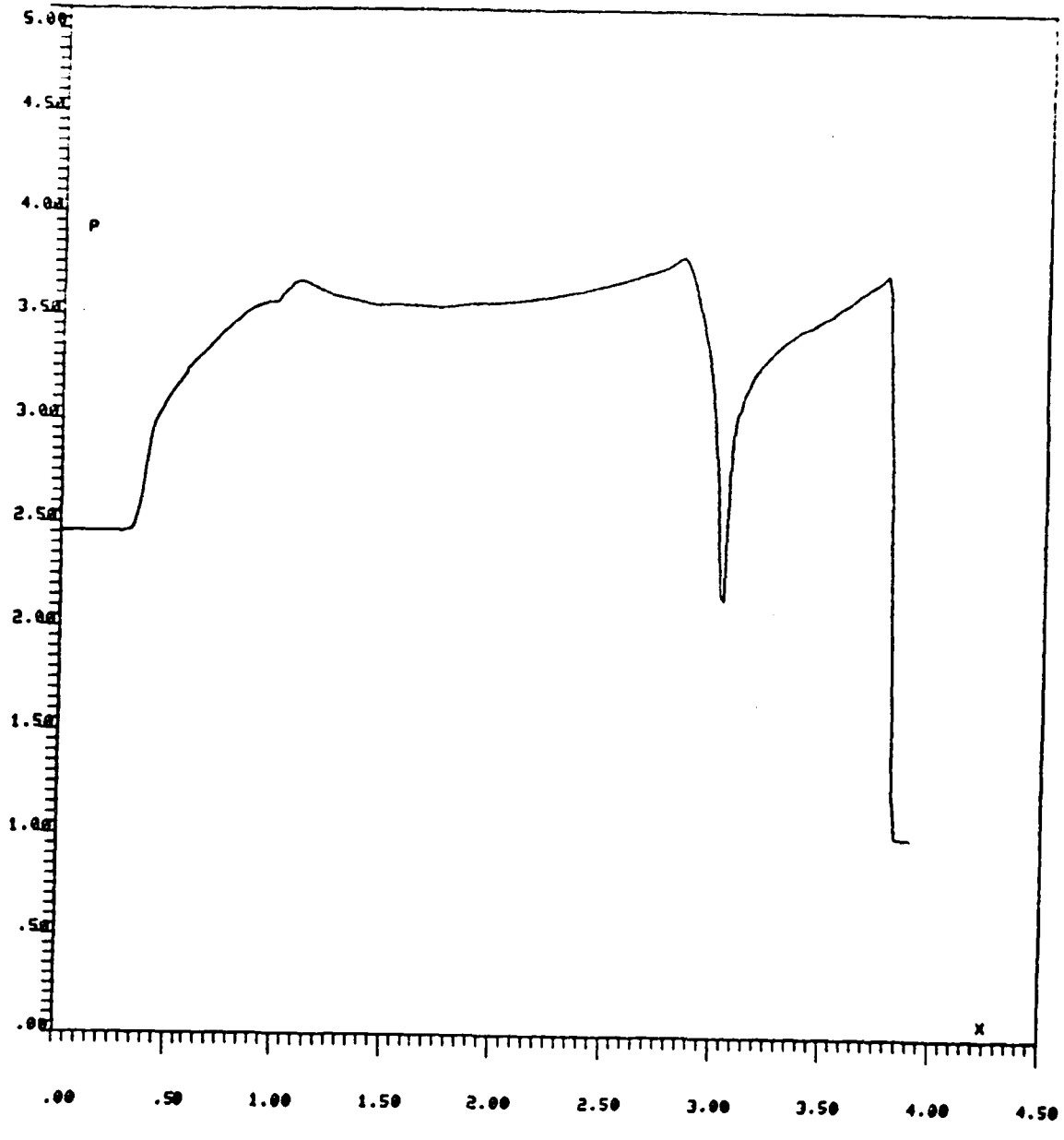
P
X
5.00
4.50
4.00
3.50
3.00
2.50
2.00
1.50
1.00
.50
.00
.00
.50
1.00
1.50
2.00
2.50
3.00
3.50
4.00
4.50

REVERT. O K

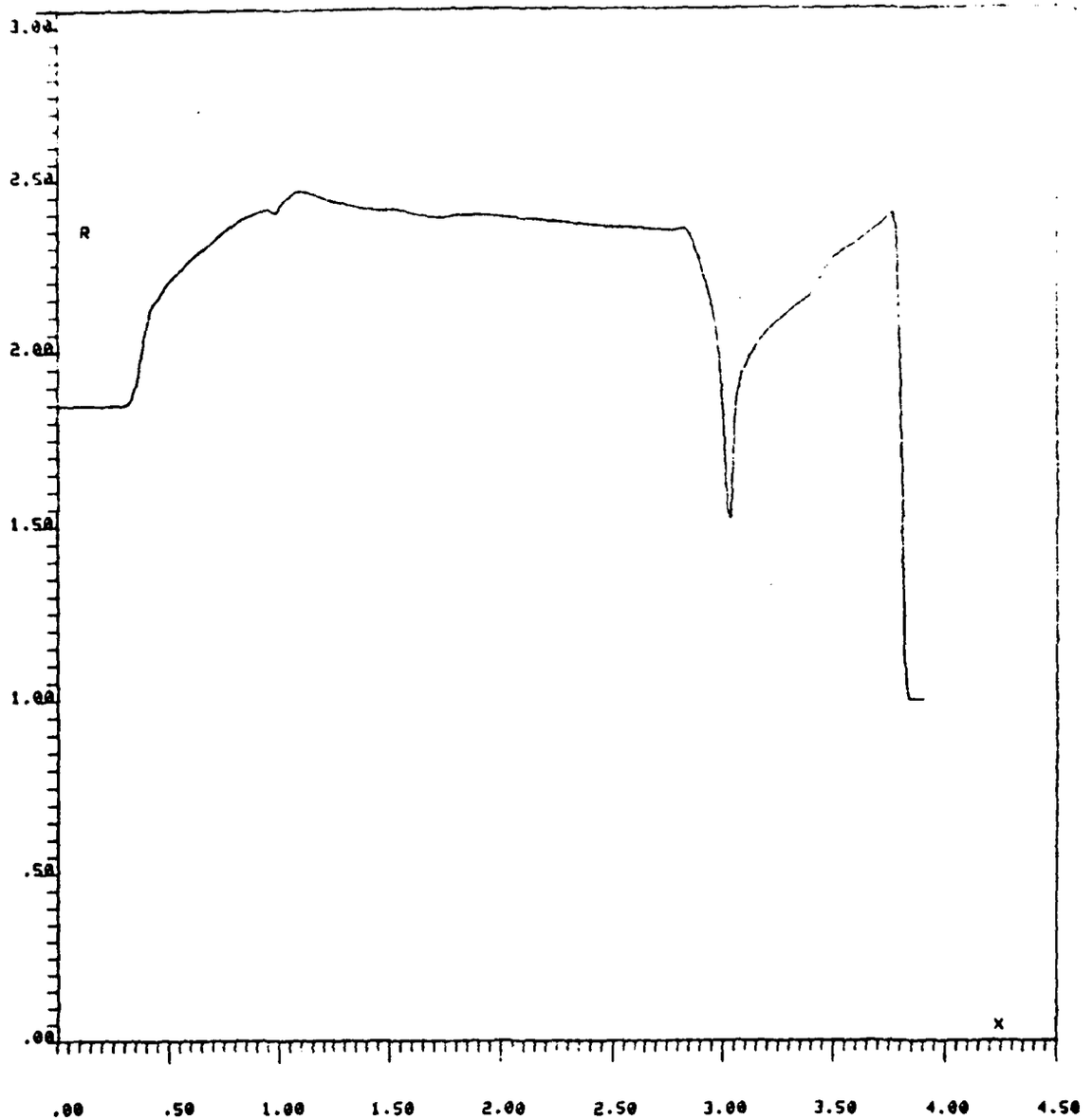

M_S = 1.47 at 66.9 kPa, 40°/25°

Case 11

fringe	ρ/ρ_0
a	2.1376
b	2.2008
c	2.2640
d	2.3272
e	2.3904
f	2.4536
g	2.5168
h	2.5800
i	2.6432
j	2.7064
k	2.7696
l	2.8328

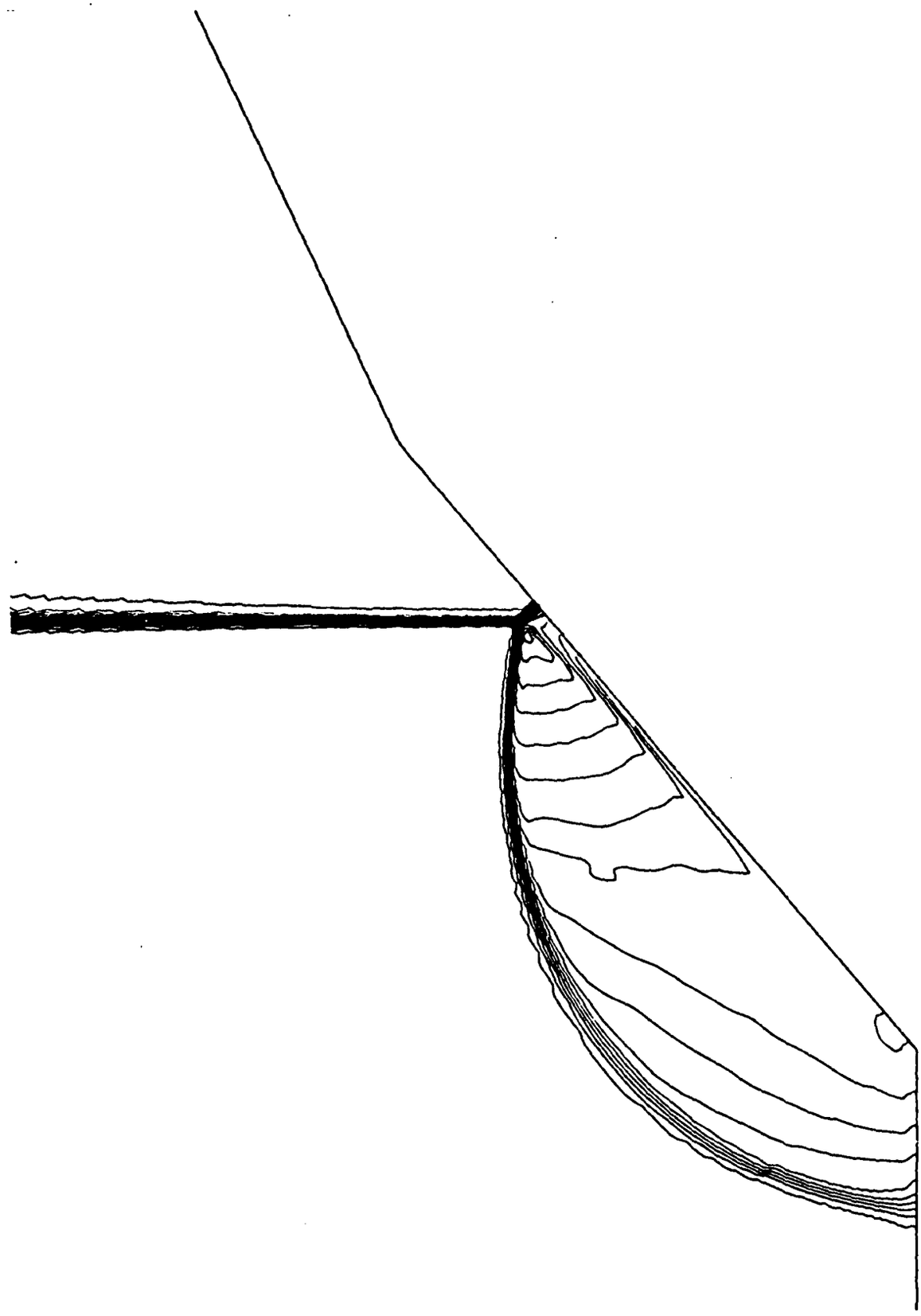

REVERT. O K

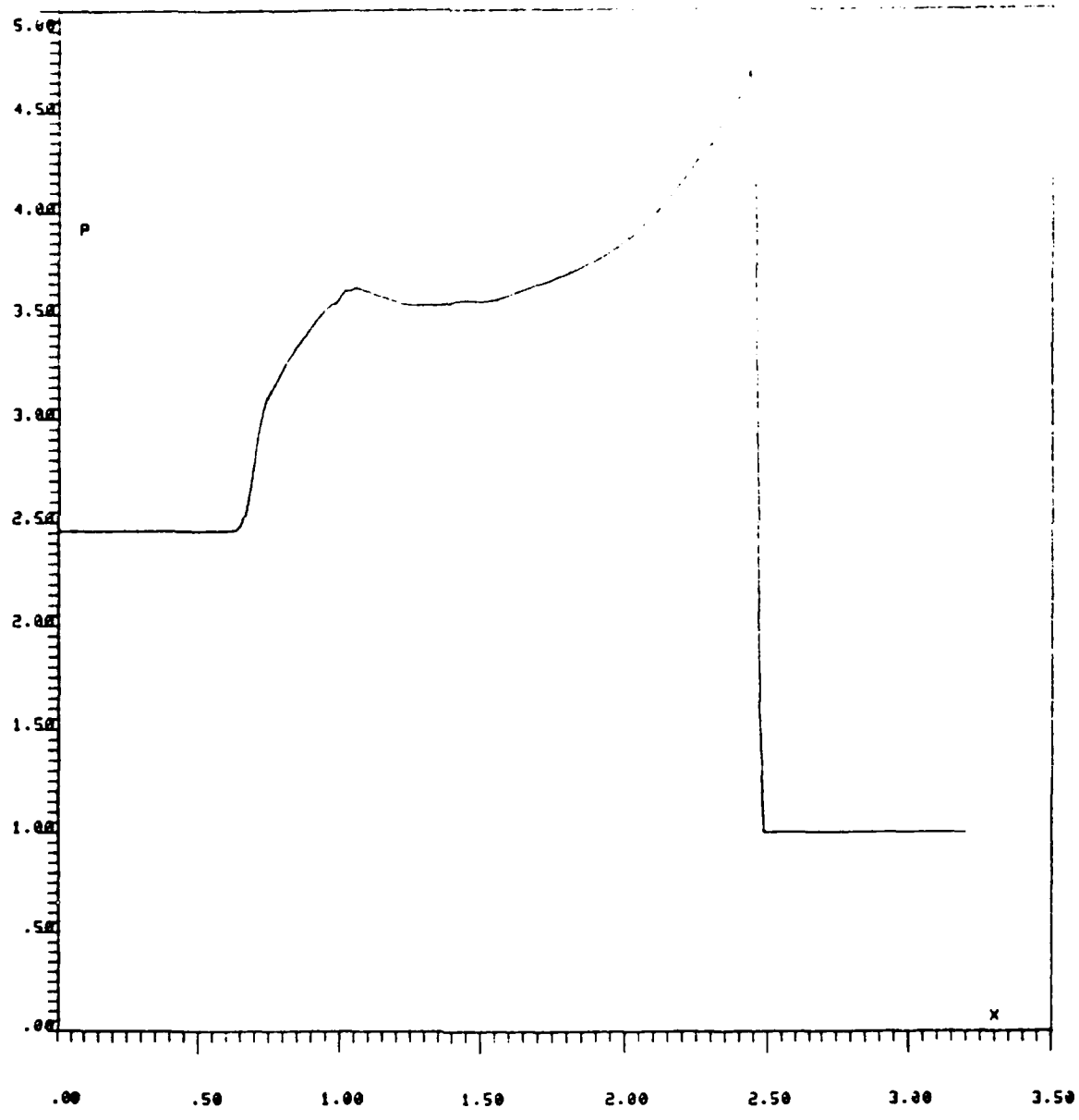

REVERT. 0 K

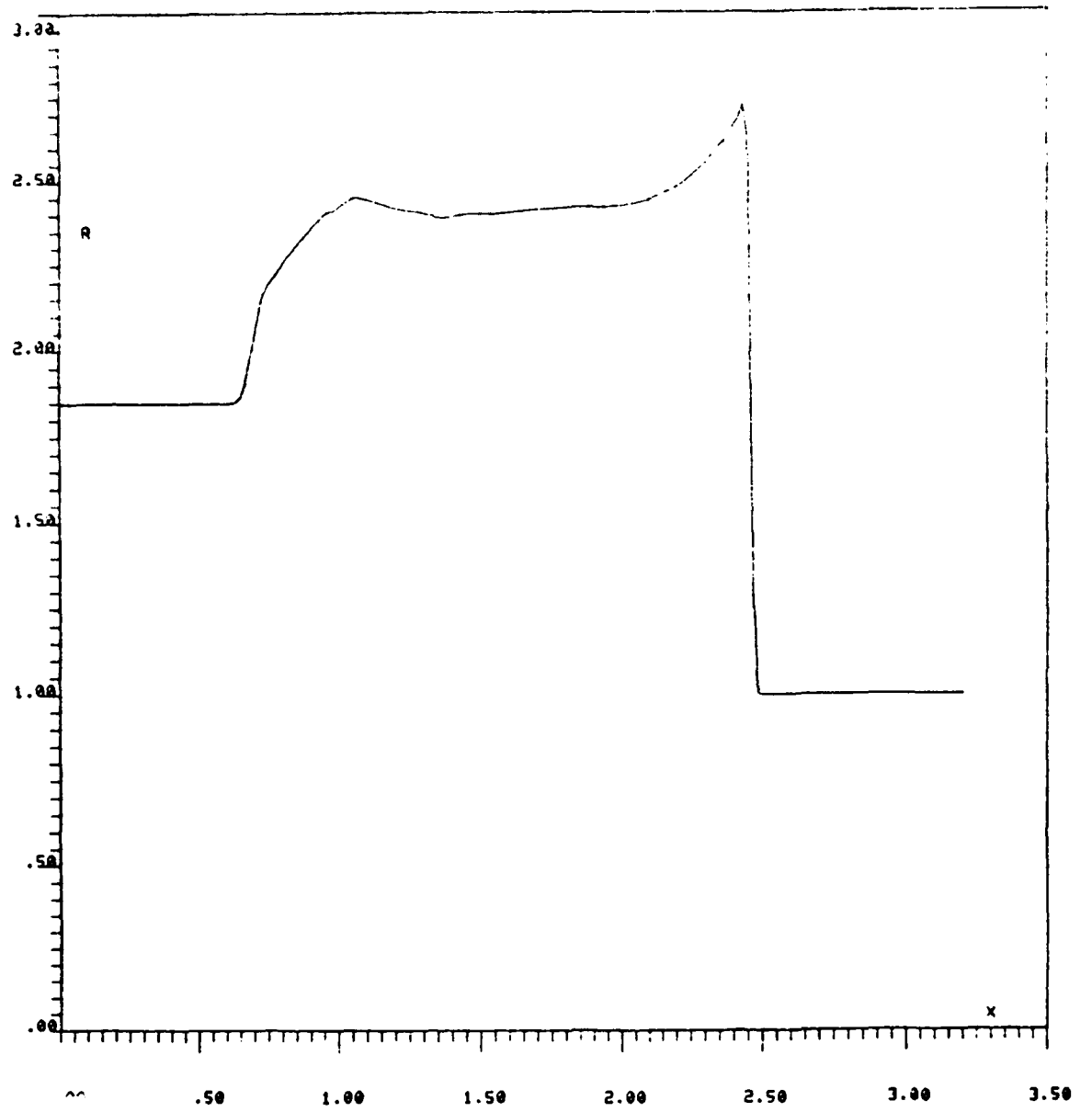


h
i
g
f
b
g
f
e
f
b
a

Case 12

fringe	ρ/ρ_0
a	2.4148
b	2.4672
c	2.5196
d	2.5720
e	2.6244
f	2.6768
g	2.7292
h	2.7816
i	2.8340
j	2.8864
k	2.9388
l	2.9912
m	3.0436

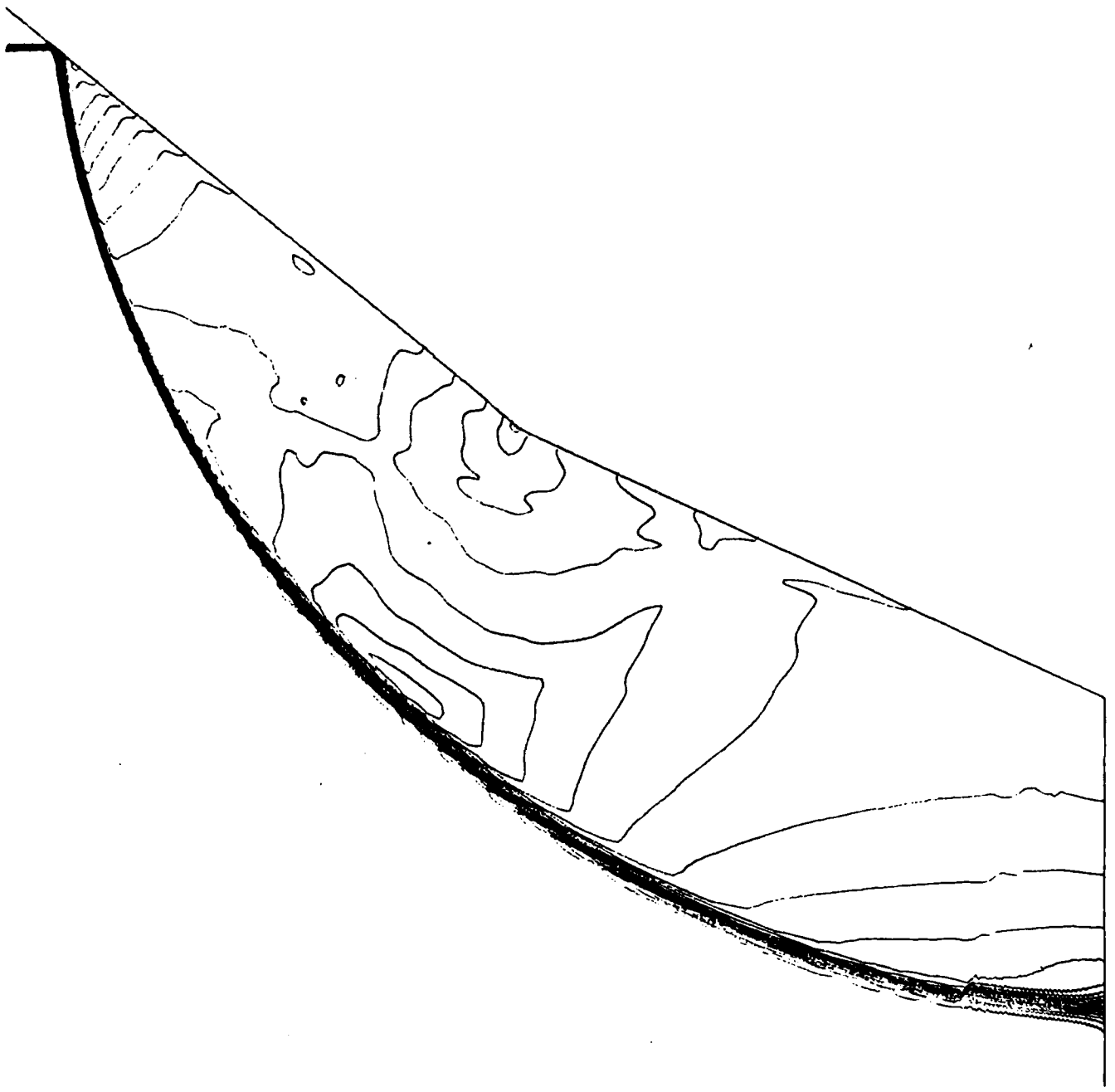

REVERT.

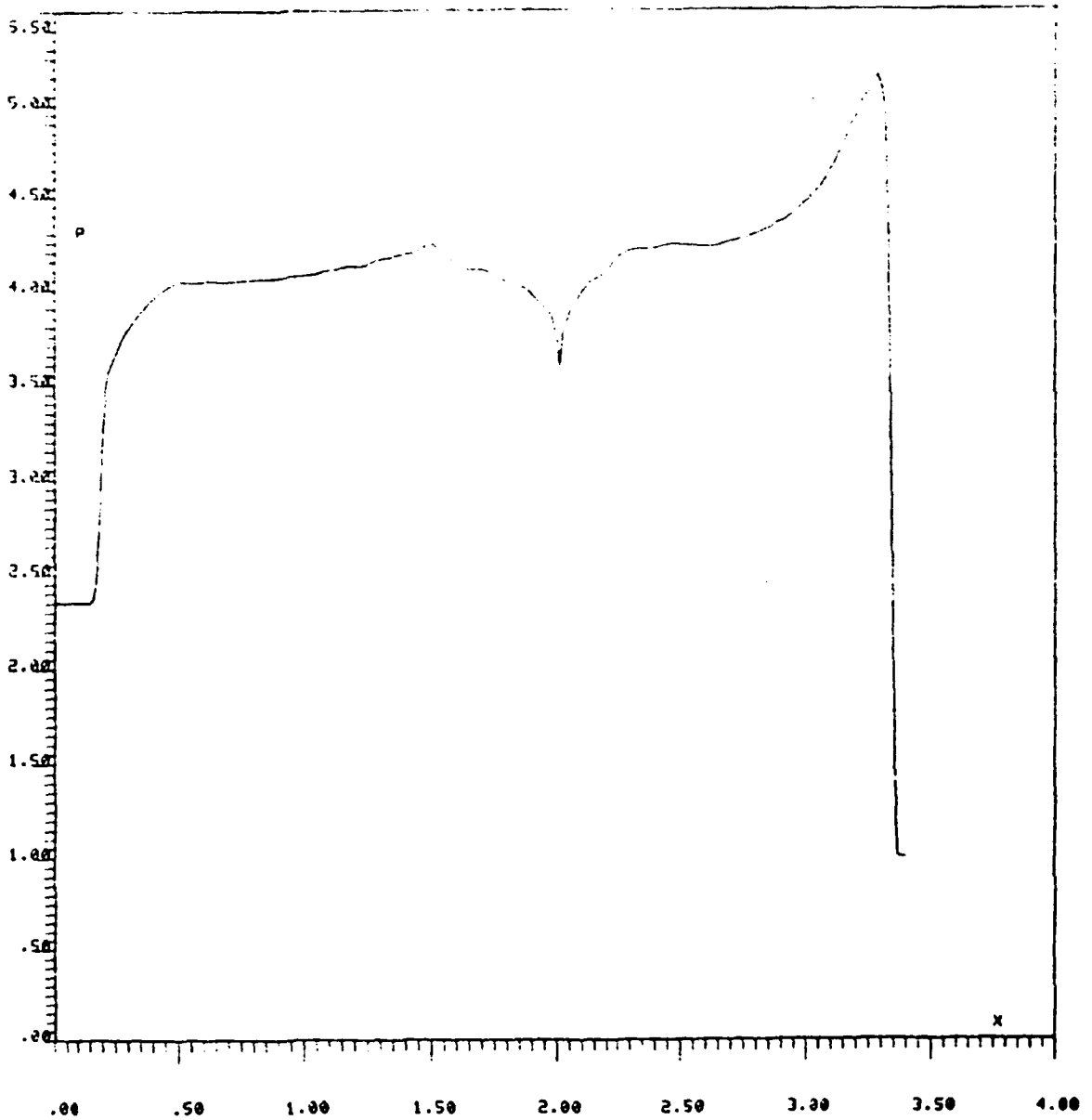

REVERT. O K